Unione Europea

Fondo Sociale Europeo

1562

UNIVERSITY OF SASSARI

PHD SCHOOL IN NATURAL SCIENCES

XXIII CYCLE

IRON AND MANGANESE ACCUMULATIONS IN SARDINIA: THE ROLE OF SUPERGENIC AND HYDROTHERMAL PROCESSES

DIRECTOR: PROF. MARCO APOLLONIO

COORDINATOR: PROF. GIACOMO OGGIANO

TUTOR:

DR. PAOLA MAMELI

CO-TUTORS:

PROF. GIOVANNI MONGELLI

PROF. GIACOMO OGGIANO

PHD STUDENT:

DR. ROSA SINISI

A Te,
a cui devo
parte del mio essere

CONTENTS

Abstract

This paper examines the compositional features of some Fe and Mn accumulations of Sardinia in order to reconstruct the palaeoenvironmental conditions of ores formation, to better characterize the processes that lead to Fe and Mn minerals formation and to compare the Fe and Mn geochemical behavior within different depositional environments. The research focused on comparison between: 1) continental Fe oxyhydroxides concentrations, formed under oxic conditions on a palaeosurfaces of the Tacchi area, and the Uppermost Ordovician oolitic ironstones of shallow anoxic marine environment of the Nurra district; 2) marine supergene Mn ores of Logudoro Basin, hosted in a littoral conglomerate laying at the base of the Miocene transgressive calcareous sediments, and continental hydrothermal Mn mineralizations of San Pietro Island and Anglona district where they are the stockwork and veins filling within Miocene volcanic sequences. Chemical analyses (XRF, INAA and ICP-MS), XRD analysis, OM and SEM-EDS observations were performed on each samples. The analyses results suggest that although the Sardinian ores formed in different environments (marine *vs* continental) and under contrasting climatic (sub-glacial *vs* tropical) and environmental (supergene *vs* hydrothermal) conditions, they share similar mineralogical or geochemical features. Therefore, not necessarily dramatic palaeoenvironmental differences find a counterpart in geochemical features of the chemical sediments.

Riassunto

L'obiettivo del presente lavoro ha riguardato la caratterizzazione composizionale di alcune mineralizzazioni a fasi di Fe e Mn prevalenti (ironstones and Mn ore, rispettivamente), presenti in diverse località della Sardegna allo scopo di ricostruire le condizioni chimico-fisiche del paleoambiente di formazione, caratterizzare in modo più dettagliato i processi che portano alla formazione di fasi minerali a Fe e Mn ed, infine, confrontare i comportamenti geochimici di questi due elementi all'interno di ambienti deposizioni differenti. In particolare, la ricerca si è focalizzata sul confronto tra: 1) concentrazioni di ossi/idrossidi di Fe di ambiente continentale, formate in condizioni ossidanti in corrispondenza di una paleo-superficie situata nell'area dei Tacchi, ed ironstones oolitici dell'Ordoviciano superiore affioranti in diverse località della Nurra e formati in ambiente di mare basso caratterizzato da condizioni anossiche; 2) mineralizzazioni di manganese precipitate a partire da soluzioni marine in condizioni supergeniche ed attualmente distribuite all'interno di un livello conglomeratico che costituisce la base dei sedimenti carbonatici trasgressivi del Miocene, e mineralizzazioni di Mn formatesi in ambiente continentale ad opera di fluidi idrotermali che hanno interessato le sequenze vulcaniche mioceniche dell'Anglona e dell'Isola di San Pietro dove gli ossidi di Mn formano stockworks o si distribuiscono in vene. Tutti i campioni sono stati sottoposti ad analisi chimiche (XRF, INAA and ICP-MS), mineralogiche (XRD) e tessiturali (SEM-EDS). I risultati mostrano che nonostante gli ores studiati si siano formati in ambienti differenti (continentale vs marino) e in condizioni climatiche (sub-glaciale vs tropicale) ed ambientali (supergenico *vs* idrotermale) contrastanti, essi mostrano simili caratteristiche chimiche e mineralogiche. Tutto ciò suggerisce che le differenze del paleoambiente deposizionale, pur essendo significative, possono anche non generare evidenti differenze geochimiche nei sedimenti di origine chimica.

INTRODUCTION AND OBJECTIVES

There is no unequivocal definition of an ore deposit. The traditional definitions embrace the concept of a natural mineral accumulation that may be profitably exploited to meet the demands of society, although the significance of profitability is often questioned because it is directly linked to fluctuations in market prices. However, not all minerals fall into the "ores" category. Indeed, whilst all natural inorganic crystalline solids (including useful raw materials such as diamond) are named minerals, more usually only those that are metalliferous are considered to constitute ores (Marshall and Fairbidge 1999). For this reason, the ores cannot be considered as industrial minerals, despite their growing importance is primarily controlled by economic interests. The industrial minerals definition, in fact, includes generally a wide range of solid material extracted for purposes other than energy and metals production (Manning 1994) implying a "for use" classification and not a mineralogical one.

Whatever their exact definition, the ore deposits are of great geochemical interest from several perspectives: first, they are comparatively rare and comparatively large natural metals accumulations which are characterized by high enrichment factors values related to average metals contents in most common rocks of the upper continental crust; second, their genesis is usually incompletely understood and often can be explain only by geochemical models; third, the ore deposits, forming from chemical precipitation processes within the supergenic cycling, are valid tools for the palaeoclimatic and/or palaeoenvironmental reconstructions. In fact the chemical sediments are able to record the climate and redox conditions.

Moreover the ores deposits, especially when they are made of oxides, have a great environmental importance due to elements adsorption capability of these mineral phases. As for this last feature, particular attention has recently been paid to Mn oxy-hydroxides. Despite the long time known tunneled crystal structures of Mn oxides and the derived properties, only recently the researches have deepened the study of manganese oxides considering them as adsorbent materials of pollutant species profitable for environmental remediation. It is well known, indeed, that element cycling on Earth is directly related to electron transfer (or redox) reactions.

Not only the environmental redox processes play key roles in the precipitation and/or dissolution of mineral phases but also such minerals often control the discharge or sequestration of inorganic contaminants. Thus, the

redox processes control the chemical speciation, bioavailability, toxicity, and mobility of many major and trace elements including Fe, Mn, C, P, N, S, Cr, Cu, Co, As, Sb, Se, Hg, Tc, and U. In addition, the redox-active mineral surfaces are able in catalyzing the transformation and degradation of organic contaminants.

Most manganese oxides, mainly hollandite group minerals, pyrolusite and todorokite are characterized by a high surface charge and a tunneled crystal structure which play a key role in geochemistry of Mn deposits.

Murray (1975) and Nicholson and Eley (1997) argue that the adsorption mechanism of the elements onto Mn oxides surface is the main process leading to the accumulation of cations, mainly heavy metals, into Mn deposits. This adsorption mechanism is also influenced by the pH of solution and, precisely, Nicholson and Eley (1997) observed experimentally that adsorption capacity of Mn oxides increases with pH increasing. This implies that in alkaline water, such as seawater, the Mn oxides absorb onto their surface the most of the dissolved cations. This important feature of Mn oxides leads to an enrichment of chemical Mn-bearing sediments in many transition metals of significant economic interest, particularly Cu, Ni, Co, Zn, Ba and Pb (Koschinsky et al. 2003; Maynard 2003).

Similar processes also involve some iron oxyhydroxides. Thiessen et al. 1996, indeed, argue that, through the adsorption processes developing on the minerals surface, the Fe oxyhydroxides, particularly goethite, are capable of fractioning and retaining many trace elements at significant amounts.

However, the adsorption is not the only inclusion mechanism of trace elements within metalliferous oxides. Other processes such as replacement through ion-exchange and co-precipitation with oxides must be considered (Koschinsky and Hein 2003). In particular, these mechanisms typically occur in the presence of the Mn minerals with tunneled crystal structure (Chen et al. 2009; Randall et al. 1998). This structure consist of MnO_6 octahedral units shared by vertices and/or edges forming a single chain. Latter in turn can bind to other octahedral chains to form a framework structure containing tunnels with variable square cross sections which may be usually filled by large mono- or divalent cations and water molecules (Post and Burnham 1986; Lei 1996).

The meaningful source of dissolved Fe and Mn concentrations, able to generate ores, is mostly linked to ocean floor hydrothermal vents. These lead to sedimentary nodules and encrustations which, due to their high content of heavy

metals (such as Ni, Co, Cu and Zn), are better known as polymetallic nodules and crusts (Cronan 1997; Nath et al. 1997).

Other significant Fe and Mn accumulations are linked to extreme weathering conditions leading to residual crusts such as ferricrusts or wad in continental environments. Less spread a less studied are continental hydrothermal Mn concentrations and shallow marine Mn sedimentary deposits.

Some good examples of manganese and iron concentrations in coastal sediments occur in the Ordovician and in Miocene sequences of Sardinia where manganese also occurs in hydrothermal veins hosted in Tertiary calcalkaline volcanites. Despite such deposits gave rise to minor exploitations during last century, no specific studies on their mineralogical, geochemical and genetic features were carried out. For this reason, these deposits represent a challenging topic on manganese and iron accumulation mechanisms in continental and shallow marine settings.

In detail, the research focused on the compositional characterization of some ironstones deposits and manganese mineralizations in order to 1) reconstruct the palaeoenvironmental conditions of ores formation, 2) better characterize the processes that lead to precipitation of Fe and Mn mineral phases and 3) compare the Fe and Mn geochemical behavior within different depositional environments.

Therefore, ore deposits that formed in different geological context and by different precipitation mechanisms were considered:

- the Fe oxyhydroxides linked to subaerial accumulation processes on a palaeosurface in the Tacchi area (SE Sardinia) were compared with the uppermost-Ordovician ironstones formed into a shallow anoxic marine environment;
- the marine Mn-ores of Logudoro Basin, which form the matrix or cement of a littoral conglomerate laying at the base of the middle-Miocene transgressive calcareous sediments, were compared with the hydrothermal Mn mineralizations of San Pietro Island and Anglona district, where they are the veins and fractures filling within Miocene volcanic sequences.

The thesis was organized into three main parts to ensure a clear exposition of the work. The first part (Part I) is a brief introduction to the geological and structural features of Sardinia and to the studied deposits emplacement within the geological context of the island. In the second part of thesis (Part II), the data presentation, discussion and conclusions concerning the iron deposits were grouped. Finally, in the third part (Part III) are exposed data and conclusions related to the Mn ores.

In this regard, it should be noted that the Part II correspond to a paper published in Clay Minerals and the Part III is the content of another manuscript currently under review to be published in Ore Geology Review.

Finally, the tables of chemical data and the analytical methods used for the research are reported in Appendix 1 and 2 respectively.

REFERENCES

CHEN T., DOU H., LI X., TANG X., LI J. AND HAO J. (2009) – *Tunnel structure effect of manganese oxides in complete oxidation of formaldehyde*. Microporous and Mesoporous Materials, 122, 270-274.

CRONAN D.S. (1997) – *Some controls on the geochemical variability of manganese nodules with particular reference to the tropical South Pacific*. In: Manganese Mineralizations: Geochemistry and Mineralogy of Terrestrial and Marine Deposits, Nicholson K., Hein J.R., Bühn B. and Dasgupta S. Eds., Geological Society Special Publication, 119, 139-151.

KOSHINSKY A. AND HEIN J.R. (2003) – *Uptake of elements from seawater by ferromanganese crusts: solid-phase associations and seawater speciation*. Marine Geology, 198, 331-351.

KOSHINSKY A., WINKLER A. AND FRITSCHE U. (2003) – *Importance of different types of marine particles for the scavenging of heavy metals in the deep-sea bottom water*. Applied Geochemistry, 18, 693–710.

LEI G. (1996) – *Crystal structures and metal uptake capacity of 10Å-manganates: An overview*. Marine Geology, 133, 103- 112.

MAYNARD J.B. (2003) – *Manganiferous Sediments, Rocks and Ore*. In: Treatise on Geochemistry: meteorites, comets and planets. Elsevier Lid., 1, 289-308.

MANNING D.A.C. (1994) – *Introduction to Industrial Minerals*. Chapman and Hall Eds., 288 pp.

MARSHALL C.P. AND FAIRBIDGE R.W. (1999) – *Encyclopedia of Geochemistry*. Kluwer Academy Publishers.

MURRAY J.W. (1975) – *The interaction of metal ions at the manganese dioxide-solution interface*. Geochim. Cosmochim. Acta, 39, 505-519.

NATH B.N., PLÜGER W.L. AND ROELANDTS I. (1997) – *Geochemical constraints on the hydrothermal origin of ferromanganese encrustations from the Rodriguez Triple Junction, Indian Ocean*. In: Manganese Mineralizations: Geochemistry and Mineralogy of Terrestrial and Marine Deposits, Nicholson K., Hein J.R., Bühn B. and Dasgupta S. Eds., Geological Society Special Publication, 119, 199-211.

NICHOLSON K. AND ELEY M. (1997) – *Geochemistry of manganese oxides: metal adsorption in freshwater and marine environments*. In: Nicholson K., Hein J., Bühn B., Dasgupta S. (Eds.), Geochemistry of manganese oxides: metal adsorption in freshwater and marine environments. Geological Society of London, Special Publications, 119, 309-326.

POST J.E. AND BURNHAM C.W. (1986) – *Modeling tunnel-cation displacements in hollandites using structure-energy calculations*. American Mineralogist, 71, 1178-1185.

RANDALL S.R., SHERMAN D.M. AND RAGNARSDOTTIR K.V. (1998) – *An extended X-ray absorption fine structure spectroscopy investigation of cadmium sorption on cryptomelane (KMn_8O_{16})*. Chemical Geology, 151, 95-106.

THIESSEN H., LO MONACO S., RAMIREZ A., SANTOS M.C.D. AND SHANG C. (1996) – *Phosphate minerals in a lateritic crust from Venezuela*. Biogeochemistry, 34, 1-17.

PART I

FE AND MN ORES WITHIN THE GEOLOGICAL EVOLUTION FRAME OF SARDINIA

1.1 The Sardinian basement and the Paleozoic geodynamic framework

The Sardinia basement retains good records of the entire Variscan cycle: in fact the Sardinia crust was only incidentally involved in the Alpine collision without any reactivation of the basement in later orogenic buildings.

The Sardinia segment of the Variscan chain, after the Cainozoic drifting of the island, shows a NW-SE trend and crops with good continuity from the North to the South.

The collisional structural frame results in three different structural zones (Carmignani et al 1994, Fig. 1.1):

- a thrusts and folds belt foreland consisting of a sedimentary succession, ranging in age from upper Vendian to lower Carboniferous, which crops in southwest portion of the island;
- a S-W verging nappe building which equilibrated under green schist facies conditions, consisting of a Palaeozoic sedimentary succession bearing a thick continental arc-related volcanic suite;
- an inner zone characterized by medium to high grade metamorphic rocks.

The inner zone consists of two different metamorphic complexes:

- A polimetamorphic high-grade complex (A) made up of anatexites and metatexites hosting orthogneiss and minor amphibolite bodies, which equilibrated in HT/LP conditions. This latter complex corresponds to the northernmost part of the island and extends to Corse. In spite of this late re-equilibration, in places granulite relic assemblages of high-intermediate P and unknown age are still detectable (Ghezzo et al. 1979; Di Pisa et al. 1993, Cortesogno et al. 2004, Franceschelli et al. 2007);
- A medium grade, chiefly metapelitic complex (B) consisting of micaschists and paragneisses bearing Ky+/- Stau+/- Gr+/- and including quartzites and N-MORB metabasalts boudines with eclogite relics (Cappelli et al. 1992).

The contact between these two complexes is well exposed along the Posada Valley (Elter 1987) as well as in Southern Gallura and Asinara island (Oggiano and Di Pisa 1992; Carmignani and Oggiano 1997).

Thrusting or wrench-thrusting of complex A onto complex B has been inferred in places where the contact is not complicated by late variscan

retrograde dextral strike-slip shear (Oggiano and Di Pisa 1992; Carosi et al. 2004).

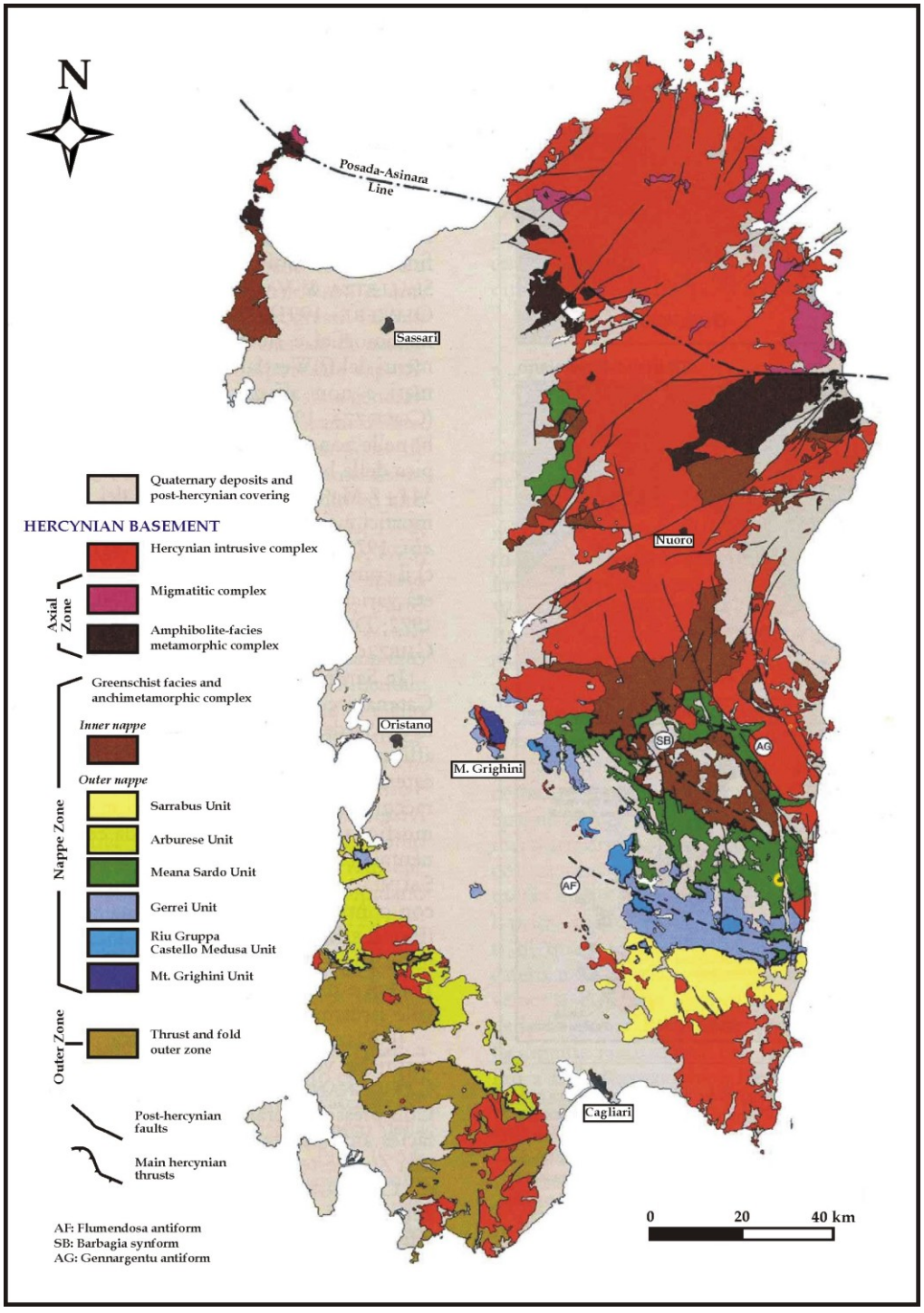

Fig. 1.1 – Major structural elements of Sardinian hercynian basement. After Carmignani et al. (2001).

This collisional frame issued from a long lasting geodynamic evolution, which starting from the onset of passive North Gondwana margin pursued with Ordovician arc-related calcalkaline magmatism (Di Pisa et al. 1993; Oggiano et al. 2010; Fig. 1.2).

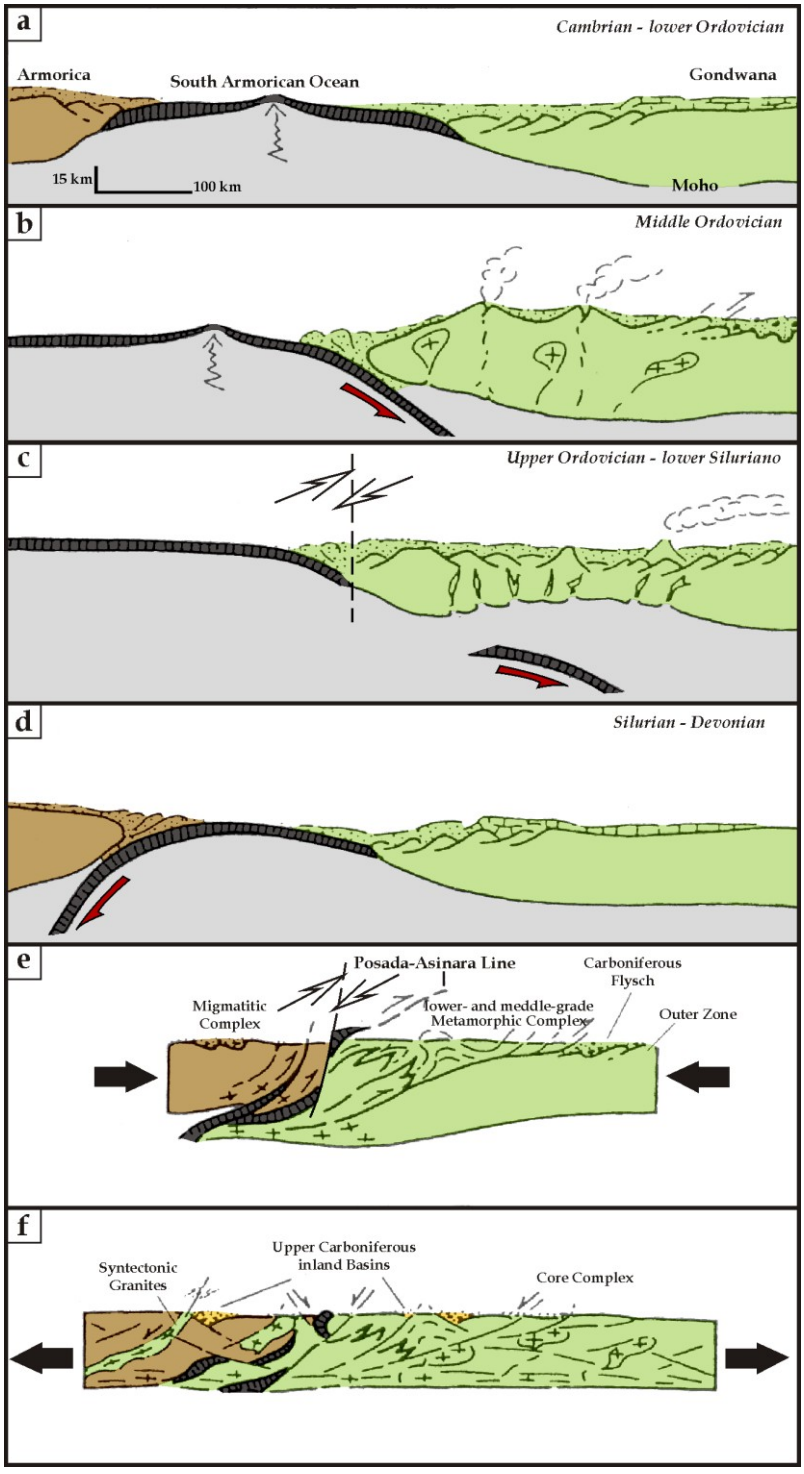

Fig. 1.2 – Geodynamic evolution scheme of Sardinian hercynian basement:
(a) lower Cambrian-Ordovician;
(b) middle Ordovician;
(c) Upper Ordovician-lower Silurian;
(d) Silurian-Devonian;
(e) lower Carboniferous;
(f) Upper Carboniferous-Permian.
After Carmignani et al. (1992) modified.

The calcalkaline magmatism turned into an alkaline one during uppermost Ordovician in concomitance with the Hirnantian glaciation, so testifying for a rifting stage possibly related to a back arc spreading followed by the detachment of the perigondwanian terranes (*Armonica Terrane Assemblage* - Rossi et al. 2009; Oggiano et al. 2010). During this cold period important oolithic ironstones and manganese-rich beds deposited.

After the Hirnantian glaciation, in concomitance with the general sea level rise, black phyllites of Orthoceras bearing limestones and Devonian shelf limestones deposited before the continental collision, which occurred during lower Carboniferous. The onset of the collisional stage is documented by Culm like flysch deposits and by Barrow time metamorphism.

The late variscan evolution (Fig. 1.3), in upper Carboniferous-Permian time, is characterized by the collapse of the chain, the HT/LP metamorphism and the emplacement of the lower Carboniferous-Permian batholith with its effusive counterpart which, along with molassic sediments, represents the infilling of extensional intracratonic basins (Cortesogno et al. 1998; Buzzi et al. 2008).

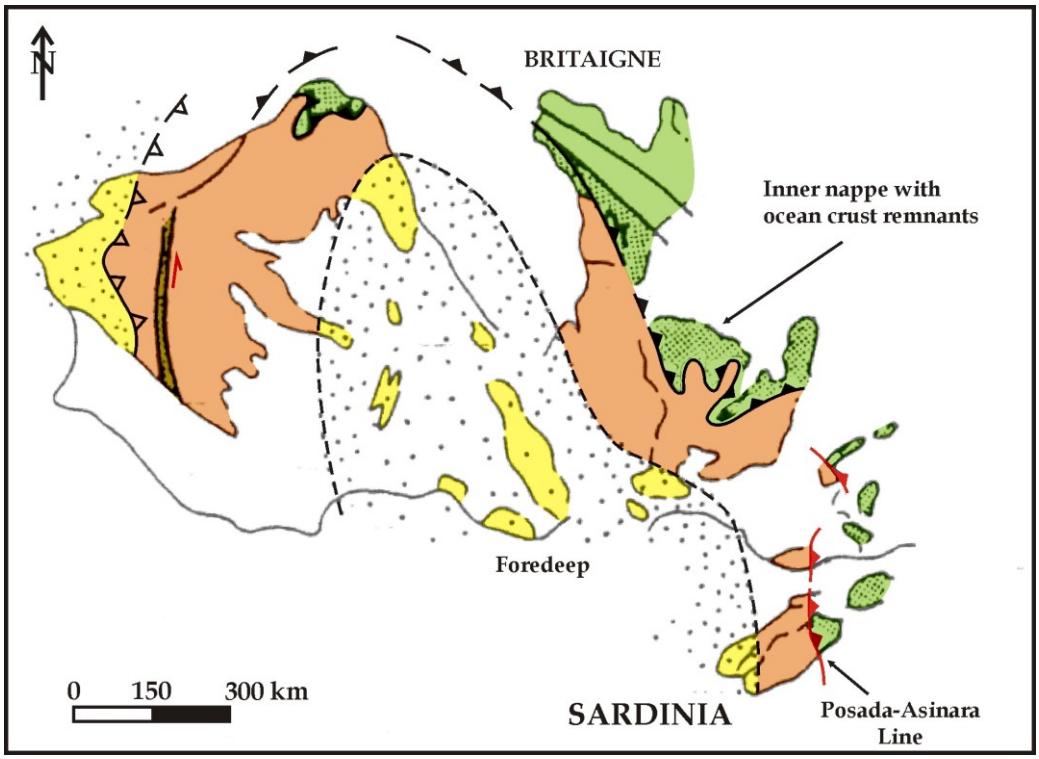

Fig. 1.3 – Reconstruction of the hercynian chain and the southern European margin at upper Carboniferous. After Carmignani et al. (2001), modified.

1.2 The Mesozoic covers and the southern Europe passive margin

Starting from middle Permian-lower Triassic, the Sardinia-Corsica Block was part of the stable Europe. During Jurassic time it was close to the passive margin of the intervening Ligure-Piemontese Ocean and, due the tropical climate, experienced notable carbonate shelf sedimentation from the middle Triassic up to the end of Cretaceous.

Iron concentration in such geodynamic setting is mainly linked to eventual emergence periods. In central Sardinia a long stratigraphic gap is recorded between Triassic and middle Jurassic (Bajocian), during which ,along a planar surface, huge concentrations of Fe oxy-hydroxide deposits formed.

A new emergence, linked to the so called "Bedoulian Movements" (Combes et al. 1993; Mameli et al. 2007) invested the western Sardinia shelf during middle Cretaceous leading to karstic bauxite deposits

A period of new tectonic instability was experienced by the Sardinia Block starting from the Oligocene up to the Burdigalian. This is documented by the general uplift of the Sardinia basement, by widespread syntectonic continental clasts and by a strike-slip dynamic. Latter generated both to transpressive (flower structures) and transtensive (pull-apart basins) crustal scale structures (Carmignani et al. 1994). This tectonic instability is also documented by orogenic, mainly calcalkaline, volcanic activity which lasted up to the Middle Miocene.

1.3 The Cenozoic successions and the Mediterranean geodynamic

During Cenozoic, Sardinia was involved, even if marginally, in some orogenic events. Due its position, between the Pyrenean orogen and the North Apennine, this sector of European crust recorded both compressive and extensional events referable to the geodynamics of the Western Mediterranean realm. Two main hypotheses concern the role played by Sardinia-Corsica Block. In the first classical hypothesis, the Sardinia-Corsica acted as foreland of the Alpine chain and then as hinterland of North Apennine. This implies the followings:

1) the nappe building of NE Corsica is a segment of the alpine chain with Europe-directed vergence. Starting from Oligocene the flip of subduction

beneath the southern margin of European plate was supposed (Boccaletti and Guazzone 1974).

2) Sardinia-Corsica crust evolves as an Andean-type arc, which migrates ocean-ward leading to the opening of the Balearic back-arc basin.

The rotation of the Sardinia-Corsica block ended because of its collision with Adria that was supposed to last until Tortonian (Giglia 1973).

Starting from the late 80's, a new hypothesis regarding Sardinia-Corsica crust as the mere hinterland of Northern Apennine arrived, so excluding an Oligocene subduction flip (Principi and Treves 1984; Carmignani et al. 1995; Lahondere et al. 1999; Oggiano et al. 2009). This hypothesis required:

- the nappe building of Northern Corsica is the consequence of the accretionary wedge deformation, which generated at the active margin of south Europe. This margin experienced subduction since mid-Cretaceous, and so, flip is required to explain the eastern vergence of North Apennine.
- collision between Adria and Europe plates started in Oligocene generating a chain with both Europe and Adria-verging tectonic units (Principi and Treves 1984; Carmignani et al. 1995; Fig. 1.4). The European hinterland was affected by strike-slip tectonics.

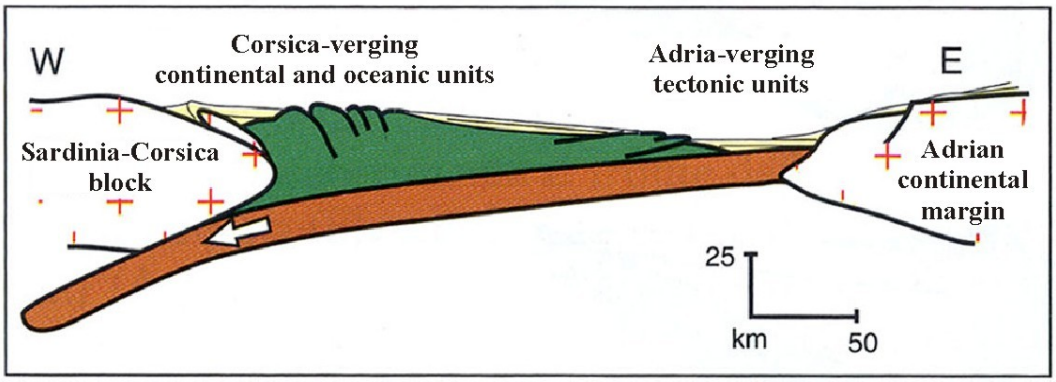

Fig. 1.4 – Scheme of Adria plate subduction and consequent formation of Europe- and Adria-verging tectonic units. After Carmignani et al. (2001), modified.

According to this hypothesis, strike-slip faults at late Oligocene generated the Aquitanian strike-slip basins that strike ENE in northern Sardinia and NW in southern Sardinia. This evidence rules out the case of Oligocene-Aquitanian E-W extension (in present day coordinates) that led to a N-S trending "Sardinian Rift". East-west extension in Sardinia started from mid-upper Burdigalian and pursued until Pliocene.

During Upper Burdigalian, the extension led to the onset of roughly N-S trending shallow basins, which experienced transgression and carbonate sedimentation from late Burdigalian up to Messinian (Funedda et al. 2003).

Regardless to above mentioned geodynamic framework, the thick volcanic and volcano-sedimentary sequences, ranging in composition from basalt to rhyolite, are related to the subduction of insubric oceanic crust beneath the south European plate palaeomargin (Coulon and Dupuy 1975; Downes et al. 2001). During Burdigalian time, back arc spreading and rotation of the Sardinia-Corsica block followed this geodynamic context (Boccaletti and Guazzone 1972).

According to Beccaluva et al. (1987) most of the volcanic activity is concentrated between 21 and 17 Ma, time during which the drift of Sardinia (Vigliotti and Langenheim 1995) and the related opening of the Balearic back arc basin (Malinverno and Ryan 1986, Fig. 1.5) occurred. The eastward slab rollback (Beccaluva et al. 1994) followed by collision and slab breakoff' generated an asthenospheric window (Royden 1988; Serri et al. 1993), resulting in anomalous heat flow below the western part of the Corsica–Sardinia microplate, which is still apparent today (Carmignani et al. 1995; Della Vedova et al. 1995).

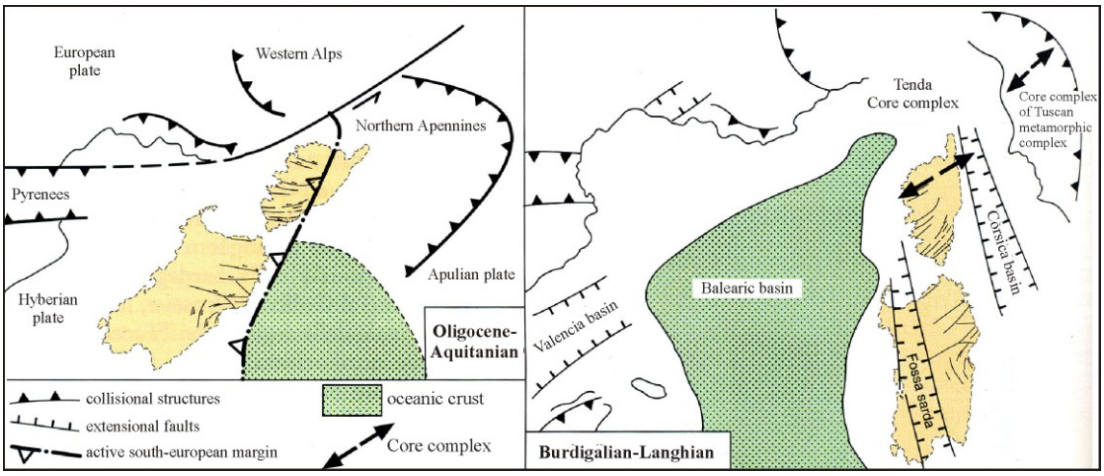

Fig. – Scheme of Sardinia-Corsica block rotation and its position in Mediterranean area at Oligocene-Aquitanian (a) and Burdigalian-Langhian (b). After Carmignani et al. (2001), modified.

Similar geodynamic context favoured the occurrence of hydrothermal deposits (de Boorder et al. 1998; Sillitoe 1997). In NW Sardinia the Oligocene porphyry copper of Calabona, near Alghero village, represents the early hydrothermal activity; it is followed by high hydrothermal, gold rich, vein deposits as well as by barren hydrothermal deposits of kaolin (Palomba et al. 2006).

This hydrothermal activity also generated Mn mineralization of some importance. Other Mn sedimentary deposits instead are linked to the Burdigalian transgression within the Late Burdigalian half-graben.

REFERENCES

BECCALUVA L., BROTZU P., MACCIOTTA G., MORBIDELLI L., SERRI G. & TRAVERSA G. (1987) – *Caenozoic tectono-magmatic evolution and inferred mantle sources in the sardo-tyrrhenian area*. In: Borani A., Bonafede M., Piccardo G.B. & Vai G.B. (Eds), The lithosphere in Italy – Advances in earth science research. Accademia Nazionale dei Lincei, 229-248.

BECCALUVA L., COLTORTI M., GALASSI B., MACCIOTTA G. & SIENA F. (1994) – *The Cenozoic Calcalkaline Magmatism of the Western Mediterranean and its Geodynamic Significance*. Boll. Geof. Teor. Appl., 36, 293-308.

BOCCALETTI M. & GUAZZONE G. (1972) – *Gli archi appenninici, il Mar Ligure e il Tirreno nel quadro della tettonica dei bacini marginali retro-arco*. Mem. Soc. Geol. It., 11, 201-216.

BOCCALETTI M. & GUAZZONE G. (1974) – *Il microcontinente sardo-corso come un arco residuo di un sistema arco-fossa miocenico*. In: Maxia C. & Cerchi A. (Eds), Paleogeografia del Terziario Sardo nell'ambito del Mediterraneo Occidentale. Rendiconti del Seminario delle Facoltà di Scienze dell'Università di Cagliari, 43, 57-68.

BUZZI L., GAGGERO L. & OGGIANO G. (2009) – *Lower Permian age of the Santa Giusta Ignimbrite (NW Sardinia): insights on the post-collisional evolution of a sector of European crust between the Lower Permian and Early Triassic*. In G. Cassinis (Guest Ed.), Special Section: Stratigraphy and palaeogeography of late- and post-Hercynian basins in the Southern Alps, Tuscany and Sardinia (Italy). Boll. Soc. Geol. It. (Italian Journal of Geosciences), 127 (3), 683-695.

CARMIGNANI L., BARCA S., DISPERATI L., FANTOZZI P., FUNEDDA A., OGGIANO G. & PASCI S. (1994) – *Tertiary compression and extension in the Sardinia basement*. Boll. Geof. Teor. Appl., 36, 45-62.

CARMIGNANI L., DECANDIA F.A., DISPERATI L., FANTOZZI P.L., LAZZAROTTO A., LIOTTA D. & OGGIANO G. (1995) – *Relationschip between the Tertiary structural evolution of the Sardinia-Corsica-Provençal Domain and the Northern Apennines*. Terra Nova, 7, 128-137.

CARMIGNANI L. & OGGIANO G. (1997) - *Terranes in the variscan segment of Sardinia: a tentative approach*. Annales geologiques des pays helleniques (Special issue on IGCP PROJECT N°276 "Terrane mappes and terrane description"), 37, 199-209.

CARMIGNANI L., OGGIANO G., BARCA S., CONTI P., SALVADORI I., ELTRUDIS A., FUNEDDA A. & PASCI S. (2001) – *Geologia della Sardegna. Note illustrative della Carta Geologica della Sardegna a scala 1:200000*. In: Memorie descrittive della Carta Geologica d'Italia, volume LX, 271 pp.

CAROSI R., FRASSI C., MONTOMOLI C. & PERTUSATI P.C. (2004) - *Le pieghe della zona di Pescaglia Alpi Apuane meridionali): un esempio di interferenza chilometrica di pieghe tardive nella falda toscana*. Atti Soc. tosc. Sci. nat., Mem., Serie A, 109, 77-83.

CAPPELLI B., CARMIGNANI L., CASTORINA F., DI PISA A., OGGIANO G. & PETRINI R. (1992) – *A Hercynian suture zone in Sardinia: geological and geochemical evidence*. Geodinamica Acta, 5, 101-118.

COMBES P.J., OGGIANO G. & TEMUSSI I. (1993) – *Geodynamique des bauxites sardes, typologie, genese et controle paleotectonique*. Comptes Rendus de l'Académie des Sciences Série II, 316, 403-409.

CORTESOGNO L., CASSINIS G., DALLAGIOVANNA G., GAGGERO L., OGGIANO G., RONCHI A., SENO S & VANOSSI M. (1998) – *The Post-Variscan volcanism in late Carboniferous-Permian sequences of Ligurian Alps, Southern Alps and Sardinia*. Lithos, 45, 305.

COULON C. & DUPUYT C. (1975) - *Evolution spatiale des caractéres chimiques du volcanisme andésitique de la Sardeigne (Italie)*. Earth Planetary Science Letters, 25, 170-176.

DE BOORDER H., SPAKMAN W., WHITE S.H. & WORTEL M.J.R. (1998) – *Late Cenozoic mineralization, orogenic collapse and s detachment in the European Alpine Belt*. Earth and Planetary Science Letters, 164, 569-575.

Della Vedova B., Lucazeau F., Pasquale V., Pellis G., Verdoja M. (1995) – *Heat flow in the tectonic provinces crossed by the southern segment of the European Geotraverse*. Tectonophysics, 244, 57-74.

DOWNES H., THIRLWALL M.F. & TRAYHORN S.C. (2001) – *Miocene subduction-related magmatism in southern Sardinia: Sr–Nd- and oxygen isotopic evidence for mantle source enrichment*. Journal of Volcanology and Geothermal Research, 106 (1-2), 1-22.

FRANCESCHELLI M., PUXEDDU M., CRUCIANI G. & UTZERI D. (2007) – *Metabasites with eclogite facies relics from Variscides in Sardinia, Italy: a review*. Int J Earth Sci (Geol Rundsch), 96, 795-815.

GHEZZO C., MEMMI I. & RICCI C.A. (1979) – *Un evento granulitico nella Sardegna nord-orientale*. Mem. Soc. Geol. It., 20, 23-38.

DI PISA A., OGGIANO G. & TALARICO F. (1993) – *Post-collisional tectono-metamorphic evolution in the axial zone of the hercynian belt in Sardinia: the exemple from the Asinara Island*. Docum. B.R.G.M.,France, 219, 216-217.

CORTESOGNO L., GAGGERO L., OGGIANO G., PAQUETTE J.L. (2004) – *Different tectono-thermal evolutionary paths in eclogitic rocks from the axial zone of the Variscan chain in Sardinia (Italy) compared with the Ligurian Alps*. Ofioliti, 29, 125-144.

FUNEDDA A., OGGIANO G. & PASCUCCI V. (2003) – *I depositi miocenici della Sardegna settentrionale: il bacino del Logudoro*. Atti del Convegno GeoSed, 381-399.

GIGLIA G. (1973) – *L'insieme Corsica-Sardegna e i suoi rapporti con l'Appennino settentrionale: rassegna dei dati cronologici e strutturali*. In: Paleogeografia del Terziario Sardo nell'ambito del mediterraneo occidentale. Rend. Seminario Fac. Sc. Univ. Cagliari, suppl. 43, 245-275.

LAHONDERE D., ROSSI P. & LAHONDERE J.C. (1999) – *Structuration alpine d'une marge continentale externe: le massif du Tenda (Haute-Corse). Implications géodynamiques au neveau de la transversale Corse-Apennins*. Geologie de la France, 4, 27-44.

MALINVERNO A. & RYAN W.B.F. (1986) – *Extension in the Tyrrhenian Sea and shortening in the Apennines as a result of arc migration driven by sinking of the lithosphere*. Tectonics, 5, 227-245.

MAMELI P., MONGELLI G., OGGIANO G. & DINELLI E. (2007) – *Geological, geochemical and mineralogical features of some bauxite deposits from Nurra (Western Sardinia, Italy): insights on conditions of formation and parental affinity*. Int. Jour. Earth Sci. (Geol. Rundsch), 96, 887-902.

OGGIANO G. & DI PISA A. (1992) – *Geologia della catena ercinica in Sardegna-Zona assiale*. In: Carmignani L., Pertusati P.C., Barca S., Carosi R., Di Pisa A., Gattiglio M., Musumeci G. & Oggiano G. (Eds), Struttura della catena ercinica in Sardegna. Guida all'escursione. Gruppo informale di Geologia strutturale, 147-167.

OGGIANO G., GAGGERO L., FUNEDDA A., BUZZI L. & TIEPOLO M. (2010) – *Multiple early Paleozoic volcanic events at the northern Gondwana margin: U-Pb age evidence from the Southern Variscan branch (Sardinia, Italy)*. Gondwana Research, 17, 44-58.

PALOMBA M., PADALINO G. & MARCHI M. (2006) – *Industrial mineral occurrences associated with Cenozoic volcanic rocks of Sardinia (Italy): Geological, mineralogical, geochemical features and genetic implications*. Ore Geology Reviews, 29, 118-145.

PRINCIPI G. & TREVES B. (1984) – *Il sistema corso-appenninico come prisma d'accrezione. Riflessi sul problema generale del limite Alpi-Appennini*. Mem. Soc. Geol. It., 28, 549-576.

ROSSI P., OGGIANO G. & COCHERIE A. (2009) – *A restored section of the "southern Variscan realm" across the Corsica-Sardinia microcontinent*. C. R. Geoscience, 341, 224-238.

ROYDEN L. (1988) – *Flexural behavior of the continental in Italy: constraints imposed by gravity and deflection data*. J. Geophys. Res., 93, 7747-7766.

SERRI G., INNOCENTI F. & MANETTI P. (1993) – *Geochemical and petrological evidence of the subduction of delaminated adriatic continental lithosphere in the genesis of the*

neogene quaternary magmatism of central Italy. Tectonophysics, 223 (1-2), 117-147.

Sillitoe R.H. (1997) – *Characteristics and controls of the largest porphyry copper–gold and epithermal gold deposits in the circum-Pacific region*. Australian Journal of Earth Sciences, 44, 373-388

VIGLIOTTI L. & LANGENHEIM V.E. (1995) – *When did Sardinia stop rotating? New paleomagnetic results*. Terra Nova, 7, 424-435.

PART II

THE FE MOBILITY AND THE IRONSTONES OF SARDINIA

Deposition of chemical sediments, and ironstones in particular, is a still debated geochemical phenomenon (Marshall and Fairbridge 1999). Beside the economic aspect, the iron-rich sediments can act as effective proxies in palaeoenvironmental reconstructions because climate and redox conditions are basic factors that determine whether iron will concentrate in sediments. Nevertheless high iron concentration by itself is not adequate to unravel, even roughly, climatic and geochemical backgrounds within a definite sedimentary palaeoenvironment.

2.1 The Fe geochemical behavior in supergenic environment

Among the different factors that control concentration and deposition of iron, Eh, pH and the iron availability are the most significant both in rocks and waters. The sources of dissolved iron can be different and are linked to the weathering of different rock types (Alibert and McCulloch 1993) or to hydrothermal vents along oceanic rift and/or at the hot spots sites (Holland 1973; Dymek and Klein 1988).

Mobility of iron can be described in term of Eh-pH diagrams (Brookins 1988). Taking in account that iron can exist both as Fe^{2+} and Fe^{3+} and that the ionic potential is considerably higher for the 3+ one (state), an unquestionably lower mobility for the oxidized form which tends to precipitate as Fe oxy-hydroxides must be expected.

The Eh-pH diagram for the Fe-O-H system (Fig. 2.1) shows as water-soluble Fe^{3+} only occurs at very low pH and oxidizing conditions not common in natural environments. Insoluble $Fe(OH)_3$ exhibits a stability field wider of that occupied by Fe^{2+} in water solutions. Ferrous ion easily undergoes oxidation during the commonest water-rock interaction processes. Therefore, the Fe^{3+} transport in water solution cannot occur in presence of free oxygen; conversely, in anoxic or low Eh condition, Fe^{2+} shows a sharp affinity for the solution. Hence the Fe^{2+} stability field in water solutions wide toward low values of Eh.

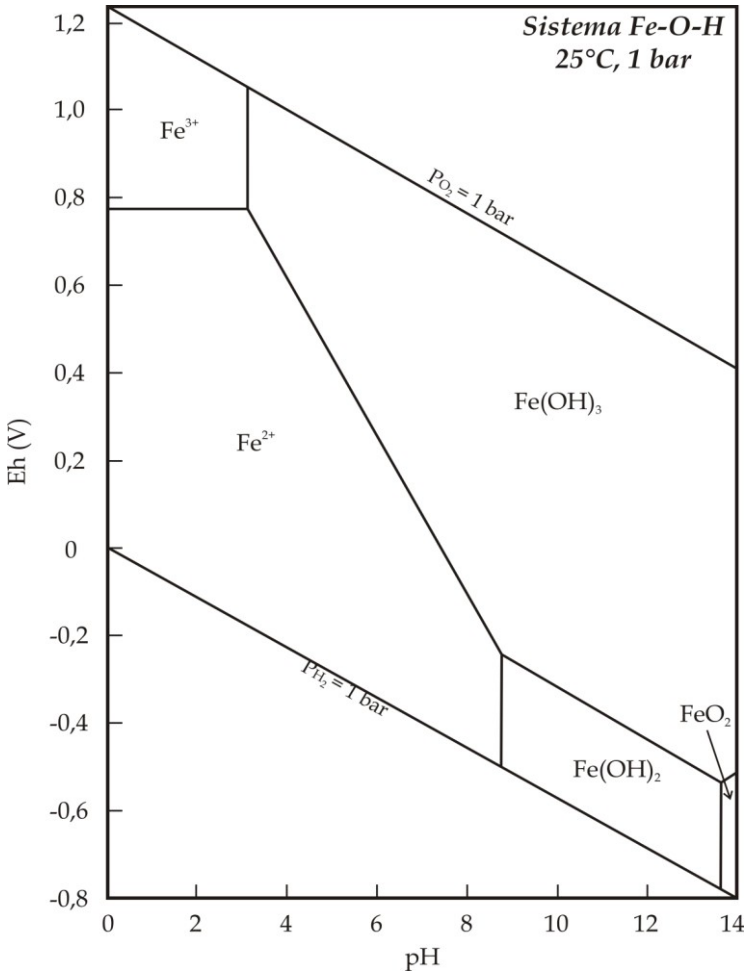

Fig. 2.1 – Eh-pH diagram for Fe-O-H system describing Fe mobility in water solution at condition standard of 25°C and 1 bar. The Fe activity is 10^{-6}. After Brookins (1988), modificato.

Nevertheless Fe^{2+} precipitation can occur as $Fe(OH)_2$ from waters characterized by high pH values (above 8.5) and reducing condition (below -0.2 Eh).

Besides pH and Eh, the P_{CO2} is critical factor responsible for the compound (carbonate, oxide, silicate or others) able to fix Fe^{2+} depending on the solution composition.

2.2 Location of studied areas and their geological settings

Within the low metamorphic grade basement of Sardinia two main concentrations of sedimentary iron occur. Their supergene nature make them of particular interest, not only as exploitable ore but also as palaeoclimatic proxies

in the reconstruction of Sardinia palaeoclimate through Paleozoic and Mesozoic time.

The outcrops are located in North-western and in central-eastern Sardinia. The older is located in the Nurra district, hosted within the inner nappe zone of the Variscan orogenic building; the more recent is hosted within a huge phyllite-made tectonic unit (the Postgotlandiano auctorum) pertaining to the external nappe zone, in the "Tacchi" district (Fig. 2.2).

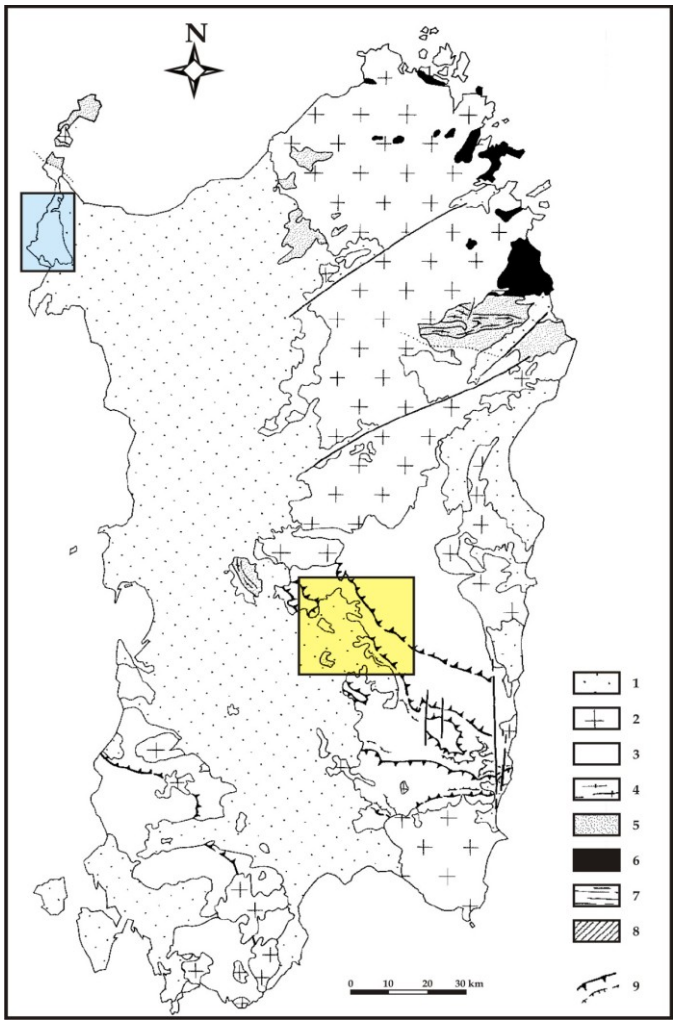

Fig. 2.2 – Tectonic sketch map of Sardinian basement. The studied areas are highlighted. The blue box represents the Nurra district; the yellow is the "Tacchi" district.
Legend: 1) post-variscan volcanics and sediments; 2) granites; 3) greenschist facies phyllites; 4) ortogneiss; 5) amphibolitic facies methamorphites; 6) amphibolitic facies migmatites; 7) covers; 8) pre-variscan basement; 9) Major and minor thrust.
After Carmignani et al. (1982) modified.

The tectonic units of the nappe zone (from Cambrian to lower Carboniferous) embrace a kilometer-thick terrigenous, volcanic and, to a lesser extent, carbonate Palaeozoic succession that experienced very low to low-grade metamorphism (Carmignani et al. 1994). Some differences exist between the

successions of the external (Sarrabus, Arburese, Gerrei, Salto di Quirra, Sarcidano and Barbagia areas) and of the inner (southern Nurra, Goceano and Gennargentu Mountain) nappe zone: the former retains huge amounts of mostly acidic, calcalkaline Ordovician volcanic products and Devonian shelf limestone; the latter is devoid of calcalkaline felsic volcanics and limestone and, in turn, it is enriched in mafic alkaline magmatic products of uppermost Ordovician age.

2.2.1 The iron deposits of Nurra district

The ironstones of Nurra district outcrop within the Canaglia tectonic unit (Oggiano and Mameli 2006). This unit is exposed along an overturned limb of a SW verging kilometer-scale anticline. It exhibits green schist facies metamorphic assemblage and it is characterized by the following succession (Fig. 2.4):

- metasandstones and phyllites (Cambrian-Ordovician);
- metarhyolites (~486 Ma U-Pb on zircon – Oggiano et al. 2010);
- metagreywackes and alkaline metabasalts (Upper Ordovician);
- metamorphic diamictite-bearing ooliths and nodules of chamosite, siliciclasts and clasts of apatite (soft ironstone, Fig. 2.3), with intercalated sequences of hardened (hard ironstone) unfoliated magnetite, chamosite and siderite (Hirnantian?);
- black metapelites with varve-like millimetre laminations (post-glacial Hirnantian?);
- black phyllite (Silurian).

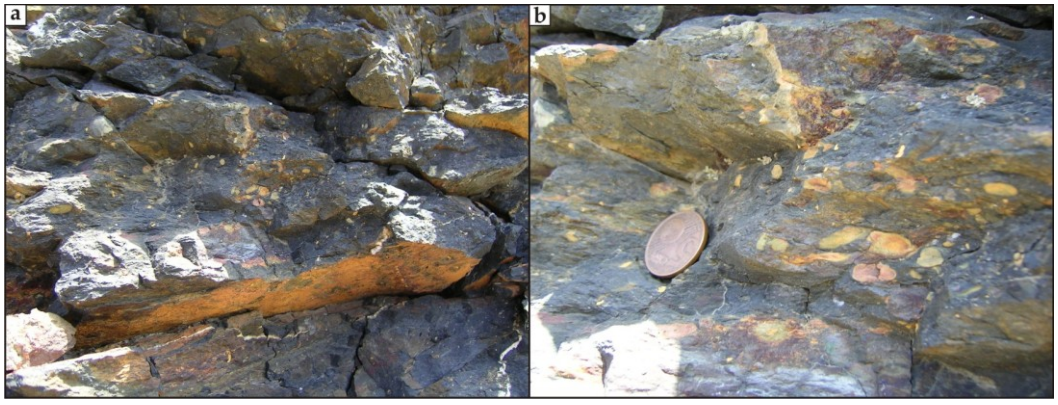

Fig. 2.3 – Soft ironstone deposit characterized by diamictic texture with oolith and nodules mainly of chamositic composition.

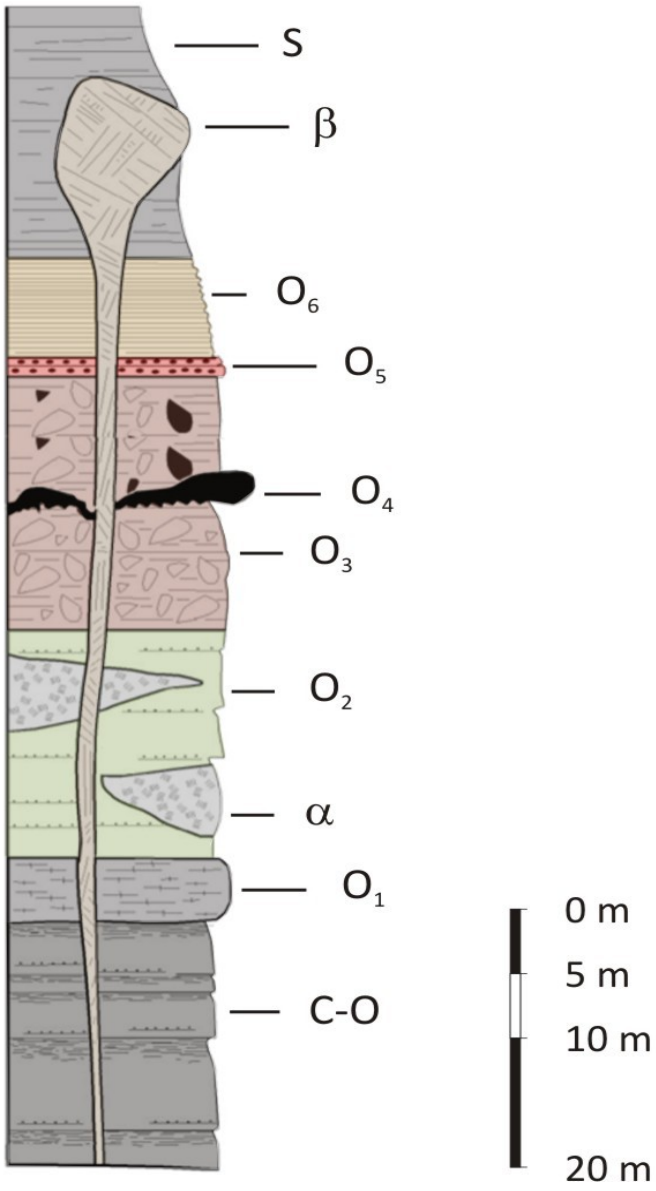

Fig. 2.4 – Schematic stratigraphic log of the oolitic ironstones.
Legend:
C-O, Metasandstones and phyllites (Cambrian-Ordovician);
O1, Metaryolites (lowermost Ordovician);
O2, Chlorite-rich metagreywackes (Upper Ordovician);
O3, metamorphic diamictite with intercalated
O4, hard ironstone and conglomerate;
O5, Thin bedded oolitic mudstone;
O6, Finely laminated metargillite;
S, Black phillytes (Silurian);
α, Alkaline metabasalts;
β, Alkaline metagabbroes and metadolerites.
After Oggiano and Mameli 2006.

The above-illustrated succession was deposited on the northern margin of Gondwana land from Cambrian to Devonian. The uppermost Ordovician sediments (diamictites), associated with the ironstones, are interpreted as sub-glacial deposits linked to Hirnantian glaciation (Oggiano and Mameli 2006) that was contemporary to a rifting stage as well as to alkaline mafic volcanism. In addition to the Sardinian example, evidence of chamosite-rich oolitic ironstones, or chamosite deposits, tied to an Upper Ordovician global cooling event are widespread (Becq-Giroudon et al. 1992; Yapp 1993).

2.2.2 The iron deposits of "Tacchi" district

The second type of iron deposit is invariably hosted within greenschist facies phyllites (Fig. 2.5) and quartzites belonging to the Postgotlandiano auctorum, a unit which corresponds to the Fiorentini Unit (Oggiano 1994).

Fig. 2.5 – Rubrified phyllites of Postgotlandiano auct. outcropping at Mt. Tonneri area.

Although the iron deposit formed on Palaeozoic metamorphic rocks, its age is post-Variscan. It consists of concretions produced under conditions of free subsurface drainage by the deposition of secondary iron oxide during or after the planation of the Variscan belt (Fig. 2.6).

Fig. 2.6 – Iron concretions deposited along a planation surface during pedogenic alteration processes. Jerzu area.

Transgressive Jurassic sediments cap the deposit; they consist of (Fig. 2.7):

- quartz conglomerate followed by fine sands to silty swamp deposits with marcasite nodules and cm-scale lignite seams of the Genna Solele Formation (Amadesi et al. 1961), which in the investigated area does not exceed about ten meters thickness (Bajocian);
- dolostones and dolomitic limestone of the Dorgali Formation (Dieni and Massari 1966) several tens of metres thick (Bathonian-Callovian).

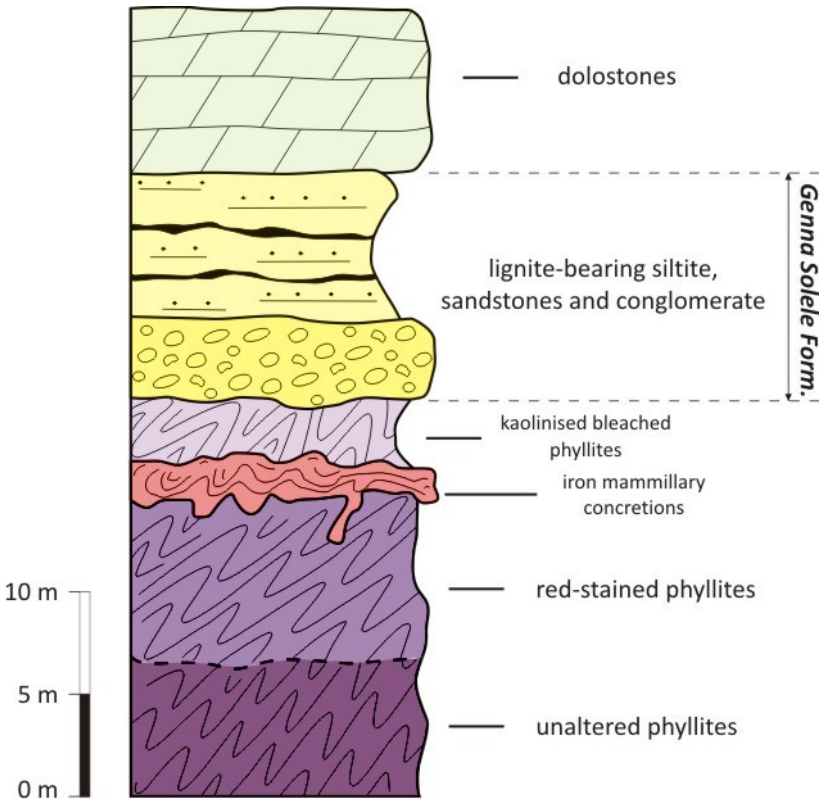

Fig. 2.7 – Schematic stratigraphic log of the "Tacchi" ironstones.

Iron oxy-hydroxides impregnate the phyllites as mammillary concretions (Fig. 2.8) along a horizon 1-3 m thick, which lies below a 1-2 m thick horizon of bleached and partially kaolinised phyllite. These deposits, if referred to Bajocian, could be due to humid sub-tropical climate with short term climate change of rainy and dry conditions (Raucsik and Varga 2008).

Fig. 2.8 – Mammillary concretions of iron oxy-hydroxides.

2.3 Sampling

The two chosen iron deposits can represent paradigmatic examples of iron accumulation under contrasting climatic and environmental conditions: marine cold environment in the first case and tropical continental in the second one. In order to have an exhaustive pictures of iron behavior in supergene conditions, in relation with other major, minor and trace elements, the sampling was carried out according to the stratigraphy and the macroscopic features of deposits. The marine Ordovician oolitic ironstones were sampled according to the textural and compositional differences.

The chlorite-rich type, also characterized by marked diamictic texture, was named soft ironstone (SI subset) while the magnetite- and siderite-rich type was named hard ironstone (HI subset) due to its massive uncleaved aspect.

The Jurassic continental ironstone was sampled according to a stratigraphyc criterion in the different localities. The first, between Jerzu and Perdasdefogu (JP subset), is characterized by prevalent mammillary texture; the other, at Monte Tonneri area (MT subset), presents a prevalent spongy texture.

2.4 Results

Thirty-eight samples of both Nurra and Tacchi ironstones were analyzed. A petrographic and mineralogical study of the samples was performed using transmitted polarized light microscopy (OM), scanning electron microscopy (SEM) using an ESEM XL30 Philips LaB6 equipped with an energy dispersive X-ray spectrometer (EDS) for microchemical determinations, and X-ray diffraction (XRD), using a Siemens D5000 diffractometer (CuKα radiation). Elemental analyses for major, V, Cr, Ni, Rb, Sr, and Ba concentrations were obtained on pressed powder disks of bulk rocks by X-ray fluorescence methods described in Franzini et al. (1975), Franzini et al. (1972) and Leoni and Saitta (1976). Loss on ignition (L.O.I.) was determined after heating the sample for three hours at 900 °C. Other trace elements, including REE, were determined by instrumental neutron activation analysis (INAA) at the Activation Laboratories, Ancaster, Canada. The precision of the trace element analyses, except Yb and Lu, is better than 5%. Yb and Lu show precision better than 8%.
The methods and operating conditions are described in detail in Appendix 2.

2.4.1 Textures and Mineralogy

The textural observations by OM and SEM-EDS on the oolitic ironstones revealed two different textural arrangements:
the subset SI, derived from the soft ironstone, shows a diamictic texture with a prevalent muddy matrix made up of chamosite, which supports siliciclasts derived from an old (Cadomian?) basement, several coated grains and non-coated grains of chamosite, clastic phosphorite and microgranular apatite involved in grano-lepidoblastic texture with chamosite (Fig. 2.9a and b).

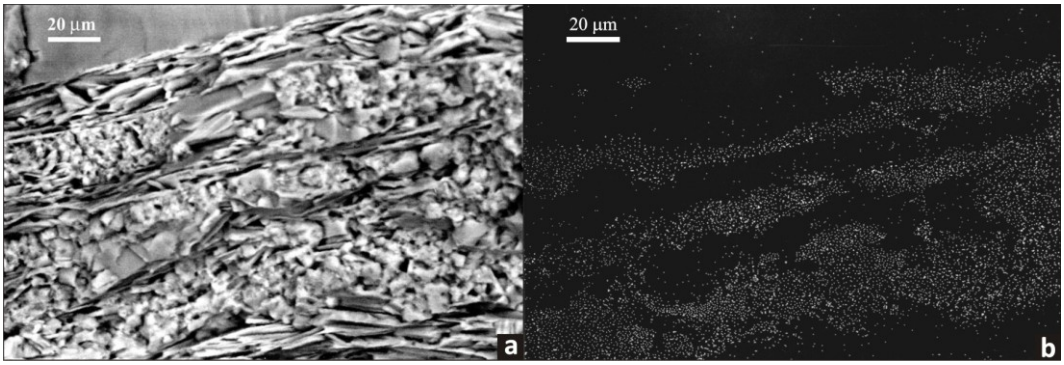

Fig. 2.9 – (a) BSE image of microgranular domains of apatite alternating lepidoblastic domains of chamosite. Groundmass of the massive diamictic metapelite. Villaggio Nurra. (b) P map of (a) (after Oggiano and Mameli, 2006).

Ooliths composed of shells of chamosite, which alternate with shells of iron oxy-hydroxides and apatite, were also seen (Fig. 2.10). The accessories phases, based on textural evidence, are authigenic monazite, ilmenite and detrital zircon;

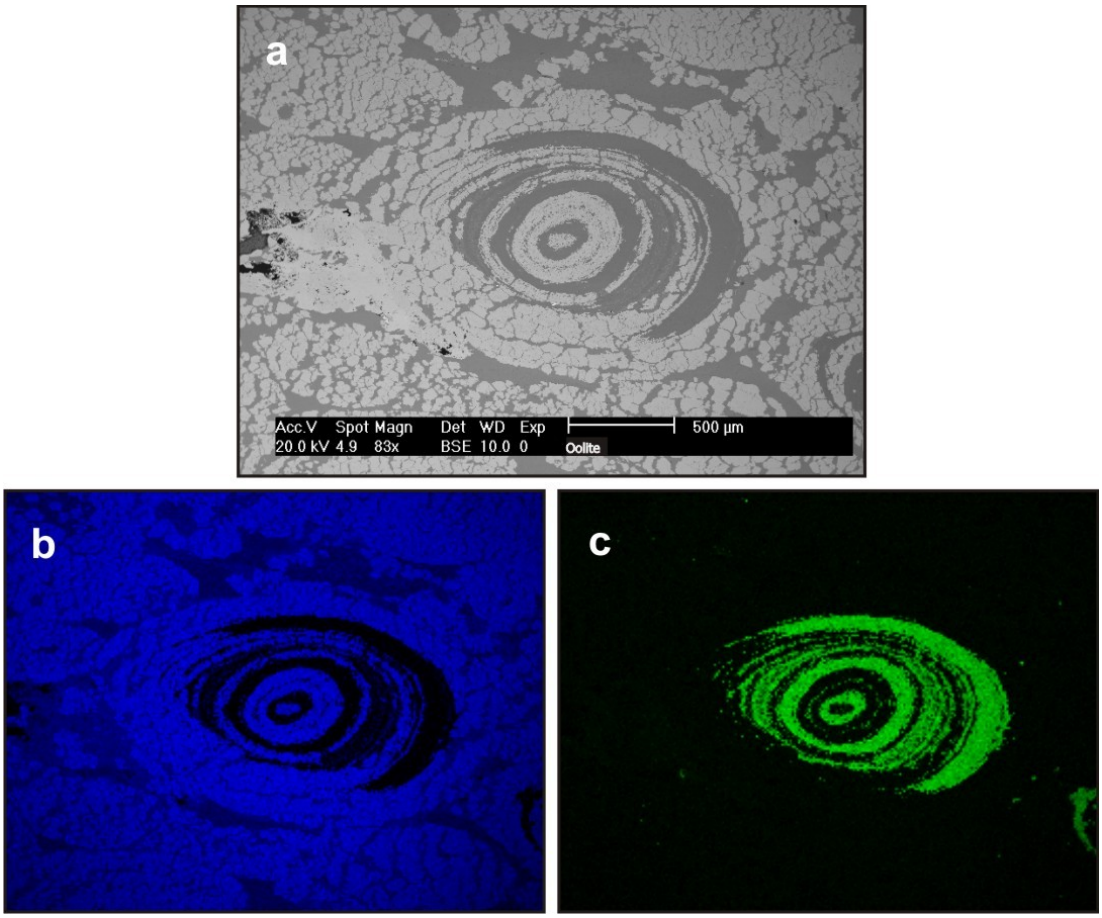

Fig. 2.10 – BSE image of an oolith (a) in which Fe-rich shells (Fe distribution map in b) alternate with P-rich shells (P distribution map in c)

Rosa SINISI – Iron and manganese accumulations in Sardinia: the role of supergenic and hydrothermal processes. PhD Thesis in Natural Sciences. Università degli Studi di Sassari

the subset HI, derived from the hard ironstone, contains magnetite and chamosite ooliths supported by secondary siderite. Some ooliths exhibit a chamosite core rimmed by magnetite shells (Fig. 2.11); in some samples siderite shells alternate with magnetite, suggesting that both phases are pseudomorphic after the original chamosite. In some cobbles of a conglomerate coming from a ruined adit at La Colti mine, EDS maps revealed that chamosite ooids are enclosed within thin phosphatic layers, suggesting that phosphorite precipitated after the nucleation of chamosite.

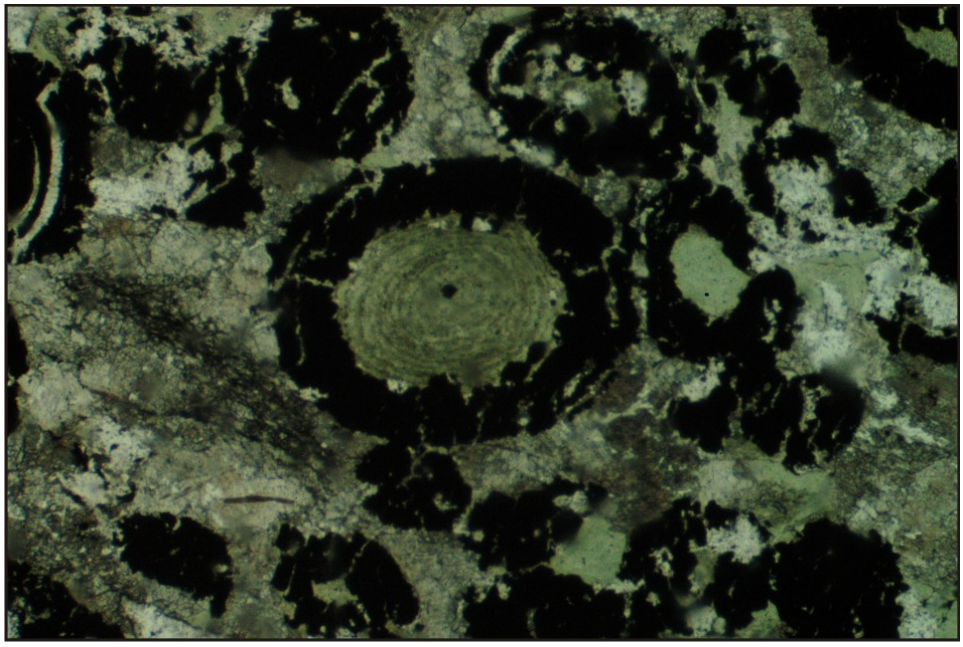

Fig. 2.11 – Photomicrograph showing ooliths with chamosite cores rimmed by magnetite

The overgrowth of phosphorite over the chamosite ooids prevented them from oxidizing during the near-surface reworking and also from being deformed, during syn-metamorphic deformation (Fig. 2.12).

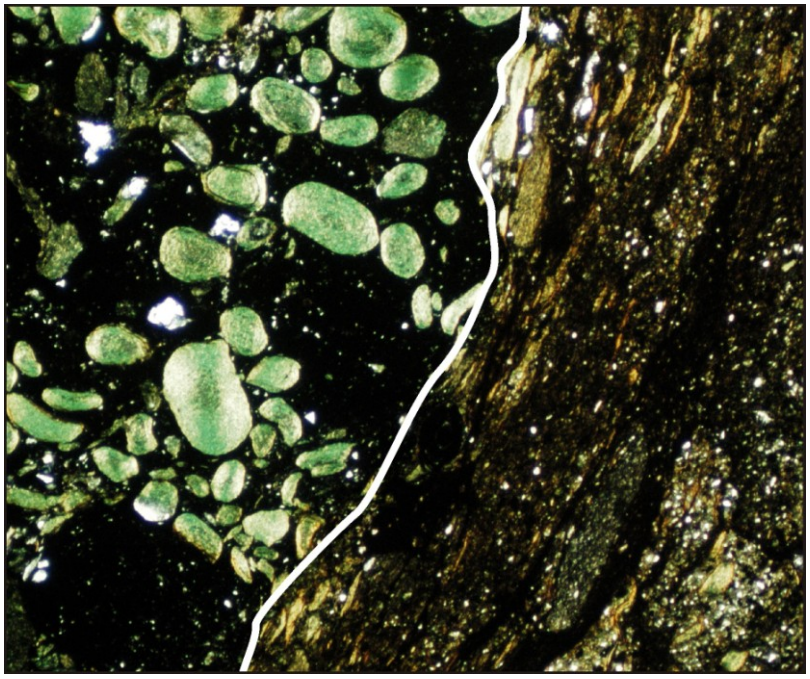

Fig. 2.12 – Chamosite ooliths enclosed in a phosphorite level. The white line is the upper boundary of this level, beyond which the ooliths are flattened and oxidized.

Authigenic monazite and detrital zircon occur as sedimentary phases, whereas stilpnomelane and chloritoid are metamorphic phases. The main phases of the two subsets are shown in Fig. 2.13 and 2.14.

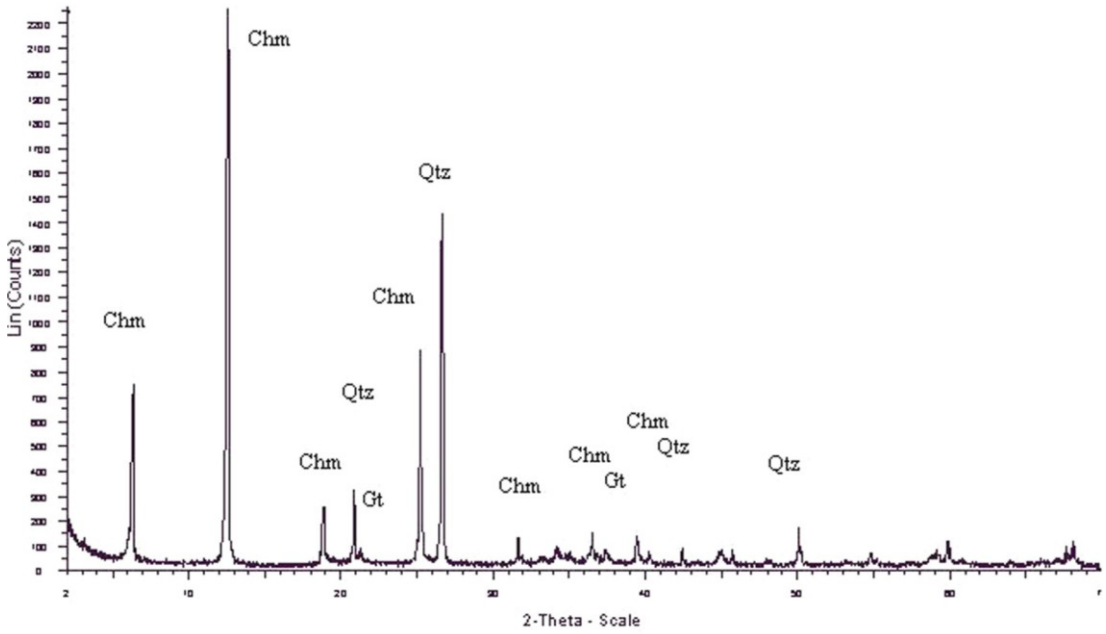

Fig. 2.13 – XRD pattern of the representative sample of the SI subset. Legend: Chm = chamosite; Gt = goethite; Qtz = quartz.

Rosa SINISI – Iron and manganese accumulations in Sardinia: the role of supergenic and hydrothermal processes. PhD Thesis in Natural Sciences. Università degli Studi di Sassari

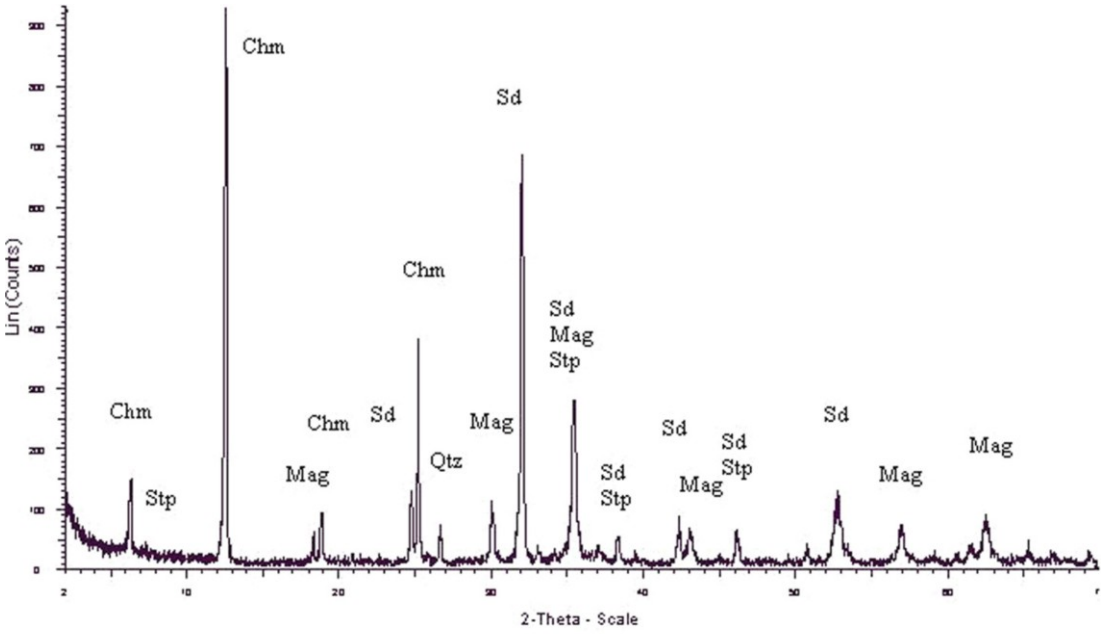

Fig. 2.14 – XRD pattern of the representative sample of the HI subset. Legend: Chm = chamosite; Mag = magnetite; Qtz = quartz; Sd = siderite; Stp = stilpnomelane.

The samples coming from the "Tacchi" ironstones were investigated only on polished surfaces by SEM-EDS due to the prevalence of opaque phases. The dominant mineralogy consists of massive goethite, which overgrows relic phyllites represented by survived muscovite lamellae (Fig. 2.15). The orientation of the muscovite is continuous with the foliation external to the goethite concretions.

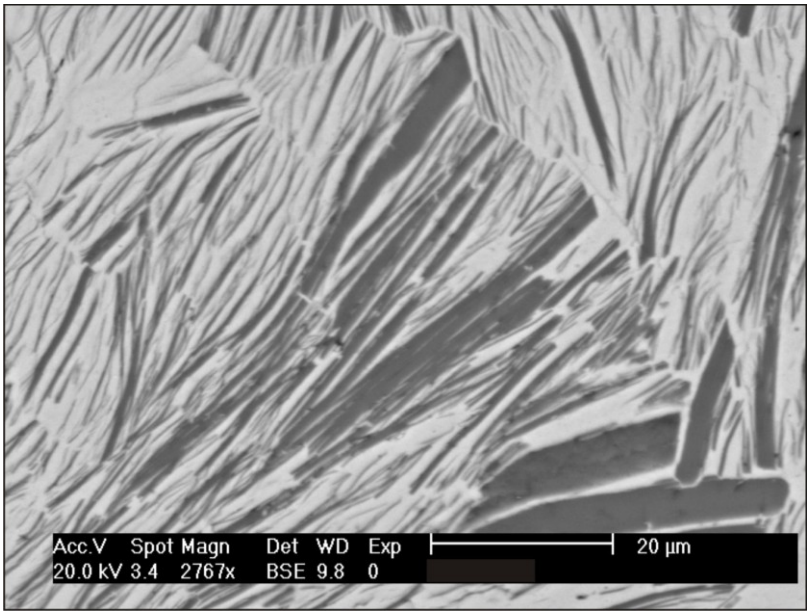

Fig. 2.15 – BSE image of muscovite lamellae (dark stripes) embedded in goethite.

The macroscopic mammillary features have a microscopic counterpart in curved accretionary bands, which grow toward the centre of the voids (Fig. 2.16). EDS maps showed P-rich bands alternating with P-depleted bands.

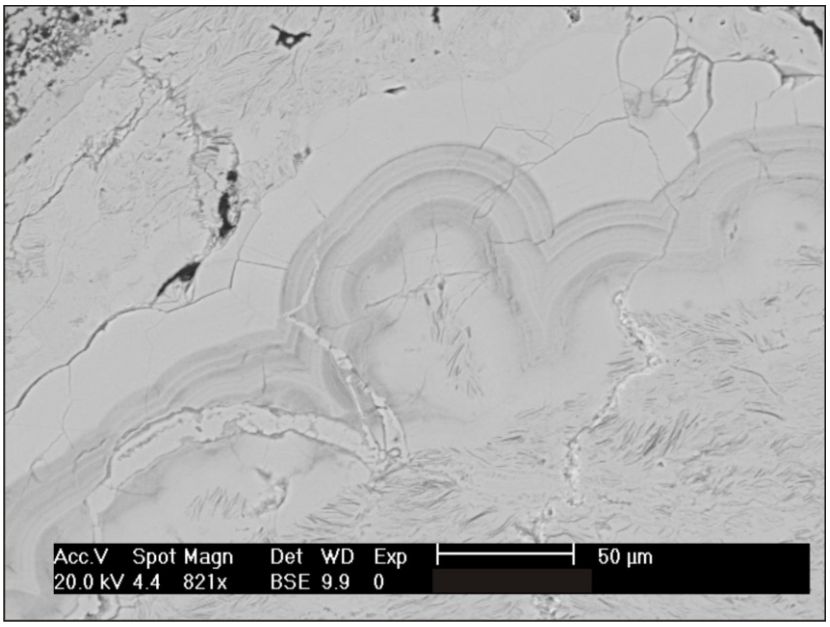

Fig. 2.16 – BSE image of concentric concretions of goethite and P-rich material (dark bands).

Quartz occurs as fractured grains, which could represent remnants of metamorphic veins (Fig. 2.17a). The accessory phases include fluorapatite, monazite, siderite, ilmenite, baryte (Fig. 2.17b), rhodochrosite and variscite.

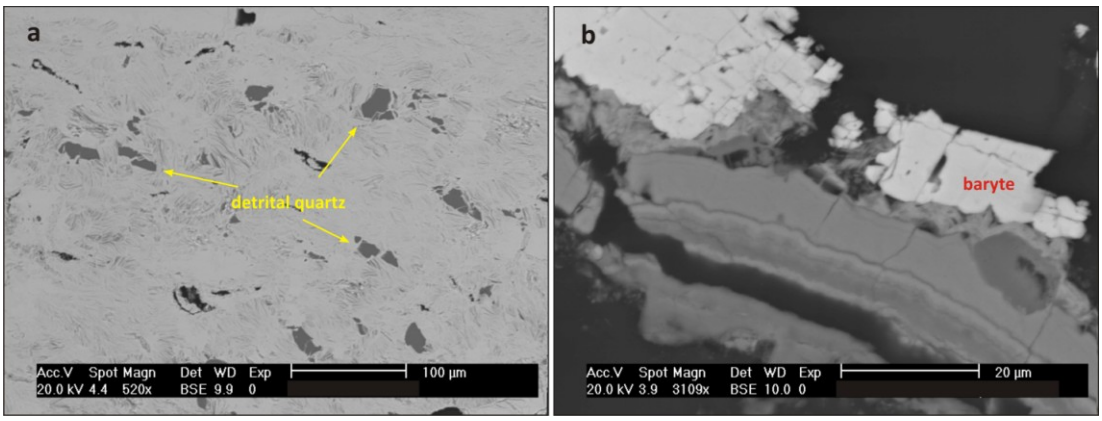

Fig. 2.17 – (a) BSE image of fractured quartz (dark) within a goethite groundmass; (b) BSE image of baryte (light) filling a void.

The primary mineral assemblages are shown in Fig. 2.18 and 2.19.

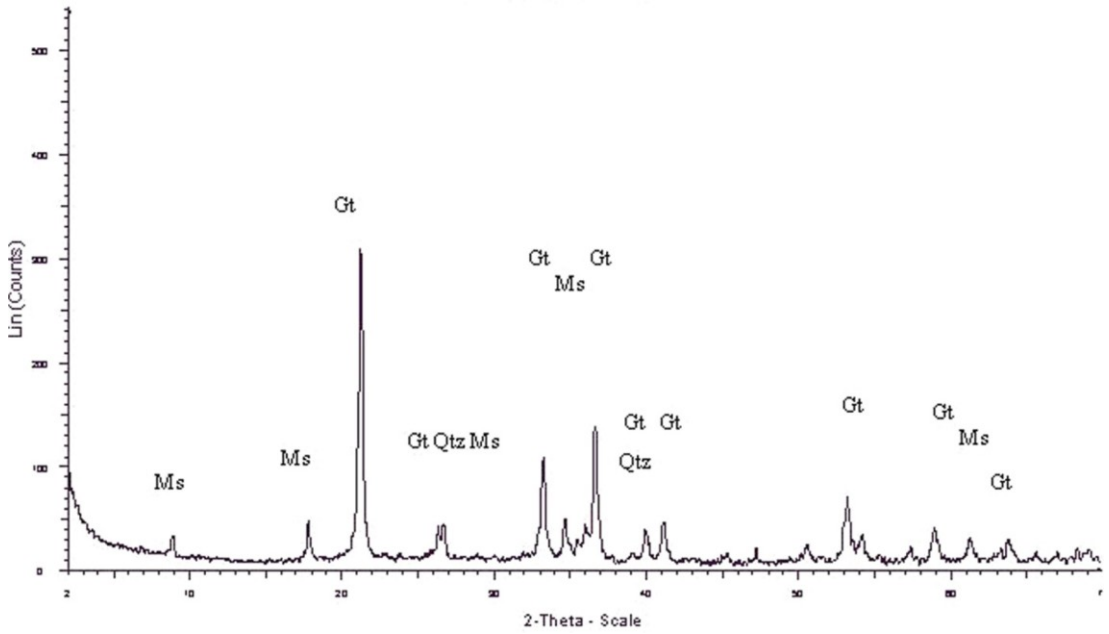

Fig. 2.18 – XRD pattern of the representative sample of the JP subset. Legend: Gt = goethite; Ms = muscovite; Qtz = quartz.

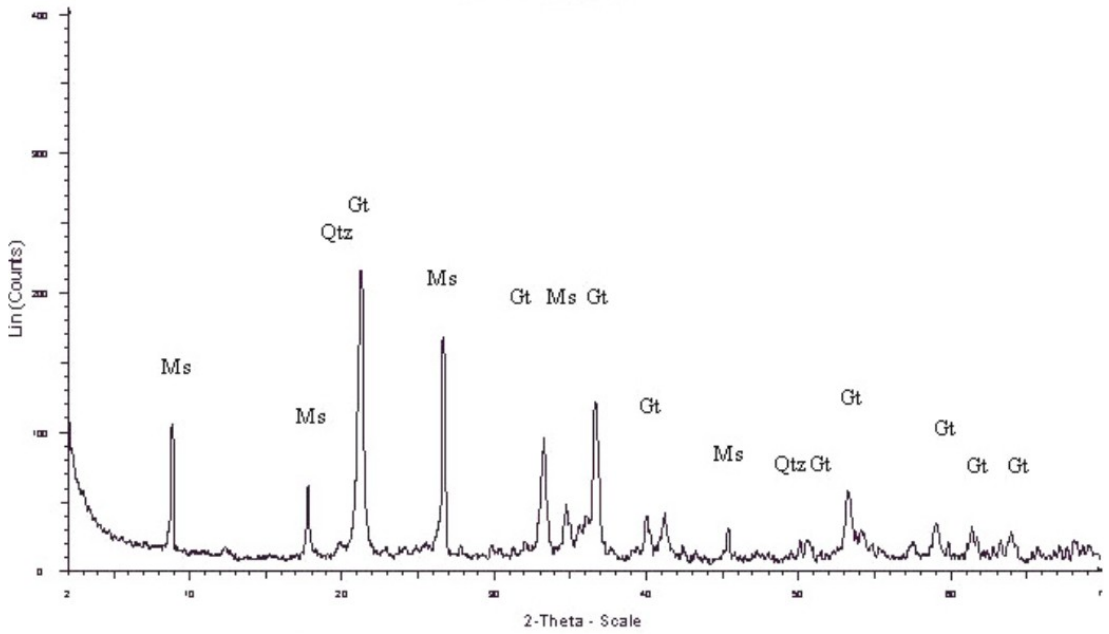

Fig. 2.19 – XRD pattern of the representative sample of the MT subset. Legend: Gt = goethite; Ms = muscovite; Qtz = quartz.

2.4.2 Chemistry

Although, as previously stated, significant textural and mineralogical differences exist between the two assemblages, the chemistry (Tabs. 1 and 2 in Appendix 1), at least for major elements, does not mirror these differences. At a first inspection Sardinian ironstones, when normalized to the GLOSS upper continental crust model (Plank and Langmuir 1998), are overall characterized by similar iron (about 10X GLOSS) and phosphorous enrichments. The P enrichment usually ranges between 5X and 10X GLOSS with the exception of the SI group samples in which P is usually <5X GLOSS. The other oxides, especially silica and alkali metals, are generally depleted relative to GLOSS, with the exception of Al and Mg in the SI group (Fig. 2.20).

Common features of the trace elements (Fig. 2.21) include Sr depletion, due to the lack of Ca-carbonate and feldspar, and Co enrichment which is higher in the continental set and especially in the MT subset (about 10X GLOSS), likely due to adsorption effects exerted by Fe oxy-hydroxides. It is also interesting to observe the strong enrichment of the redox-sensitive elements U and Zn in the continental set and especially in the JP subset.

Hafnium and Zr are usually depleted relative to GLOSS with the exception of the SI subset where elemental abundances are close to that of the standard. Some trace elements, such as Pb, Th, and Y, are either enriched and depleted, often within the same group of samples likely due to local variability and/or small-scale changes. Conversely other elements, including Cs and Nb, show minor variability and are generally close to the standard values. Finally Ba, Ni, and Rb were detected only in few samples. Ba was detected only in the continental set and, as previously stated, SEM observations revealed the occurrence of barite. As is well known, Ba is immobile as barite over most of the Eh-pH field of water stability (Brookins 1988; Takeno 2005) and its occurrence cannot be used to infer palaeoenvironmental conditions.

A significant difference between the REE contents of the marine and the continental sets is the occurrence of Ce-anomalies in the latter set (Fig. 2.22). A negative Ce-anomaly was observed in all the samples of the MT subset, ranging from 0.20 to 0.60, whereas in the JP subset both negative and positive Ce-anomalies were usually observed.

The Eu/Eu* index in the marine set varies from 0.69 to 1.15, whereas in the continental set it ranged between 0.71-0.91. In addition, overall the Eu-anomaly was generally larger than the GLOSS value (0.73). Finally in all the groups of samples large fluctuation of the LREE-HREE fractionation index was observed. The $(La/Yb)_{ch}$ ranged between 1.5 and 5.3 in the marine set of the HI group, well below the GLOSS value (7.1), and this ratio was in the 5.2-13.4 range for the SI group; in the continental set the variation was larger, ranging from 1.8 to 25.7 for the MT group and from 2.8 to 24.5 in the JP group of samples.

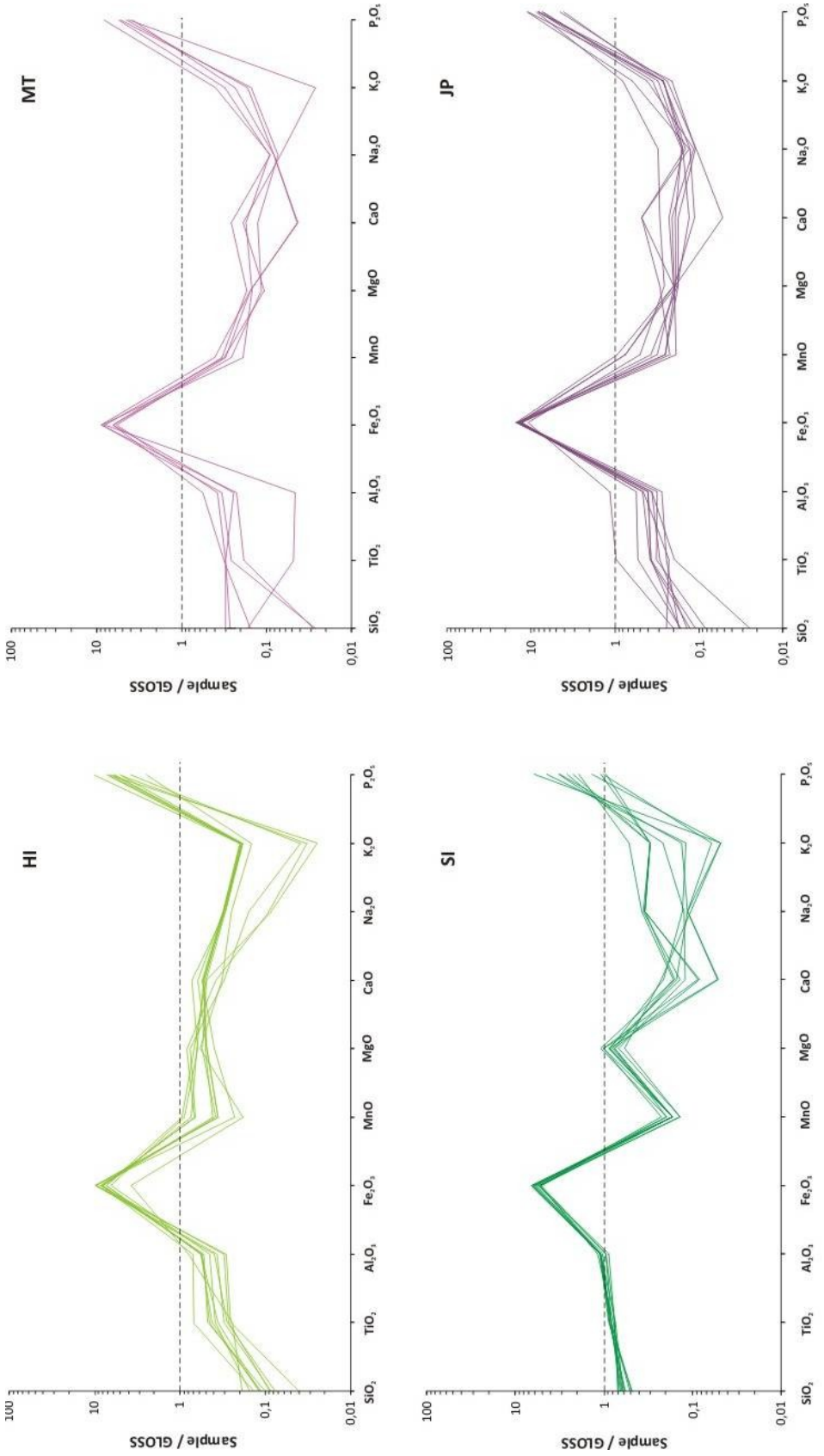

Fig. 2.20 – GLOSS-normalized major-elements patterns of the four subset analyzed.

Rosa SINISI – Iron and manganese accumulations in Sardinia: the role of supergenic and hydrothermal processes. PhD Thesis in Natural Sciences. Università degli Studi di Sassari

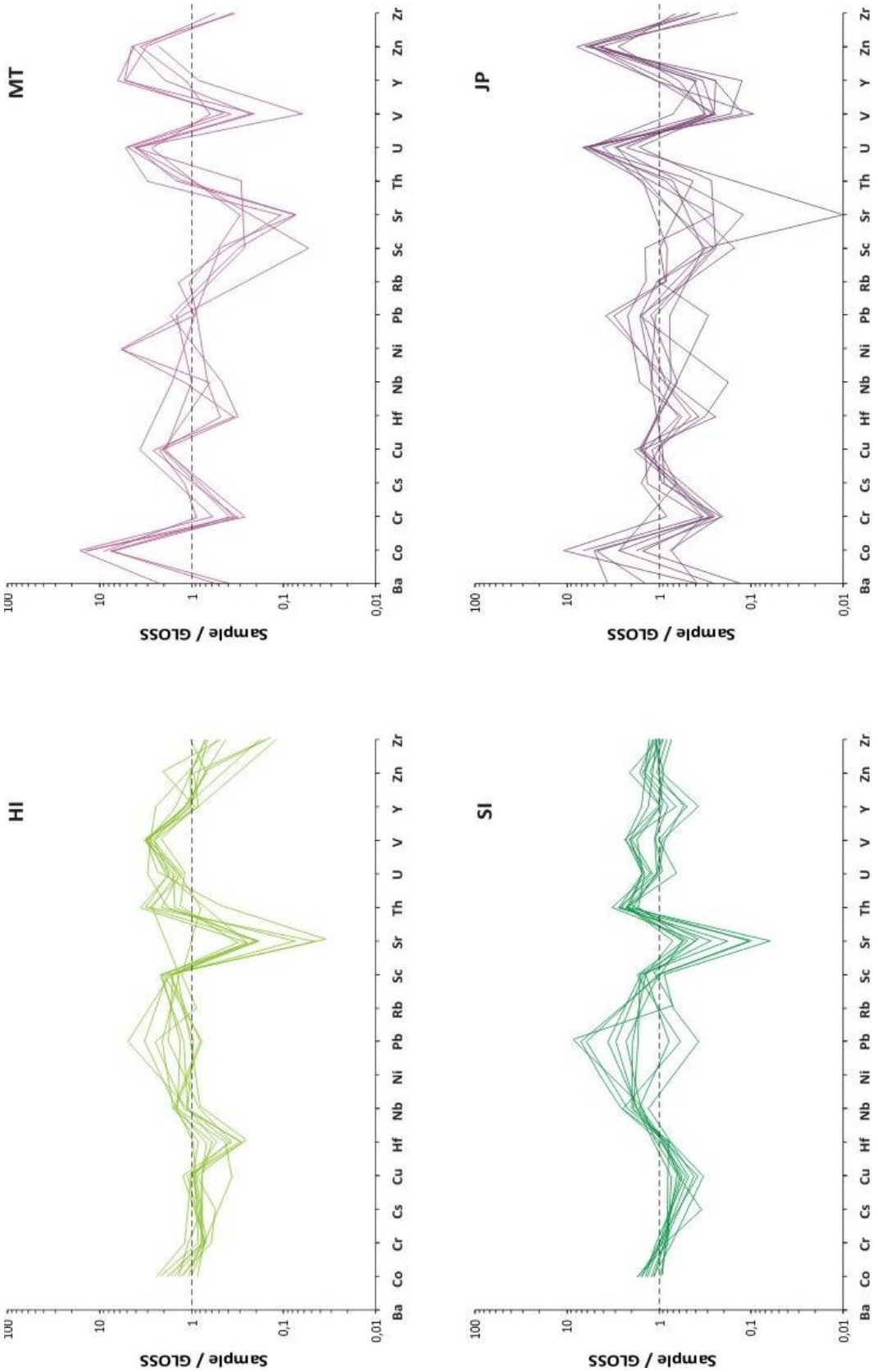

Fig. 2.21 – GLOSS-normalized trace-elements patterns of the four subset analyzed.

Rosa SINISI – Iron and manganese accumulations in Sardinia: the role of supergenic and hydrothermal processes. PhD Thesis in Natural Sciences. Università degli Studi di Sassari

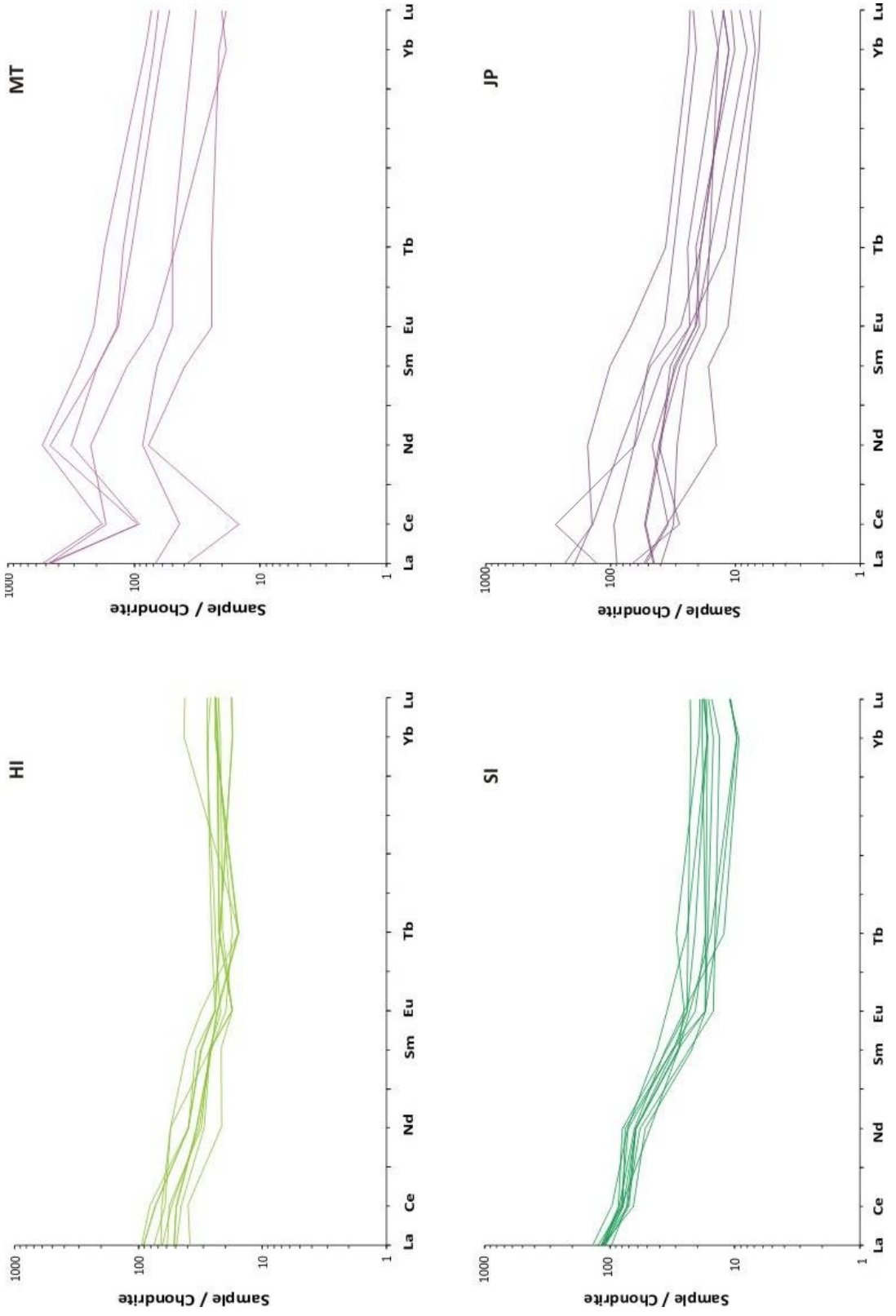

Fig. 2.22 – REE chondrite-normalized patterns of the four subset analyzed.

2.5 Discussion

Following the amount of presented data, the discussion was divided into two parts: in the first one the chemical, mineralogical and textural features of marine ironstones are analyzed; in the second one, are exposed those concerning of continental ironstones.

2.5.1 Marine set

Recently, Mücke (2000, 2006) and Mücke and Farshad (2005) improved our understanding of the origin of Phanerozoic chamosite ironstones through analyses of ironstones from 31 sites distributed over the world. The work of others who have studied the Sardinian chamosite ironstone (Franceschelli et al. 2000; Oggiano and Mameli 2006), particularly concerning reducing conditions is in good agreement with the conclusions of Mücke.

Redox sensitive trace-elements concentrations or ratios have been widely used to estimate palaeoredox conditions (e.g., Algeo and Maynard 2004), and the V/Cr ratio has proven to be one of the most useful (Jones and Manning 1994). In oxic conditions both elements occur in solution, as $H_2VO_4^-$ and CrO_4^{2-}, respectively, whereas under reducing conditions they are largely insoluble. Reducing conditions of the depositional-to-diagenetic environment of the HI samples are supported by both the mineral assemblage, including magnetite and siderite, and the V/Cr proxy. Jones and Manning (1994) stated that reducing conditions are associated with V/Cr ratios >4.25 and in our case V/Cr is usually above this value, suggesting that these samples formed under reducing conditions and not were exposed to post-diagenetic oxidation.

Further insights on palaeoenvironmental conditions in which HI samples formed can be deduced from the occurrence of siderite. Anoxic environments (after Berner 1980) are divided in sulphidic and non-sulphidic. The latter is further subdivided into post-oxic and methanic. Sulphidic conditions are typically driven by bacterial reduction of seawater dissolved sulphate to H_2S and HS^-. Further decomposition of organic matter results in the occurrence of the highly reducing anoxic non-sulphidic methanic environment in which abundant siderite forms (Mücke 2006) and where magnetite is also stable (e. g., Maynard 1982). Thus we assume that samples of the HI subset formed in such an environment.

Several lines of evidence for the protolith seem to exclude that kaolinite and iron-oxyhydroxides, originating from continental weathering, acted as chamosite precursors, as proposed by Mücke (2006) for other Phanerozoic ironstones. These evidences include diamictitic texture and the palaeogeographical location of Sardinia close to the South Pole during uppermost Ordovician (von Raumer et al. 2003; Tait et al. 2000). It is likely that detrital chlorite and illite, as products of physical weathering, acted as precursors and that they successively underwent diagenetic transformation to chamosite (Becq-Giraudon et al. 1991; Kim and Lee, 2000, and references therein). Indeed, chlorite and illite typically characterize the recent sedimentary record around the Antarctic craton (Ehrmann et al. 2005). Both paragenesis and the V/Cr proxy indicate for the SI samples that they experienced an additional event in comparison with the HI samples. The V/Cr ratio ranges from 1.45 to 3.62, indicating an oxic to intermediate environment. It is likely that all samples of the marine set derived from the same protolith and experienced the same diagenetic conditions but that SI samples suffered oxic conditions during an emergence stage, leading to goethite replacement of siderite and magnetite according to the reactions, respectively:

$$(1) \quad 4FeCO_3 + O_2 + 2H_2O \rightarrow 4FeO(OH) + 4CO_2$$

$$(2) \quad 4Fe_3O_4 + O_2 + 6H_2O \rightarrow 12FeO(OH)$$

2.5.2 Continental set

Iron as Fe^{3+} is hosted primarily by oxy-hydroxides during weathering in the continental environment, and these oxy-hydroxides can occur in a large range of environmental conditions (e.g., Brookins 1988; Drever 1997). Schwertmann and Murad (1983) observed maximum ferric-oxy-hydroxide formation under circum-neutral pH conditions and Marshall and Fairbridge (1999) suggested that these phases are expected to form under high Eh conditions where little or no decomposable organic matter is present. Iron oxy-hydroxides likely also played a role in concentrating P due to the high goethite P-sorption capability (e.g. Thiessen et al. 1996).

Jones and Manning (1994) concluded that oxic to highly oxic conditions are associated with values of the V/Cr proxy <2 and in our case all samples of the

continental set show V/Cr values <<2, ranging from 0.33 to 1.58. In addition, Zn and U, due to their redox chemistry, have been proposed as indicators of euxinic conditions (Algeo and Maynard 2004 and references therein). Although Zn possesses only one common valence in nature (Zn^{2+}) its distribution is dependent on redox conditions because of the stability of sphalerite (ZnS) in reducing environments (Brookins, 1988). However SEM inspection did not show the presence of sulphides minerals in the continental set, and, in fact, under oxidizing conditions a large stability field for zincite (ZnO) occurs. In addition maximum sorption of Zn^{2+} on hydrous ferric oxide occurs in 6-7 pH range (Stumm 1992). Thus we suggest that Zn enrichment in the continental set can be related to surface processes in an oxidizing environment. It is well known that the behavior of U in the sedimentary environment is Eh dependent, and in oxidizing environments U is most soluble in the hexavalent oxidation state. However sorption of U^{6+} on goethite and hematite and occlusion by Fe-oxide coatings can retard U transport in the environment (Bruno et al. 1995; Duff et al. 2002). As a consequence, the enrichment of U in the continental set may be related to surface concentration processes under oxidizing conditions and not to redox changes pointing toward more reducing conditions.

In addition to the above redox-sensitive elements, Ce is a useful proxy as a result of the $Ce^{3+} \rightarrow Ce^{4+}$ reaction. Ce anomalies are common in our samples, a feature that has been frequently observed during weathering and soil formation as well as in ancient ironstones. In the continental set, particularly in the MT subset, negative Ce anomalies were observed, similarly to what was observed by Hren et al. (2006) in ironstones, suggestive of an oxy-hydroxide origin from Ce-depleted solutions likely due to the precipitation of Ce^{4+} minerals or adsorption of Ce^{4+} onto pre-existing oxy-hydroxides (Braun et al. 1990; Mongelli 1997) prior the formation of the iron phases. In the JP subset, however, a few samples showed a positive Ce-anomaly. At a pH<5 the surfaces of iron oxyhydroxides catalyse the oxidation of dissolved Ce^{3+} to the less-soluble Ce^{4+} causing Ce precipitation and resulting in positive Ce anomalies (Bau 1994, 1999). In addition, iron oxyhydroxides forming at low pH display lower REE sorption (Koeppenkastrop and De Carlo 1992; Bau et al. 1998; Bau 1999) and in our case the sample having the highest positive Ce-anomaly (JP7, Ce/Ce*=2.61) has a significantly lower REE content (ΣREE=369.18 ppm) relative to the sample showing the lowest Ce anomaly (MT5, Ce/Ce*= 0.20, ΣREE= 672.94 ppm).

Thus, we assume that continental samples likely formed in oxidizing environment under different pH conditions, and that acidic conditions were not the rule. In addition, based on the high Mn contents observed in these samples, it may be assumed that manganese oxy-hydroxides, due to their relevant REE adsorption capacity, may play a role in causing positive Ce anomalies.

2.6 Conclusions

Sardinian ironstones hosted in the Variscan basement are of different ages and formed under different palaeoenvironmental and palaeoclimatic conditions. The V/Cr proxy proved to be a useful and comparatively simple mean to determine palaeoenvironmental settings and, in particular, to assess redox conditions.

In marine ironstones formed under highly reducing, anoxic, non-sulphidic methanic environments (HI subset), the Fe-phases are chamosite, siderite and magnetite. Detrital chlorite and illite, as products of physical weathering acted as chamosite precursors.

The SI subset of these ironstones experienced an immersion stage that caused goethite replacement after siderite and magnetite in a transitional to oxic environment.

The dominant Fe-phase in continental ironstones formed under oxic conditions is goethite, which is capable of adsorbing Zn^{2+} and U^{6+}, which in these samples are strongly enriched relatively to the average upper crustal composition. Ce-anomalies generally occur in this set of samples, a feature that has been frequently observed during soil formation as well as in ancient ironstones. Negative Ce anomalies were observed in the MT subset, suggesting oxyhydroxides origin from Ce-depleted solutions likely due to the precipitation of Ce^{4+} minerals prior the formation of the iron phase. In the JP subset a few samples showed a positive Ce-anomaly. At pH<5, the surfaces of iron oxyhydroxides can catalyse the oxidation of dissolved Ce^{3+} to the less-soluble Ce^{4+} thereby causing Ce precipitation and positive Ce anomalies. In addition, iron oxyhydroxides forming at lower pH values display lower REE sorption. In our study, the sample having the highest positive Ce-anomaly (JP7, Ce/Ce*=2.61)

has a lower REE content (ΣREE=369.18 ppm) than the sample with the lowest Ce anomaly (MT5, Ce/Ce*= 0.20, ΣREE= 672.94 ppm).

We therefore conclude that continental samples formed in oxidizing environment under variable pH conditions and that acidic conditions were not the rule.

In spite of the fact that Sardinian ironstones formed in different environments (marine *vs* continental) and under contrasting climatic conditions (sub-glacial *vs* tropical), they share many geochemical features, particularly their similar Fe and P contents. If the occurrence of phosphorous in oolitic ironstones is common and related to the occurrence of authigenic apatite linked to the decay of organic matter in an anoxic sub-oxic environment, it does not follow that it would occur in the strongly oxic conditions of the continental ironstones. Probably in this case the phosphorous abundance is related to the ability of goethite to adsorb P (Thiessen et al. 1996). Our results demonstrate that comparatively subtle differences in palaeoenvironments can give rise to important geochemical differences in some chemical sediments.

REFERENCES

ALGEO T.J. AND MAYNARD J.B. (2004) – *Trace-element behavior and redox facies in core shales of Upper Pennsylvanian Kansas-type cyclothems*. Chemical Geology, 206, 289-318.

ALIBERT C. & MCCULLOCH M.T. (1993) – *Rare earth element and neodymium composition of the banded iron formations and associated shales from Hamersley, Western Australia*. Geochim. Cosmochim. Acta, 57,187-204.

AMADESI E., CANTELLI C., CARLONI G.C., RABBI E. (1961) – *Ricerche geologiche sui terreni sedimentari del foglio 208 Dorgali*. Giornale di Geologia, 28, 59-87.

BAU M. (1994) – *Modeling of Rare-Earth Element partitioning between particles and solution in aquatic environments-comment*. Geochimica et Cosmochimica Acta, 58, 4521-4523.

BAU M. (1999) – *Scavenging of dissolved yttrium and rare earths by precipitating iron oxyhydroxide: experimental evidence for Ce oxidation, Y-Ho fractionation and lanthanide tetrad effect*. Geochimica et Cosmochimica Acta, 63, 67-77.

BAU M., USUI A., PRACEJUS B., MITA N., KANAI Y., IRBER W., DULSKI P. (1998) – *Geochemistry of low-temperature water-rock interaction: evidence from natural waters, andesite, and iron oxyhydroxide precipitation at Nishiki-numa iron spring, Hokkaido, Japan*. Chemical Geology, 151, 293-307.

BECQ-GIRAUDON J.F., BOUILLÉ S., CHAUVEL J.J. (1992) – *Genesis and significance of the silico-aluminous nodules in the Ordovician of the Montagne Noire and the Massif Armoricain (France)*. Sedimentary Geology, 77, 77-87.

BERNER R.A. (1980) – *A new geochemical classification of sedimentary environments*. Journal of Sedimentary Petrology, 51, 359-365.

BRAUN J.J., PAGEL M., MULLER J.P., BILONG P., MICHERD A. AND GUILLET B. (1990) – *Cerium anomalies in lateritic profiles*. Geochimica Cosmochimica Acta, 54, 781-795.

BROOKINS D.G. (1988) – *Eh-pH diagrams for geochemistry*. Springer-Verlag, Berlin, 176 pp.

BRUNO J., DE PABLO J., DURO L., FIGUEROLA E. (1995) – *Experimental study and modeling of the U(VI)-Fe(OH)3 surface precipitation/coprecipitation equilibria*. Geochimica et Cosmochimica Acta, 59, 4113-4123.

BUZZI L., GAGGERO L., FUNEDDA A., OGGIANO G. AND TIEPOLO M. (2007) – *Zircon geochronology and Sr-Nd isotopic study of the Ordovician magmatic events in the southern Variscides (Sardinia)*. Geologie de la France, 2, 73.

CAPELLI B., CARMIGNANI L., CASTORINA F., DI PISA A., OGGIANO G., PETRINI R. (1992) – *A Hercynian suture zone in Sardinia: geological and geochemical evidence*. Geodinamica Acta, 5, 101-118.

CARMIGNANI L., COCOZZA T., GHEZZO C., PERTUSATI P.C. & RICCI C.A. (1982) – *Lineamenti del Basamento Sardo. Guida alla geologia del Paleozoico sardo*. Guide Geologiche Regionali Soc. Geol. It., 11-23.

CARMIGNANI L., CAROSI R., DI PISA A., GATTIGLIO M., MUSUMECI G., OGGIANO G., PERTUSATI P.C. (1994) – *The Hercynian chain of Sardinia (Italy)*. Geodinamica Acta, 7, 31-47.

DIENI I. AND MASSARI F. (1966) – *I Foraminiferi del Valanginiano superiore di Orosei (Sardegna)*. Paleontologia Italiana, 61, 75-186.

DREVER J.I. (1997) – *The geochemistry of natural waters: surface and groundwater environments*. Prentice Hall, Upper Saddle River, NJ, III ed., 436 pp.

DUFF M.C., COUGHLIN J.U. AND HUNTER D.B. (2002) – Uranium co-precipitation with iron oxide minerals. Geochimica Cosmochimica Acta, 66, 3533-3547.

DYMEK R.F. & KLEIN C. (1988) – *Chemistry, petrology and origin of banded iron-formation lithologies from the 3800 Ma Isua supracrustal belt, west Greenland*. Precambrian Research, 39, 247-302.

EHRMANN W., SETTI M. AND MARINONI L. (2005) – *Clay minerals in Cenozoic sediments off Cape Roberts (McMurdo Sound, Antarctica) reveal palaeoclimatic history*. Palaeogeography, Palaeoclimatology, Palaeoecology, 229, 187-211.

FRANCESCHELLI M., PUXEDDU M., CARTA M. (2000) – *Mineralogy and geochemistry of late Ordovician Phosphate-bearing oolitic ironstones from NW Sardinia, Italy*. Mineralogy and Petrology, 69, 267-293.

FRANZINI M., LEONI L., SAITTA M. (1972) – *A simple method to evaluate the matrix effects in X-ray fluorescence analysis*. X-ray spectrometry, 1, 151-154.

FRANZINI M., LEONI L., SAITTA M. (1975) – *Revisione di una metodologia analitica per fluorescenza X basata sulla correzione degli effetti di matrice*. Società Italiana di Mineralogia e Petrologia, 31, 365-378.

HOLLAND H.D. (1973) – *The oceans: a possible source of iron in iron formations*. Economic Geology, 68, 1169-1172.

HREN M.T., LOWE D.R., TICE M.M., BYERLY G. AND CHAMBERLAIN C.P. (2006) – *Stable isotope and Rare Earth Element evidence for recent ironstone pods within the Archean Barberton greenstone belt, South Africa*. Geochimica et Cosmochimica Acta, 70, 1457-1470.

JONES B. AND MANNING D.A.C. (1994) – *Comparison of geochemical indices used for the interpretation of palaeoredox conditions in ancient mudstones*. Chemical Geology, 111, 111-129.

KIM Y. AND LEE Y.I. (2000) – *Ironstones and green marine clays in the Dongjeom Formation (Early Ordovician) of Korea*. Sedimentary Geology, 130, 65-80.

KIMBERLEY M.M. (1979) – *Origin of oolitic iron formations*. Journal of Sedimentary Petrology, 49, 111-132.

KOEPPENKASTROP D. AND DE CARLO E.H. (1992) – *Sorption of Rare-Earth Elements from seawater onto synthetic mineral particles – an experimental approach*. Chemical Geology, 95, 251-263.

LEONI L. AND SAITTA M. (1976) – *Determination of yttrium and niobium on standard silicate rocks by X-ray fluorescence analysis*. X-ray Spectrometry, 5, 29-30.

MARSHALL C.P. AND FAIRBRIDGE R.W. (1999) – *Encyclopedia of Geochemistry*. Kluwer Academy Publishers, Dordrecht, 768 pp.

MAYNARD J.B. (1982) – *Extension of Berner's 'New geochemical classification of sedimentary environments' to ancient sediments*. Journal of Sedimentary Petrology, 52, 1325-1331.

MONGELLI G. (1997) – *Ce-anomalies in the textural components of Upper Cretaceous karst bauxites from the Apulian Carbonate platform (southern Italy)*. Chemical Geology, 140, 69-79.

MÜCKE A. (2000) – *Environmental conditions in the late Cretaceous African Tethys: conclusion from a microscopic-microchemical study of ooidal ironstones from Egypt, Sudan and Nigeria*. Journal of African Earth Sciences, 30, 25-46.

MÜCKE A. (2006) – *Chamosite, siderite and the environmental conditions of their formation in chamosite-type Phanerozoic ooidal ironstones*. Ore Geology Reviews, 28, 235-249.

MÜCKE A. AND FARSHAD F. (2005) – *Whole-rock and mineralogical composition of Phanerozoic ooidal ironstones: comparison and differentiation of types and subtypes*. Ore Geology Review, 26, 227-262.

OGGIANO G. (1994) – *Lineamenti stratigrafico-strutturali del basamento del Goceano (Sardegna centro-settentrionale)*. Bollettino della Società Geologica Italiana, 113, 471-480.

OGGIANO G. AND MAMELI P. (2006) – *Diamictite and oolitic ironstones, a sedimentary association at Ordovician-Silurian transition in the North Gondwana Margin: new evidence from the Inner Nappe of Sardinia Variscides (Italy)*. Gondwana Research, 9, 500-511.

OGGIANO G., GAGGERO L., FUNEDDA A., BUZZI L. & TIEPOLO M. (2010) – *Multiple early Paleozoic volcanic events at the northern Gondwana margin: U-Pb age evidence from the Southern Variscan branch (Sardinia, Italy)*. Gondwana Research, 17, 44-58.

PLANK T. AND LANGMUIR C.H. (1998) – *The chemical composition of subducting sediment and its composition for the crust and mantle*. Chemical Geology, 145, 325-394.

RAUCSIK B. & VARGA A. (2008) – *Climato-environmental controls on clay mineralogy of the Hettangian–Bajocian successions of the Mecsek Mountains, Hungary: an evidence for extreme continental weathering during the early Toarcian oceanic anoxic event*. Palaeogeogr. Palaeoclimatol. Palaeoecol., 265, 1-13.

SCHWERTMANN U. AND MURAD E. (1983) – *Effect of pH on the formation of goethite and hematite from ferrihydrite*. Clays and Clay Minerals, 31, 277-284.

STUMM W. (1992) – Chemistry of the solid-water interface, Wiley and Sons, NJ, 428 pp.

TAKENO N. (2005) – *Atlas of Eh-pH diagrams. Intercomparison of thermodynamic databases*. Geological Survey of Japan, 419, 285 pp.

TAIT J., SCHATZ M., BACHTADSE V. AND SOFFEL H. (2000) – *Palaeomagnetism and Palaeozoic palaeogeography of Gondwana and European terranes*. In: Orogenic Processes: Quantification and Modelling in the Variscan Belt (W. Franke, V. Haak, O. Oncken and D. Tanner, editors). Geological Society of London, Special Publications, 179, 21-34.

THIESSEN H., LO MONACO S., RAMIREZ A., SANTOS M.C.D. AND SHANG C. (1996) – *Phosphate minerals in a lateritic crust from Venezuela*. Biogeochemistry, 34, 1-17.

VON RAUMER J.F., STAMPFLI G.M. AND BUSSY, F. (2003) – *Gondwana-derived microcontinents—the constituents of the Variscan and Alpine collisional orogens*. Tectonophysics, 365, 7-22.

YAPP C.J. (1993) – *Paleoenvironment and the oxygen isotope geochemistry of ironstone of the Upper Ordovician Neda Formation, Wisconsin, USA*. Geochimica et Cosmochimica Acta, 57, 2319-2327.

PART III

THE MN MOBILITY AND THE MN ORES OF SARDINIA

3.1 The Mn geochemical behavior in supergenic and hydrothermal systems

The redox potential and pH of an aqueous system are the main controls on the geochemical behavior of Mn and, ultimately, the competition between its affinity for solution or for the growth of solid-state Mn phases. Manganese occurs in three oxidation states: Mn^{2+}, which is soluble under reducing and acidic conditions; and Mn^{3+} and Mn^{4+}, which are less soluble and are stable under relatively oxidizing and alkaline conditions (Fig. 3.1a).

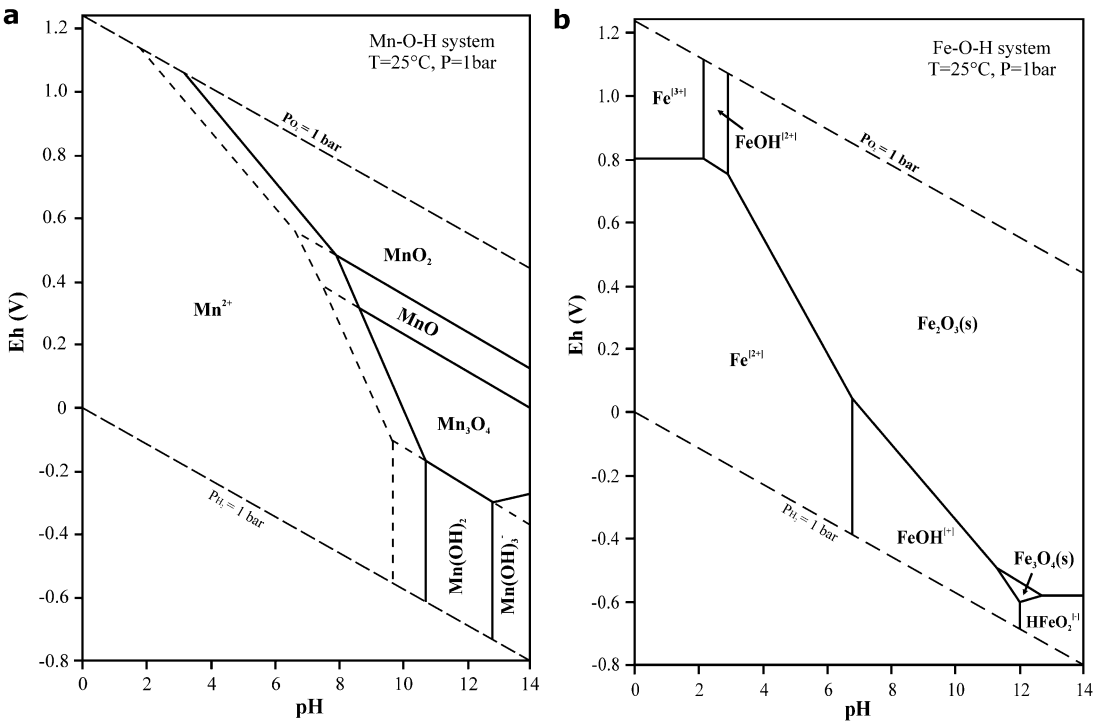

Fig. 3.1 – Eh-pH diagrams of Mn-O-H (a) and Fe-O-H (b) systems at standard conditions of 25°C and 1 bar. The dissolved ions molality is 10^{-6}. More details in the text. After Brookins 1988; Takeno 2005.

At first inspection, therefore, the geochemical behavior of manganese in the hydrosphere is similar to that of iron. However, two differences amid Fe and Mn are relevant:

1) the reduction of Mn^{3+} or Mn^{4+} to dissolved Mn^{2+} occur at higher redox potentials than those of $Fe^{3+} \longrightarrow Fe^{2+}$ reduction;

2) the oxidation of Mn^{2+} to Mn^{3+} or Mn^{4+}, is usually slower than the oxygenation of Fe^{2+} (Stumm 1992). The comparison of the manganese phase diagram with the iron one (Fig. 3.1b) shows that higher oxidation potentials are

required to stabilize pyrolusite than hematite. This fact provides a possible explanation for the spatial and stratigraphycal separation between iron and manganese ore in nature (Robb 2005).

The accumulation of Mn in solution and its deposition as a mineral phase occur in a variety of modern and ancient geological settings (Roy 1992). Supergene and hydrothermal processes, active in both marine and continental environments, are responsible for the origin of most Mn ores. The occurrence of Mn-ores and their classification have been the subject of many studies (Roy 1981, 1997; Nicholson 1992; Fan and Yang 1999; Liakopoulos et al. 2001; Shah and Moon 2004, 2007; Brugger and Meisser 2006), which have shown that each deposit must be studied independently using multidisciplinary research.

Unfortunately, a few data on the geochemical behavior of Mn at different redox conditions within a hydrothermal system are available.

For this reason the equilibrium reaction products were calculated here, using the Fact-Sage™ 6.2 Gibbs free energy database (Bale et al. 2002). Three Eh-pH diagrams at growing temperatures (from 25 to 75 °C) were derived for Mn-H_2O system with a constant Mn molality of 10^{-6} (Fig. 3.2). The comparison amid these diagrams shows that the Mn behavior not change significantly with the temperature (at least up to 75°C). Only a weak widening of the solids stability fields - at the same dissolved ion activity value – was noted.

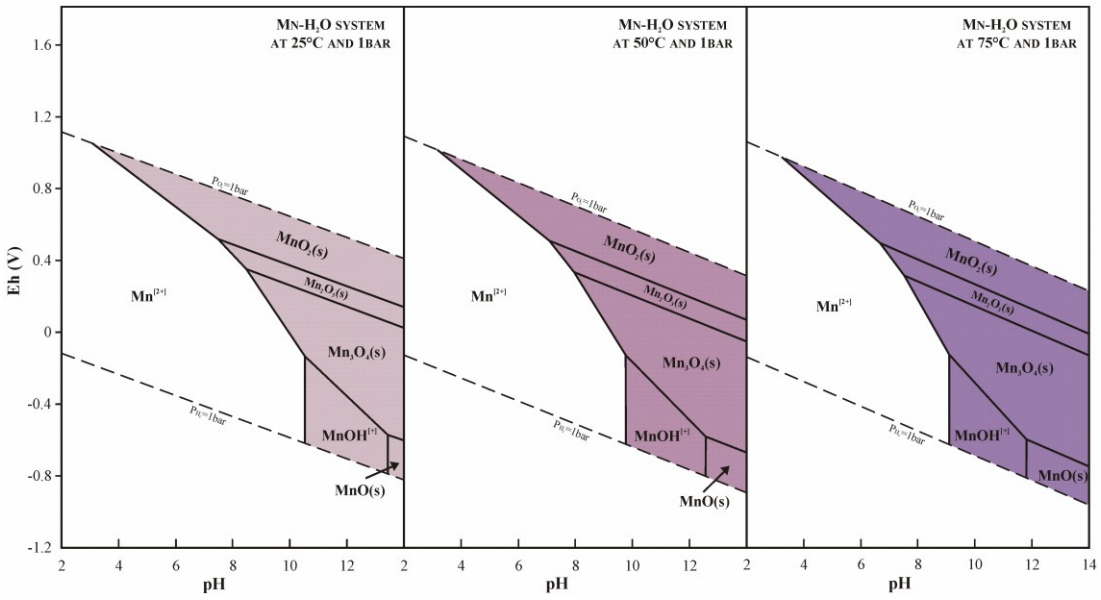

Fig. 3.2 – Eh-pH diagram of Mn-H_2O system at 25°C (a), 50°C (b) and 75°C (c) performed by FactSage™ database (Bale et al. 2002). The Mn molality of each system is 10^{-6}.

3.2 Deposits geology

In Sardinia different types of Mn-ore deposits occur within shallow-marine sediments and volcanic rocks (Fig. 3.3). Based on the classification scheme proposed by Nicholson (1992), these ores can be classified as follows: *a)* marine supergene Mn deposits hosted within clast-supported conglomerate deposited upon calcalkaline volcanic rocks during a Miocene marine transgression, and *b)* continental vein-type hydrothermal Mn-ores that cross-cut volcanic rocks ranging in composition from andesite to rhyolite and comendite.

No previous study has analyzed these deposits, and they differ from the widespread and better-known Mn ores that occur in sedimentary and hydrothermal ocean-floor settings.

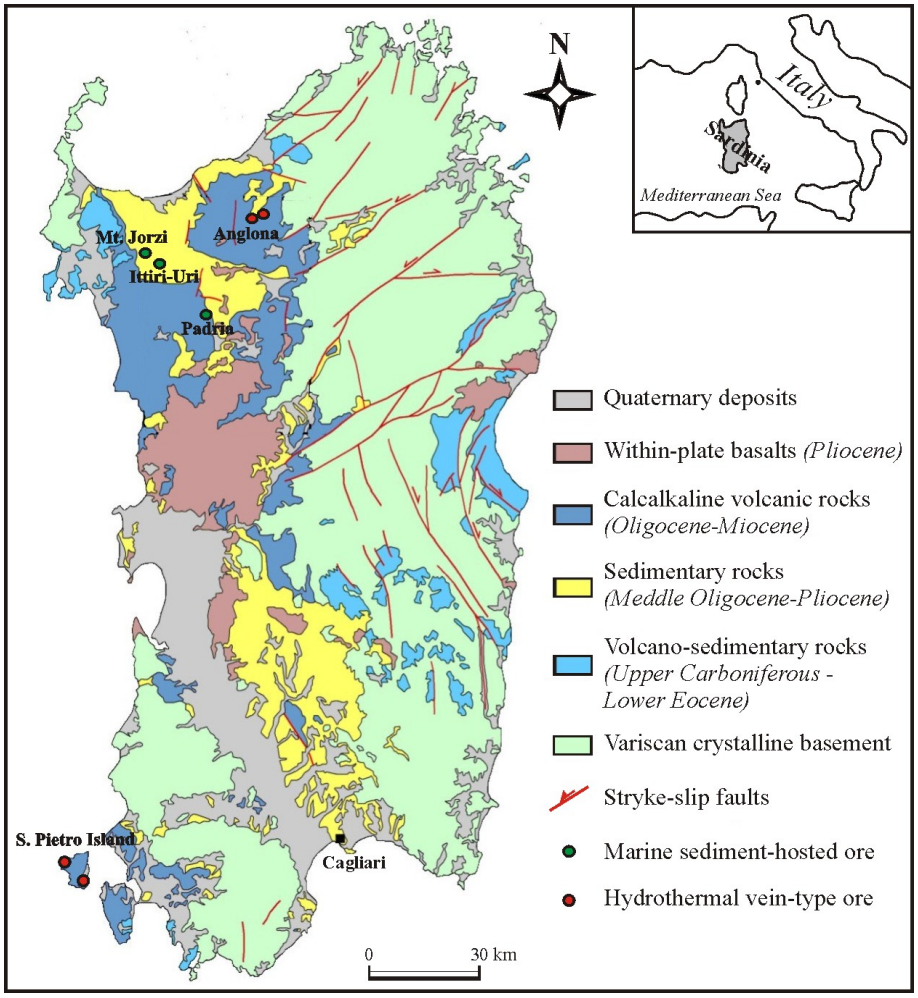

Fig. 3.3 - Geological sketch map of Sardinia and sampling sites. After Carmignani et al. 2001, modified.

3.2.1 *Marine supergene Mn ores (hereafter called mar group)*

In northwest Sardinia, several sediment-hosted Mn deposits occur at the base of a carbonate marine transgressive sequence deposited within the Logudoro Basin during the upper Burdigalian–Langhian (Funedda et al. 2000). Manganese oxides occur as matrix and cement within littoral conglomerates that comprise rounded, decimeter-sized cobbles and rare boulders derived from the underlying volcanic calcalkaline succession (Fig. 3.4). The Mn-bearing conglomerate is continuous over a distance of 5 km. Its thickness rarely exceeds 1.5 m and it is capped by a coarse bioclastic layer of oyster shells (Ostrea Lamellosa) which are locally cemented by sparitic calcite and Mn oxides. Fine, reworked Mn oxides occur locally in silty layers that cap the conglomerate.

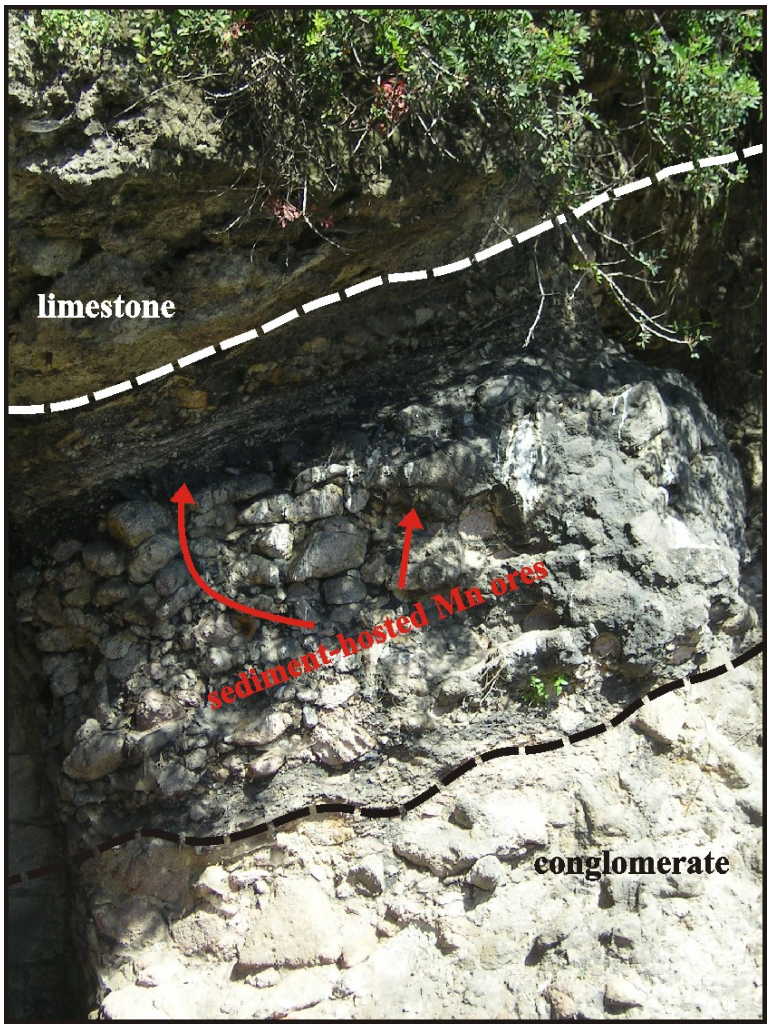

Fig. 3.4 - Littoral conglomerate cemented by Mn ores.

These marine Mn deposits occur in the Padria (mar1 subgroup), Ittiri-Uri (mar2 subgroup) and Monte Jorzi (mar3 subgroup) areas, where they were mined during the 20th century. At Ittiri-Uri and Monte Jorzi, the Mn-bearing conglomerate and its calcareous cap are cut by E–W-striking normal faults that are possibly related to Serravallian extensional tectonics. These faults post-date the calcalkaline volcanic activity in this part of the island. There exists no evidence to suggest the faults acted as hydrothermal pathways. The transgressive conglomerate is deposited on pyroclastic flows at Ittiri-Uri and Monte Jorzi, whereas at Padria it rests on andesites.

3.2.2 Continental hydrothermal Mn deposits (hereafter called hyd group)

In the Anglona district of northwest Sardinia, hydrothermal Mn mineralization (the hyd1 subgroup) is hosted within a latite lava dome and, to a lesser degree, within a welded pyroclastic flow that yields an age of 18 ± 0.6 Ma (Oudet et al. 2010; Fig. 3.5).

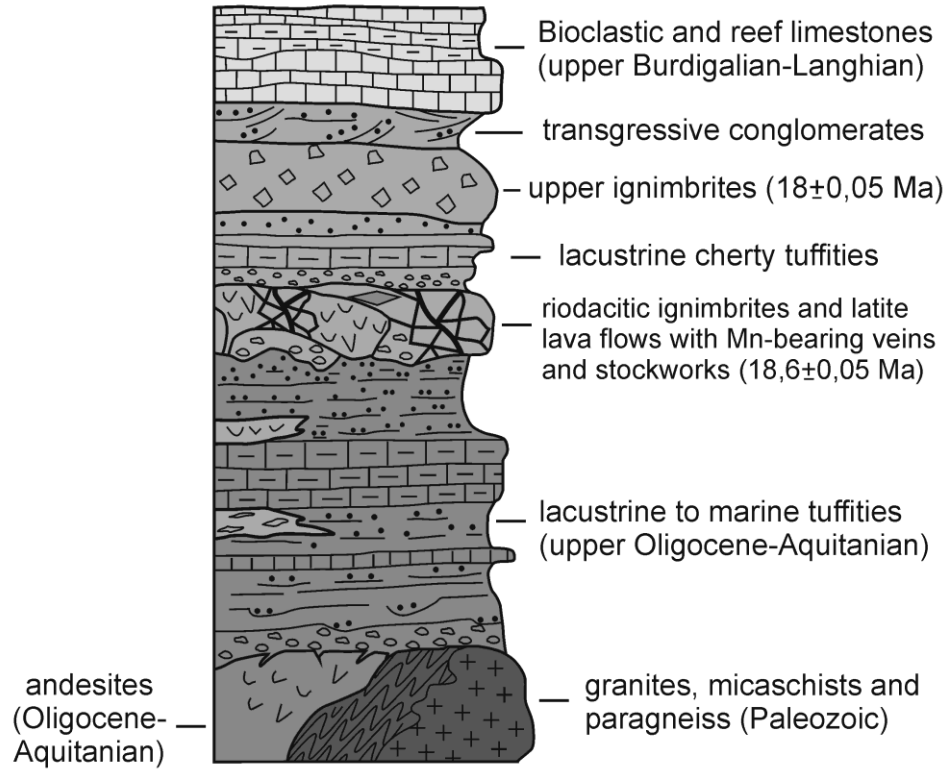

Fig. 3.5 - Stratigraphic column of Anglona volcanic sequences. Note the occurrence of Mn-bearing stockworks and veins within Burdigalian ignimbrites and lava flows.

The area is characterized by a volcanic–sedimentary succession consisting of andesite domes, lacustrine to marine Oligocene–Aquitanian tuffites, welded ignimbrites and latite to high-K basaltic andesites, and lacustrine cherty tuffites capped by a weakly welded pyroclastic flow. This succession is uncomformably overlain by transgressive marine deposits of late Burdigalian age. Manganese ore occurs both as vein fill (Fig. 3.6) and as stockwork in zones oriented approximately parallel to NNE–SSW-trending faults. The Mn ore in these deposits is commonly associated with cherty gangue, which also fills the stockwork. The gangue minerals, mainly opal-CT and quartz, and the Mn phases are interfingered, precluding the possibility of establishing a precipitation sequence based on textural features.

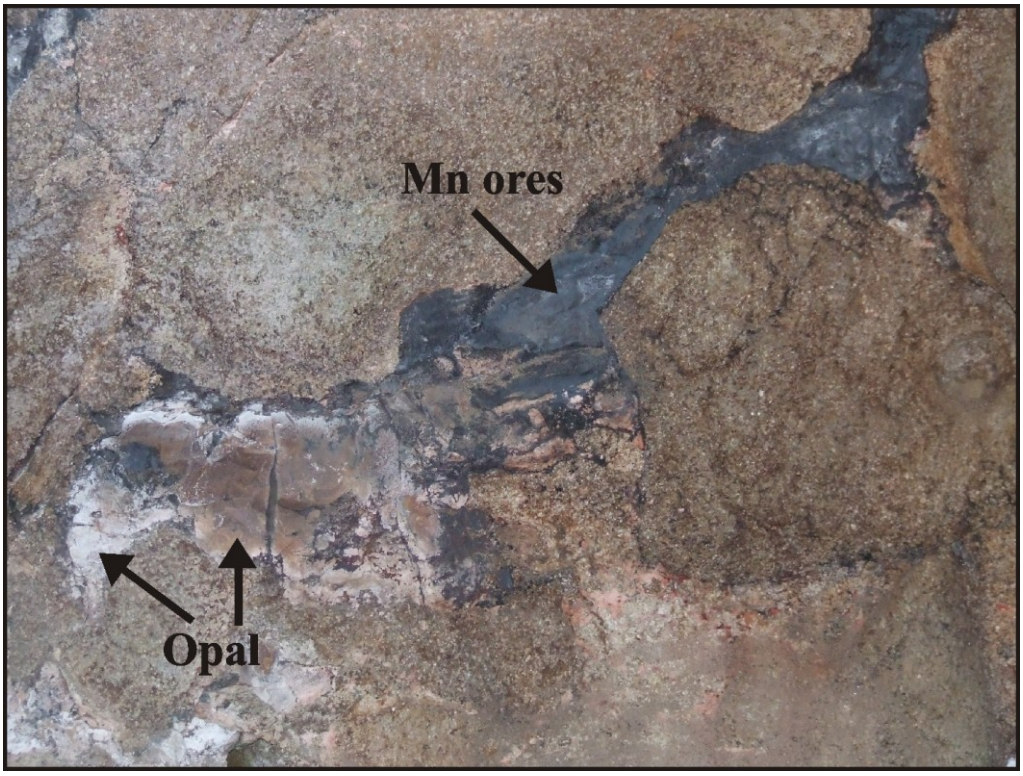

Fig. 3.6 - Hydrothermal mineralization (hyd1) within Anglona andesites. Mn oxyhydroxides and opal fill the fracture.

Continental hydrothermal Mn ore within a volcanic sequence consisting of alternating pyroclastic and comenditic lava flows (Cioni and Funedda 2005) occurs at San Pietro Island, southwest Sardinia (Fig. 3.7). Field observations, including geological and structural data, suggest subaerial deposition of the ore.

In fact, San Pietro Island is located on a structural high that was not submerged during the Late Miocene transgression, as indicated by the absence of erosional surfaces or transgressive sediments above the volcanic rocks. The island consists of Miocene volcanic rocks with well-preserved structures indicative of subaerial emplacement (Cioni and Funedda 2005). The Mn mineralization occurs within rhyolitic lavas and within an ignimbritic complex, which Arana et al. (1974) attributed to the final phases of Miocene magmatism (~15 Ma).

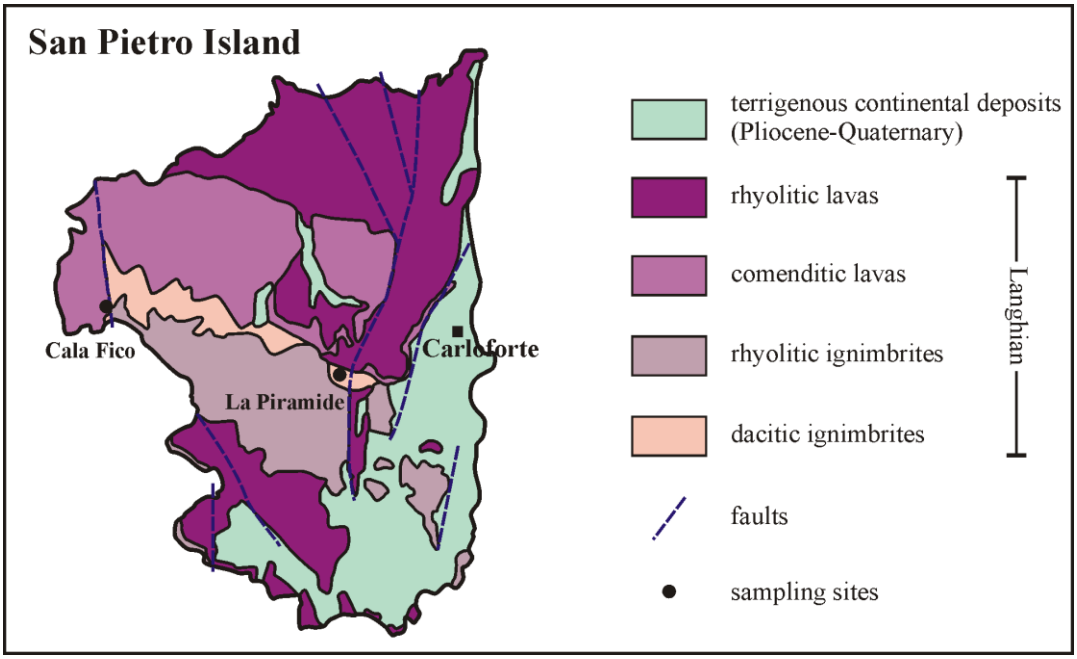

Fig. 3.7 - Geological map of San Pietro Island (after Morra et al. 1994) and sampling sites of *hyd2* and *hyd3* subgroups.

San Pietro Island contains two types of Mn mineralization:

1) in the La Piramide area, mineralization occurs within a welded ignimbrite (hyd2 subgroup) as individual centimeter-wide veins (Fig. 3.8a) and as aggregates which mimic eutaxitic structure (Fig. 3.8b); opal-CT and quartz are the main gangue phases;

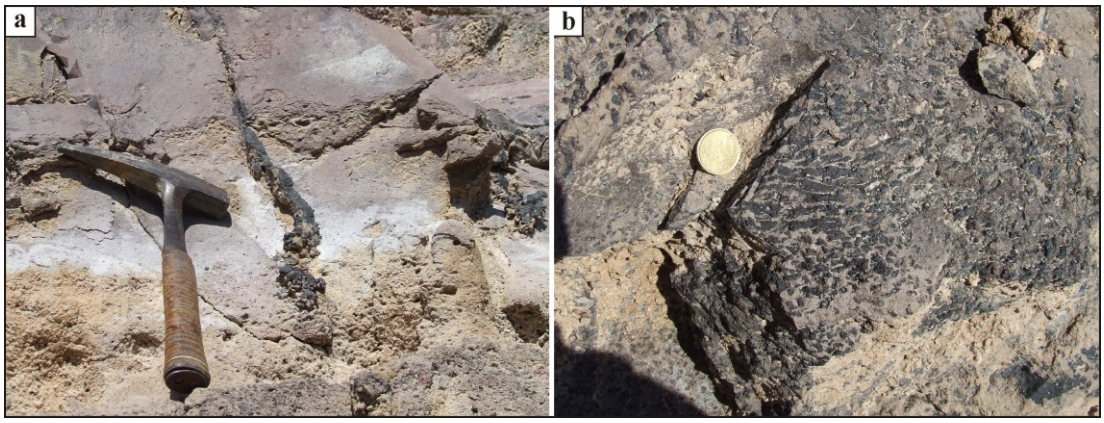

Fig. 3.8 - (a) Centimeter vein-type Mn mineralization and (b) Mn oxyhydroxides aggregates within a welded rhyolitic ignimbrite at La Piramide district (San Pietro Island).

2) in the Cala Fico area, mineralization (hyd3 subgroup) is hosted within comenditic lavas, consisting of vein swarms of massive ore oriented parallel to the main faults and of Mn-rich bands oriented parallel to rheomorphism-related anisotropies (Fig. 3.9). Both types of mineralization are developed along an E–W-striking fault that separates the lower part of the comenditic lava flows from the underlying Matzaccara Ignimbrite unit, both of which are Langhian in age (Cioni and Funedda 2005).

Fig. 3.9 - Mn-rich bands hosted by comendite lavas (*hyd3* mineralizations)

The free wall of fractures contains clinoptilolite as a gangue mineral (Fig. 3.10). The occurrence of zeolite may indicate the presence of slightly alkaline solutions produced by interaction between fluids and alkaline/peralkaline rocks such as rhyolites and comendites (Zhang et al. 2001).

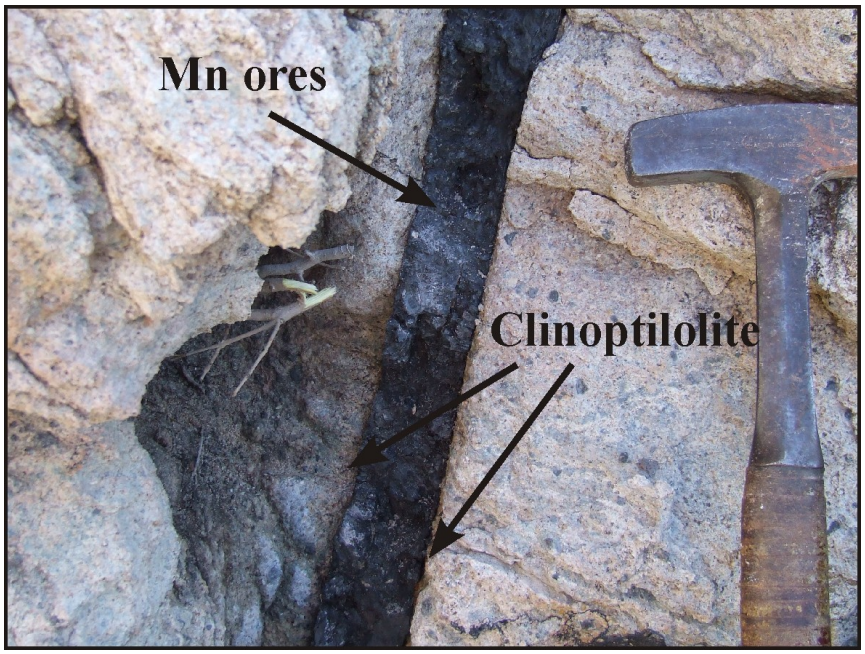

Fig. 3.10 - Fractures within a comendite lavas at Cala Fico area (San Pietro Island). The Mn ores fill the fracture while zeolite constitute the free wall

3.3 Sampling and analytical methods

Nineteen samples of hydrothermal Mn-ores and 18 samples of marine Mn mineralization were subjected to textural, mineralogical and chemical analysis. The unaltered samples were collected from natural exposures or disused mines. Care was taken to prevent contamination of the samples during their collection, transport and subsequent storage. Whole-rock samples were first dried and then reduced to fine powder in a planetary mill equipped with an agate jar and agate milling balls.

The mineralogy of the samples was analyzed from randomly oriented whole-rock powders analyzed at 2°–70° 2θ with a step size of 0.02° 2θ, using a Siemens D5000 diffractometer (Cu-Kα radiation, 40 kV and 30 mA).

The petrography of the samples was studied by optical transmission microscopy (OM), using a binocular microscope, and by scanning electron microscopy (ESEM XL30 Philips LaB6) equipped with an energy-dispersive X-ray spectrometer (SEM–EDS).

The abundances of major and trace elements were determined by inductively coupled plasma-mass spectrometry (ICP-MS) and instrumental neutron activation (INAA) analysis, respectively, at Activation Laboratories, Ancaster, Canada. Average errors were less than ±5%, except for those elements occurring at a concentration of 10 ppm or lower, for which the errors were ±5%–10%. Total loss on ignition (LOI) was gravimetrically estimated after overnight heating at 950° C.

3.4 Results

3.4.1 Mineralogy and texture

3.4.1.1 Marine supergene ores

The paragenesis of the studied ores is dominated by pyrolusite [MnO2] with minor hollandite [$Ba_x(Mn^{4+},Mn^{3+})_6O_{16}$], as found in samples RS4, RS5 and RS8. Todorokite [$(Mg, Ca, Na, K)_x(Mn^{4+},Mn^{3+})_6O_{12}\cdot 3.5H_2O$] and manganite [MnO(OH)] occur as accessory phases in samples RS9 and RS1, and RS3, respectively. Gangue minerals are quartz, calcite, plagioclase and K-feldspar. The XRD data also indicate trace amounts of 2:1 clay minerals in samples RS4, RS5, RS8, RS9, Mn4 and Mn5.

Microscopic examinations reveal that the Mn oxides occur as microcrystalline cement that contains fragments of volcanic material. The texture of the cement varies with the different Mn phases. Samples dominated by pyrolusite are characterized by a heterogeneous texture consisting of large prismatic and acicular pyrolusite crystals (20–60 μm) within a fine matrix of smaller pyrolusite crystals (Fig. 3.11a). In samples with hollandite as the main mineral phase, it occurs as concretions that grow as botryoidal nodules (Fig. 3.11b).

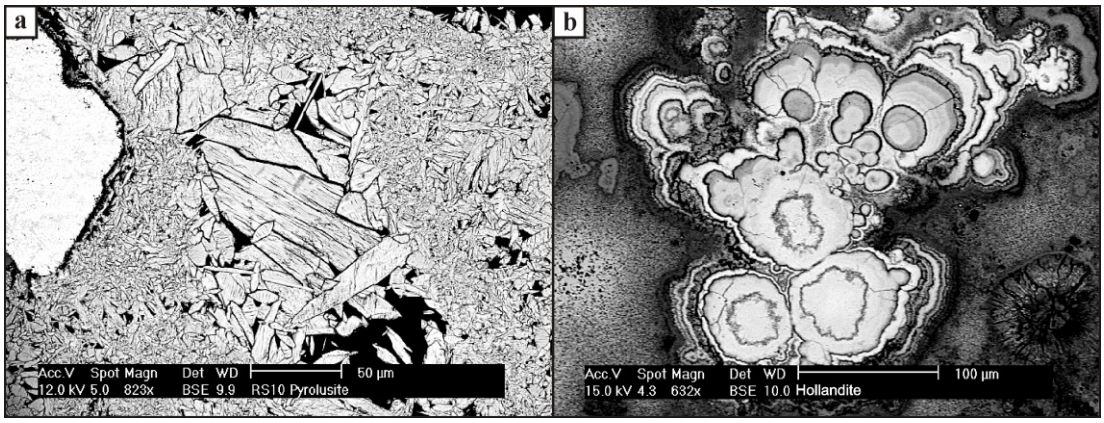

Fig. 3.11 - BSE images showing the non homogeneous pyrolusite texture (a) and the botryoidal hollandite concretion (b) of mar mineralizations

3.4.1.2 Continental hydrothermal ores

Ores from San Pietro Island (hyd2, hyd3) have a different paragenesis to that of the Anglona ore (hyd1). Hyd2 and hyd3 ores consist of pyrolusite, cryptomelane [$K_x(Mn^{4+},Mn^{3+})_8O_{16}$] and hollandite as the main Mn minerals. Coronadite [$Pb_x(Mn^{4+},Mn^{3+})_8O_{16}$] was detected in a sample from the hyd3 subgroup. Micromorphological observations reveal that Mn minerals form a muddy matrix which contains accessory phases such as quartz, plagioclase and K-feldspar. In most of the hyd samples, K-feldspar is intergrown with or replaced by Mn oxides or Fe-bearing phases (Fig. 3.12). Some samples also contain calcite, biotite, chlorite and clinoptilolite.

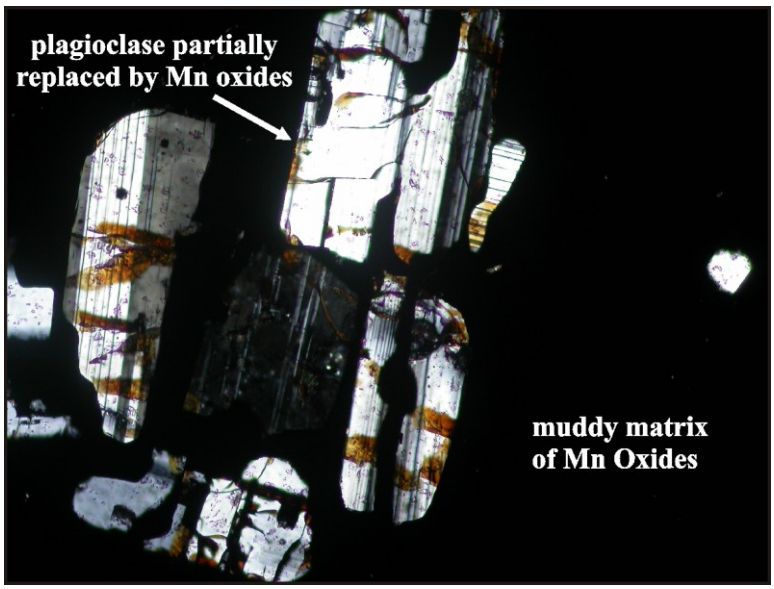

Fig. 3.12 - OM image of a hyd samples composed of K-feldspars partially replaced by Mn phases

The accessory phases detected by EDS microanalyses include sub-euhedral zircon crystals, commonly associated with biotite and fluorapatite, which are probably remnants of the wall rock, and secondary ilmenite and kaolinite. The latter phase appears at the margins of cryptomelane cores, and cryptomelane occurs as pseudomorphs after biotite (Fig. 13).

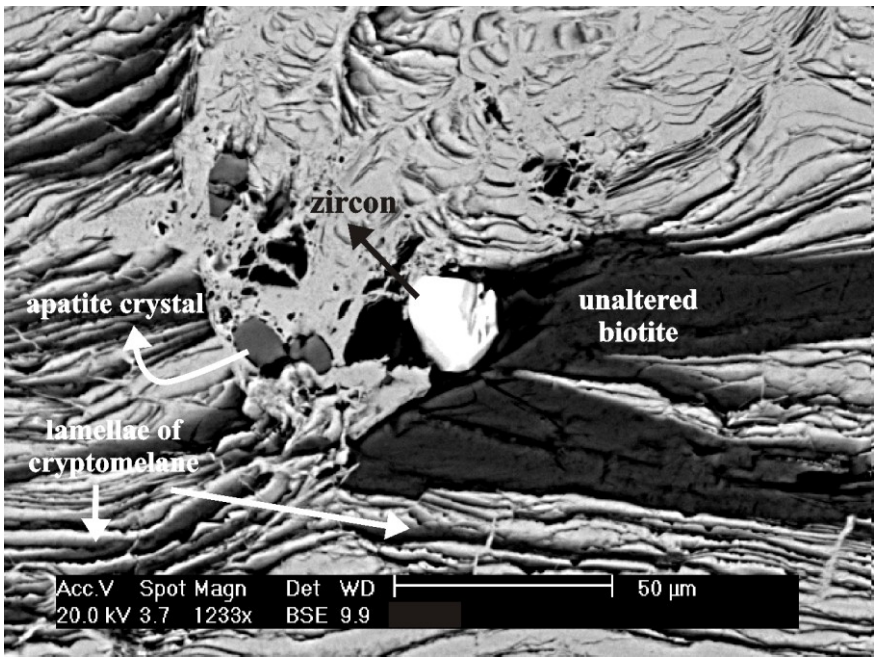

Fig. 3.13 - BSE image showing the biotite lamellae replaced by cryptomelane. Zircon and apatite crystals are also detected

Pyrolusite is the only Mn-phase in the hyd1 subgroup. The mineralization in this area is characterized by opal-CT, feldspar and clinoptilolite, and SEM–EDS analysis reveals the occurrence of baryte (Fig. 14). The observed textural relationships suggest that baryte crystallized in cavities within the massive pyrolusite.

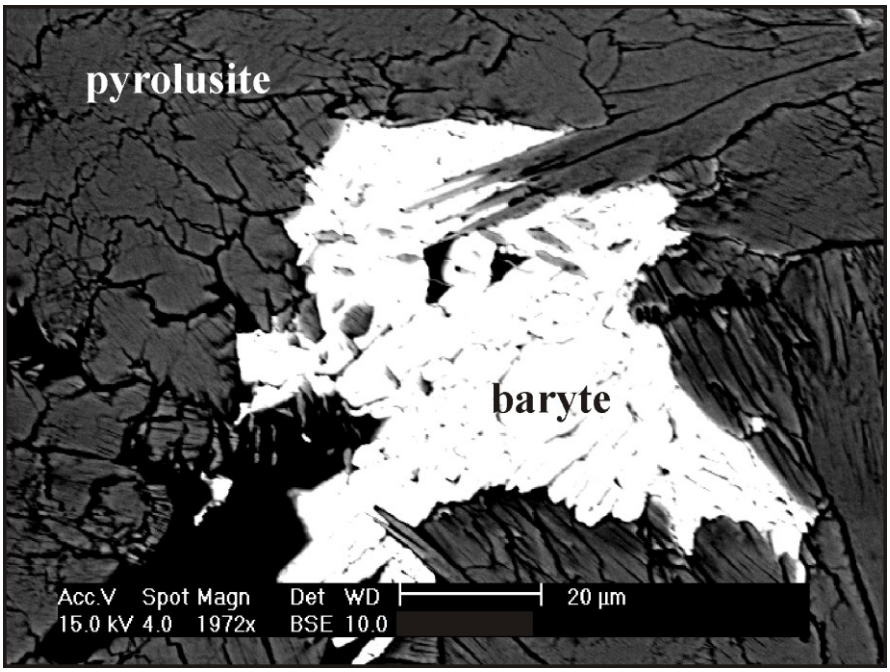

Fig. 3.14 - BSE images of baryte crystallized within cavities of pyrolusite masses

3.4.2 Chemistry

The elemental concentrations of the *mar* and *hyd* Mn-rich ores are given in Tables 3 and 4 (see Appendix 1), respectively. The elemental distributions, normalized to the GLOSS upper continental crust model (Plank and Langmuir 1998), are shown in Figs. 15 and 16.

3.4.2.1 Major elements

The Mn deposits all have Mn contents that are commonly equal to or higher than 100X GLOSS (Fig. 15). However, the *mar* and *hyd* ores show a certain degree of variability due to varying amounts of gangue material. In the hydrothermal ores, the MnO content ranges from 31.16 to 81.67 wt %, in the marine ores, it varies between 4.26 and 80.84 wt %. For the other major elements, the Anglona hydrothermal ores (*hyd1*) are characterized by concentrations lower than standard values, except for P_2O_5, which occurs at concentrations similar to those of the standard.

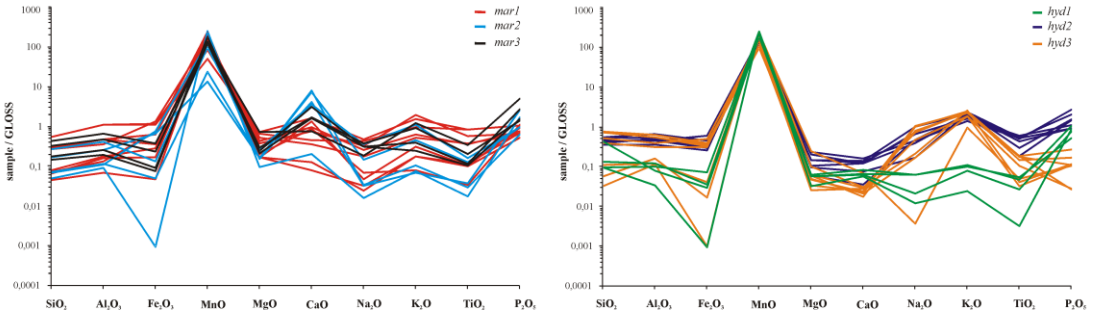

Fig. 3.15 - GLOSS normalized major elements patterns of mar (a) and hyd (b) samples

All the *hyd2* and *hyd3* samples, except for CF6, show moderate enrichments in K_2O (1–2X GLOSS) and moderate depletions in SiO_2, Al_2O_3, Fe_2O_3, Na_2O and TiO_2. MgO and CaO are always depleted relative to the standard values. The P_2O_5 concentrations are highly variable: within *hyd2* ores, the concentrations are similar to or higher than those of GLOSS, whereas they are depleted within *hyd3* samples.

The GLOSS-normalized distribution of major elements in the supergene marine deposits is similar to that in the hydrothermal ores, although most mar samples contain CaO concentrations higher than that in GLOSS, and K_2O concentrations are similar to or lower than that of the standard. The mar samples also show greater variability in SiO_2, Al_2O_3 and Fe_2O_3 than that seen in the hydrothermal ores.

3.4.2.2 Trace elements

The Mn ores of hydrothermal origin show different trace element patterns to those of marine ones. The *hyd2* and *hyd3* samples are characterized by a wide range of trace element contents. Co, Zn, Sr, Y, Ba, Hf, Pb and U are enriched relative to GLOSS, whereas the transition elements (mainly Cr, Sc, Cu and V) are depleted. Rb, Zr, Nb, Cs, Ta and Th are either depleted or enriched, while the Ni content is always comparable to that of the standard. In the *hyd1* samples, large-ion lithophile elements (LILE) and Zn are enriched, whereas most of the high-field strength elements (HFSE) are depleted. Ni concentrations are usually similar to that of GLOSS, whereas Cu is strongly enriched.

At first inspection, the patterns of trace elements in *mar* ores are similar to

those of the Anglona hydrothermal deposits.

The *mar* ores differ from the *hyd2* and *hyd3* ores in terms of their Ni, Zn, Rb, Cu and Ta contents. Indeed, the behavior of these elements in the *mar* samples is the opposite of that in the samples from San Pietro Island (Fig. 16). Of note, V was only detected in hydrothermal samples of the *hyd2* and *hyd3* subgroups.

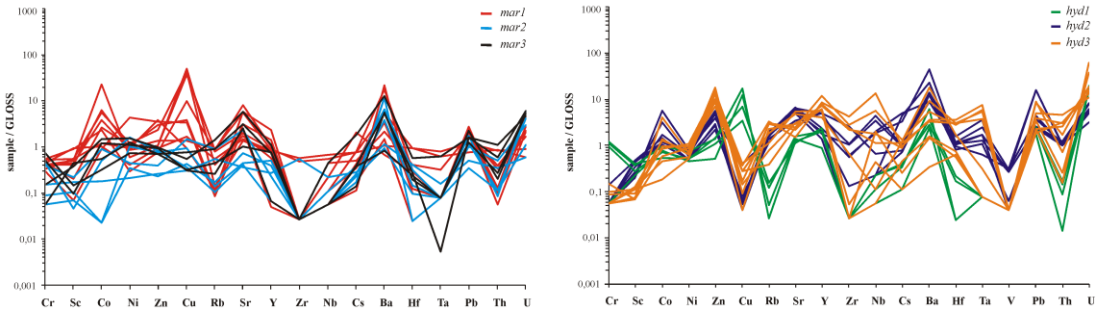

Fig. 3.16 - GLOSS normalized trace elements patterns of mar (a) and hyd (b) samples

3.4.2.3 Rare earth elements

Figure 3.16 shows the chondrite-normalized REE patterns of hydrothermal and marine Mn-ores (Taylor and McLennan 1985). The patterns are different from each other in terms of their shape and concentrations, and differ from patterns reported previously, especially with regard to the average concentrations of REEs in the main Mn deposits worldwide (Toth 1980; Hein et al. 1997; Nath et al. 1997; Maynard 2003; Shah and Moon 2004). REE concentrations in the hydrothermal and marine Mn-ores are extremely high with respect to the reference chondrite, and the hydrothermal ores have ΣREE values (105.02–3309.15) that are several orders of magnitude higher than those of most of the marine deposits (9.86–195.36).

Large negative Eu anomalies are observed in the hydrothermal deposits and Eu/Eu* values range from 0.01 to 0.67. Positive Ce anomalies are observed in *hyd2* ores, whereas most of the *hyd3* and all of the *hyd1* samples have a negative Ce anomaly. Most of the *hyd1* and *hyd2* ores have (La/Yb)ch values (6.96–8.52, except for LP3 = 4.13, RS18 = 4.51 and LP5 = 9.84) similar to that of GLOSS (7.1), whereas the LREE/HREE fractionation index in the *hyd3* ores is

highly variable (10.23 < $(La/Yb)_{ch}$ < 47.11).

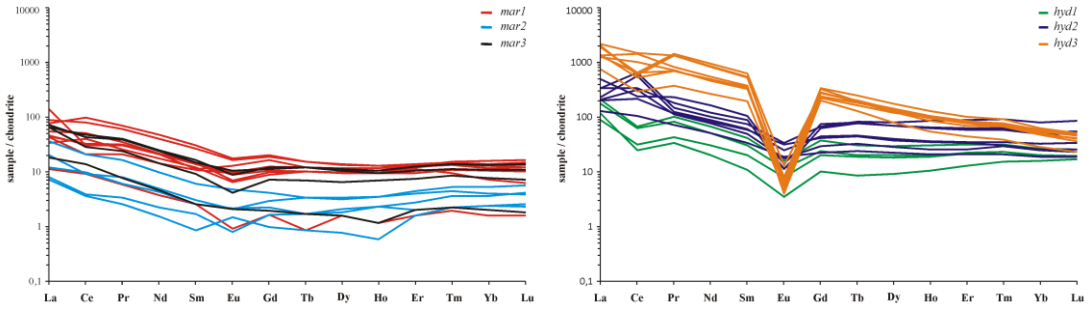

Fig. 3.16 - Chondrite normalized REE patterns of mar (a) and hyd (b) samples

The *mar* samples contain both negative and positive Ce anomalies (0.36 < Ce/Ce* < 1.39), and generally show a negative Eu anomaly. The $(La/Yb)_{ch}$ ratio varies from 2.13 to 9.19 (although sample RS10 yielded a value of 19.03).

3.5 Discussion

3.5.1 Marine Mn mineralization

Redox-controlled processes govern Mn behavior in the sedimentary environment. Diagrams showing the Eh–pH relation (e.g., Brookins 1988; Takeno 2005) indicate a relatively large stability field for dissolved Mn^{2+} compared with that for solid oxides, which precipitate, at a given value of dissolved Mn^{2+} activity, in an alkaline environment. The mineralogical association of Mn-phases in manganiferous deposits does not allow the unique identification of the depositional environment, because many of the Mn^{4+} oxides occur under a wide range of conditions. Consequently, none of the minerals within the supergene deposits can be used to distinguish marine from continental mineralization (Nicholson 1992). In addition, mineral assemblages similar to those of the Sardinian deposits have been documented in mineralization related to both marine solutions (El-Hasan et al. 2008) and hydrothermal fluids (Post 1999; Glasby et al. 2005; Fitzgerald and Gillis 2006).

Regardless of the depositional environment and processes, the present Mn oxides are characterized by high surface charge, which influences the mineralogy

and geochemistry of Mn deposits. Murray (1975) and Nicholson and Eley (1997) argued that the adsorption of elements onto the surface of Mn oxides is the main process leading to the accumulation of cations (mainly heavy metals) in Mn deposits.

The pH of the solution also influences the adsorption mechanism: the adsorption capacity of Mn oxides increases with increasing pH (Nicholson and Eley 1997). In alkaline water, such as seawater, Mn oxides mainly absorb onto the surface cations dissolved in solution, resulting in the enrichment of economic transition metals, particularly Cu, Ni, Co, Zn, Ba and Pb in Mn-rich marine sediments (Koschinsky et al. 2003; Maynard 2003).

Adsorption is unlikely to be the only mechanism of including trace elements within Mn minerals. Other processes must be considered, including replacement through ion exchange and co-precipitation with Mn oxides (Koschinsky and Hein 2003). These mechanisms typically occur in the presence of Mn minerals with a tunnel crystal structure (Chen et al. 2009; Randall et al. 1998).

Pyrolusite, hollandite and todorokite, which are the main Mn phases in the studied marine ores, are characterized by a tunnel structure (Post 1999) consisting of MnO6 octahedra units shared by apexes or edges. In pyrolusite, single chains of edge-sharing MnO6 octahedra share corners with adjacent chains to form a framework structure containing tunnels of ~2.3 Å in diameter. The crystal structure of hollandite consists of two double edge-sharing MnO6 octahedral chains which share vertices to form tunnels with a square cross-section with a width twice that of tunnels in pyrolusite (~4.6 Å; Post et al. 1982; Miura 1986). The structure of todorokite consists of triple chains of edge-sharing MnO6 octahedra that form the largest tunnels among the Mn minerals, with a square tunnel cross-section. Tunnels within pyrolusite are too small to accommodate other chemical species (Kijima et al. 2009), but those within hollandite and todorokite are usually filled with large monovalent or divalent cations (mainly K^+, Ba^{2+}, Sr^{2+}, Pb^{2+} and Na^+) and water molecules (Post and Burnham 1986; Lei 1996). Therefore, the occurrence of these minerals in the marine Mn mineralization of Sardinia may explain in part the high contents of certain alkali and alkaline earth metals that also occur in other minerals such as feldspars. Unlike pyrolusite, todorokite can accommodate in its structure both Mn^{3+} and Mn^{4+} ions, indicating that the precipitation of todorokite and pyrolusite occurs from solutions characterized by different redox conditions.

The large availability of dissolved ions in solution may also affect the mineralogy of Mn oxides (Nahon et al. 1983), promoting the precipitation of todorokite in some of the mineralized areas. Furthermore, the absence of calcite in samples containing todorokite suggests that this mineral played a significant role in the removal of Ca from solution.

The occurrence of manganite requires a separate discussion. Although it is metastable, manganite is the most stable of the Mn^{3+} oxyhydroxides in a supergene environment. As with the other Mn oxides, manganite is ubiquitous, occurring as a weathering product from parent rocks of varying origin and mineralogy (Nahon et al. 1983), or, as is most likely in the present case, as an authigenic mineral formed during the initial stages of oxidation of dissolved Mn^{2+} (Roy 2006). Accordingly, the precipitation of manganite requires a solution with lower Eh values than those from which pyrolusite forms (Takeno 2005). In addition, the crystal structure of manganite is similar to that of pyrolusite (Post 1999), indicating a similar ability to uptake cations.

Marine Mn deposits contain high concentrations of As, Sb and U. The behavior of As and Sb depends largely on redox conditions. Because of their similar chemistry, these elements form similar aqueous species, complexes and minerals. Previous studies have argued that isomorphic replacement, adsorption, and oxidization processes may be responsible for the uptake of these trace elements in Mn ores (Ouvrard et al. 2005; Mohapatra et al. 2006; Landrum et al. 2009). This proposal is supported by the weak correlation between S and each of As and Sb in the studied ores (As versus S: $r = 0.14$; Sb versus S: $r = -0.19$). The SEM–EDS observations showed no evidence of a uranium phase, hence the adsorption mechanism exerted by Mn-oxides is probably responsible for the uranium enrichment observed in marine deposits (Koppi et al. 1996; Webb et al. 2006).

Algeo and Tribovillard (2009) suggested that the amount of uranium in marine sediments, coupled with the Mo content, provides useful information on the redox conditions of the depositional environment. Under oxic–suboxic conditions, both U and Mo are largely unreactive, occurring as uranyl carbonate complexes and molybdate oxyanion, respectively, meaning that their enrichment in sediment is limited. In contrast, under anoxic conditions, sediments can easily uptake U and Mo (Algeo and Tribovillard 2009, and references therein).

However, the onset of U enrichment occurs under less-intensely reducing conditions (Morford et al. 2009), meaning that the pattern of covariation in molybdenum and uranium within sediments can be used to infer the redox conditions (Algeo and Tribovillard 2009).

As shown in Fig. 18a, the *mar* samples of the present study plot in several different areas in the Mo/U diagram, indicating that differences in palaeo-redox conditions are probably related to variations in the concentrations of organic matter in the depositional environment. The *mar1* and *mar3* samples have Mo/U values that generally differ from the typical seawater value, and were deposited in a transitional environment characterized by shallow and probably oxygen-poor waters. In contrast, the mar2 samples have Mo/U values comparable to those of seawater, indicating their formation in an open shelf environment (Fig. 18b).

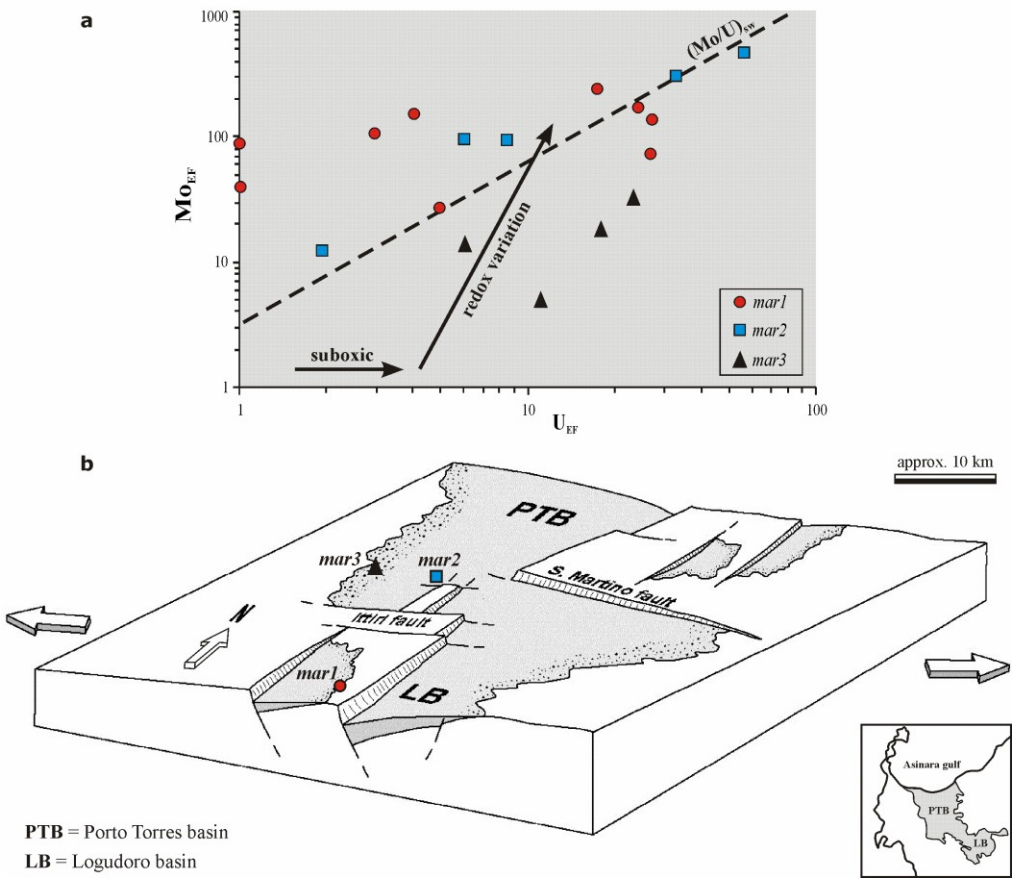

Fig. 3.18 - (a) Mo/U diagram related to mar mineralizations (after Algeo & Tribovillard 2009). The different samples distribution reflect the redox conditions of different depositional environments shown in (b)

Among the trace elements, REEs may also be adsorbed onto the surface of Mn oxides (Toth 1980; Fodor et al. 1994; Koppi et al. 1996). REE geochemistry has been widely used to estimate the redox conditions of marine depositional environments and sedimentary processes (Hein et al. 1997; Dia et al. 2000). The concentrations and distribution patterns of REEs may indicate a change in the redox potential of the solution and could be linked to changes in the sorption properties of solid phases (El-Hasan et al. 2008).

However, REEs are relatively immobile, resulting in low REE contents in seawater (e.g., Temple and Walsh 1994). Thus, the weak correlations observed between MnO and REEs in the present study (MnO versus La: r = –0.02; MnO versus Eu: r = –0.10; MnO versus Yb: r = 0.07) suggest that the very fine detrital component trapped within the ore yield most of the REEs in the Sardinian Mn mineralization of marine origin.

3.5.2 Hydrothermal Mn mineralization

The chemical signatures of the continental hydrothermal Mn mineralization examined in the present study are markedly different from those of the widespread and better-known marine hydrothermal Mn ores which commonly occupy the ocean floor near hydrothermal vents. Mn crusts related to hydrothermal vents are characterized by very low values of Mn/Fe, high SiO_2/Al_2O_3 values, extremely low concentrations (ppb) of transition metals, low ΣREE contents, and a strongly negative Ce anomaly (Bonatti et al. 1972; Toth 1980; Nath et al. 1997). These values are different to those obtained for the hydrothermal Mn mineralization at Sardinia, indicating contrasting origins for the two types of ores.

Few studies have examined hydrothermal Mn-rich vein mineralization precipitated within a continental environment (e.g., O'Reilly 1992). Nevertheless, several models have been proposed to explain the origin of the fluid in such a setting and its evolution (Robb 2005, and reference therein). Among the models, the mixing of magmatic fluids with meteoric water at shallow levels in the crust appears most relevant to the geological setting of the Sardinian vein-type Mn ores. The high concentrations of some significant trace elements, such as W, Mo, Cu, Be, U and Pb, in the studied ores suggest that the mineralizing fluid was magmatic in origin (O'Reilly 1992).

The dilution and cooling of magmatic fluids, and mixing with surface waters, are common phenomena in geological contexts favorable to the development of hydrothermal convective cells during and after magma emplacement (Mangas and Arribas 1988). During convection, the heated fluid may be enriched in metals and other trace elements leached from the host rocks. The high concentrations of trace elements in the Sardinian deposits suggest they formed from a solution previously enriched in such elements. Abrupt changes in the physical and chemical conditions of the mineralizing solution may result in the precipitation of ore and the sequential fractionation of elements between the fluid and minerals. Fractionation may occur not only by mineral precipitation but also by particle scavenging, which is significant in the presence of Mn oxy-hydroxides (Nicholson and Eley 1997; Mohapatra et al. 2009). Consequently, the high adsorption capacity onto Mn oxides surface and high cations uptake into the crystal structure likely play a key role in the hydrothermal environments as much as in supergene ones. These geochemical properties of Mn ores, combined with the lack of mineral phases that contain high concentrations of Co, Cu, Zn, Sb and As, could explain the high contents of these elements in the *hyd* samples. Conversely, the high contents of K, Ba and Pb may reflect the partitioning of these elements into the lattices of cryptomelane, hollandite and coronadite, respectively.

The subgroups of Sardinian hydrothermal mineralization show some differences in chemical composition. The Anglona ores (*hyd1*) have high Cu contents compared with *hyd2* and *hyd3*, possibly reflecting the presence of a hydrothermal fluid that was previously enriched in Cu during interaction with Cu porphyry, which is widespread in NW Sardinia. We also observed differences in the REE patterns of samples from Anglona and from San Pietro Island. The concentrations and distribution of REEs in the Anglona samples, as well as Eu anomalies, are comparable to those of andesitic lava, suggesting the mineralizing solution retained the chemical features of the rocks through which it migrated. The negative Ce anomalies in these ores, as well as those observed in the *hyd3* ores, may indicate oxidizing conditions for the fluids, which promoted Ce depletion prior to Mn mineralization. Furthermore, the *hyd3* ores have high REE contents, high LREE/HREE values and strongly negative Eu anomalies, which may reflect the chemical features of a fluid related to the highly evolved comenditic lava.

The moderate Eu anomalies and flat REE patterns observed in the *hyd2* subgroup may indicate a fluid related to the less-evolved rhyolitic ignimbrite.

3.6 Summary and conclusions

This paper reported, for the first time, detailed mineralogical and chemical data regarding supergene and hydrothermal Mn mineralization at Sardinia, yielding the following findings.

1- With several exceptions, the two types of mineralization in Sardinia contain two main Mn-phases: pyrolusite and hollandite. In greater detail, the marine supergene group comprises pyrolusite, hollandite, manganite and todorokite as Mn-phases, and calcite and clay minerals as accessory phases. The continental hydrothermal mineralization consists of pyrolusite, hollandite, cryptomelane and coronadite as Mn-phases, and quartz, opal-CT and baryte as gangue minerals.

2- Both the supergene and hydrothermal Mn deposits are characterized by highly variable chemical compositions. Relative to GLOSS, most of the samples are enriched in As, Co, Zn, Sr, Ba, Pb and U, regardless of mineralogy. This finding suggests that the Mn oxides had an influence on trace element behavior in both deposits. Previous studies have proposed that metal enrichment occurs via adsorption, cations exchange and co-precipitation reactions. This view is supported by SEM–EDS observations in the present study, because the trace elements are not associated with a specific mineral phase; instead, they are homogenously distributed throughout the ores samples. The two types of deposit also show clear chemical differences, especially in terms of REE patterns. Compared with the supergene deposits, the hydrothermal deposits have higher values of total REE content, a higher degree of fractionation between LREEs and HREEs, and larger Eu anomalies. These differences are related to the compositional diversity of the solutions from which the ore minerals formed rather than to the contrasting uptake capacities of the various Mn phases.

3- Based on chemical and mineralogical data, and field observations, we propose that the *mar* deposits formed during a marine transgression when continental waters rich in Mn and trace elements reached the shore, mixing with relatively high-pH marine waters and inducing the sudden precipitation of Mn oxyhydroxides. The redox conditions vary among the subsets, from oxic–suboxic

to weakly reducing, as indicated by Mo/U values.

The *hyd* ores originated from the mixing of magmatic fluids and meteoric waters, as indicated by field observations and chemical data. Additional isotope-based studies are required to clarify the nature of the Mn-bearing fluids.

REFERENCES

ALGEO T.J. AND TRIBOVILLARD N. (2009) – *Environmental analysis of paleoceanographic systems based on molybdenum-uranium covariation*. Chemical Geology, 268, 211-225.

ARANA V., BARBERI F. AND SANTACROCE R. (1974) – *Some data of comenditic type aea (S. Pietro and S. Antioco Islands, Sardinia)*. Bulletin Volcanologique, 38, 725-736.

BALE C.W., CHARTRAND P., DEGTEROV S.A., ERIKSSON G., HACK K., BEN MAHFOUD R., MELANÇON J., PELTON A.D. AND PETERSEN S. (2002) – *FactSage Thermochemical Software and Databases*. Calphad, 26 (2), 189-228.

BECCALUVA L., COLTORTI M., PREMTI I., SACCANI E., SIENA F. AND ZEDA O. (1994) – Mid-Ocean ridge and suprasubduction affinities in the ophiolitic belts of Albania. Ofioliti, 19, 77-96.

BONATTI E., KRAMER T. AND RYDELL H. (1972) – *Classification and genesis of sub-marine iron manganese deposits*. In: Ferromanganese Deposits on the Ocean Floor, D. Horn Eds, National Science Fundation, Washington, D.C., 146-165.

BROOKINS D.G. (1988) – *Eh-pH diagrams for geochemistry*. Springer-Verlag, Berlin.

BRUGGER J. AND MEISSER N. (2006) – *Manganese-rich assemblages in the Barrhorn Unit, Turtmanntal, central Alps, Switzerland*. The Canadian Mineralogist, 44, 229-248.

CARMIGNANI L., DECANDIA F.A., DISPERATI L., FANTOZZI P.L., LAZZOROTTO A., LIOTTA D. AND OGGIANO G. (1995) – *Relationship between the Tertiary structural evolution of the Sardinia-Corsica-Provençal Domain and the Northern Apennines*. Terra Nova, 7, 128-137.

CARMIGNANI L., OGGIANO G., BARCA S., CONTI P., SALVADORI I., ELTRUDIS A., FUNEDDA A. AND PASCI S. (2001) – *Geologia della Sardegna. Note illustrative della Carta Geologica della Sardegna a scala 1:200000*. In: Memorie descrittive della Carta Geologica d'Italia, vol. LX, 271 pp.

CHEN T., DOU H., LI X., TANG X., LI J. AND HAO J. (2009) – *Tunnel structure effect of manganese oxides in complete oxidation of formaldehyde*. Microporous and Mesoporous Materials, 122, 270-274.

CIONI R. AND FUNEDDA A. (2005) – *Structural geology of crystal-rich, silicic lava flows: a case study from San Pietro Island (Sardinia, Italy)*. Geological Society of America, Special Paper, 396, 1-14.

DE BOORDER H., SPAKMAN W., WHITE S.H. AND WORTEL M.J.R. (1998) – *Late Cenozoic mineralization, orogenic collapse and s detachment in the European Alpine Belt*. Earth and Planetary Science Letters, 164, 569-575.

DELLA VEDOVA B., LUCAZEAU F., PASQUALE V., PELLIS G. AND VERDOJA M. (1995) – *Heat flow in the tectonic provinces crossed by the southern segment of the European Geotraverse*. Tectonophysics, 244, 57-74.

DIA A., GRUAU G., OLIVIÉ-LAUQUET G., RIOU C., MOLÉNAT J. AND CURMI P. (2000) – *The distribution of rare earth elements in groundwaters: assessing the role of source-rock composition, redox changes and colloidal particles*. Geochimica et Cosmochimica Acta, 64 (24), 4131-4151.

DOWNES H., THIRLWALL M.F. AND TRAYHORN S.C. (2001) – *Miocene subduction-related magmatism in southern Sardinia: Sr–Nd- and oxygen isotopic evidence for mantle source enrichment*. Journal of Volcanology and Geothermal Research, 106 (1-2), 1-22.

EL-HASAN T., AL-MALABEH A. AND KOMURO K. (2008) - *Rare Earth Elements Geochemistry of the Cambrian Shallow Marine Manganese Deposit at Wadi Dana, South Jordan*. Jordan Journal of Earth and Environmental Sciences, 1, 45-52.

FAN D. AND YANG P. (1999) – *Introduction to and classification of manganese deposits of China*. Ore Geology Reviews, 15, 1-13.

FITZGERALD C.E. AND GILLIS K.M. (2006) - *Hydrothermal manganese oxide deposits from Baby Bare seamount in the Northeast Pacific Ocean*. Marine Geology, 225, 145-156.

FODOR R.V., JACOBS R.S. AND BAUER G.R. (1994) – *Hollandite in Hawaiian basalt: a relocation site for weathering-mobilized elements*. Mineralogical Magazine, 58, 589-596.

FUNEDDA A., OGGIANO G. AND PASCI S. (2000) – *The Logudoro basin: a key area for the terziary tectono-sedimentary evolution of North Sardinia*. Boll. Soc. Geol. It., 119, 31-38.

GLASBY G.P., CHERKASHOV G.A., GAVRILENKO G.M. RASHIDOV V.A. AND SLOVTSOV I.B. (2006) – *Submarine hydrothermal activity and mineralization on the Kurile and western Aleutian island arcs, N.W. Pacific*. Marine Geology, 231,163-180.

GLASBY G.P., PAPAVASSILIOU C.T., MITSIS J., VALSAMI-JONES E., LIAKOPOULOS A. AND RENNER R.M. (2005) - *The Vani manganese deposit, Milos island, Greece: A fossil stratabound Mn−Ba−Pb−Zn−As−Sb−W-rich hydrothermal deposit*. Developments in Volcanology, 7, 255-291.

HEIN J.R., KOSCHINSKY A., HALBACH P., MANHEIM F.T., BAU M., KANG J.K., LUBICK N. (1997) – *Iron and manganese oxide mineralization in the Pacific*. In: Nicholson K., Hein J.R., Bühn B. and Dasgupta S. (Eds.), Manganese Mineralization: Geochemistry and Mineralogy of Terrestrial and Marine Deposits. Geological Society of London, Special Publication, 119, 123-138.

KIJIMA N., SAKATA Y., TAKAHASHI Y., AKIMOTO J., KUMAGAI T., IGARASHI K. AND SHIMIZU T. (2009) – *Synthesis and lithium ion insertion/extraction properties of hollandite-type MnO2 prepared by acid digestion of Mn_2O_3*. Solid State Ionics, 180, 616–620.

KOPPI A.J., EDIS R., FIELD D.J., GEERING H.R., KLESSA D.A. AND COCKAYNE D.J.H. (1996) – *Rare earth elements trends and cerium-uranium-manganese associations in weathered rock from Koongarra, Northern Territory, Australia*. Geochimica et Cosmochimica Acta, 60 (10), 1695-1707.

KOSCHINSKY A. AND HEIN J.R. (2003) – *Uptake of elements from seawater by ferromanganese crusts: solid-phase associations and seawater speciation*. Marine Geology, 198, 331-351.

KOSCHINSKY A., WINKLER A. AND FRITSCHE U. (2003) – *Importance of different types of marine particles for the scavenging of heavy metals in the deep-sea bottom water*. Applied Geochemistry, 18, 693–710.

LANDRUM J.T., BENNETT P.C., ENGEL A.S., ALSINA M.A., PASTÉN P.A. AND MILLIKEN K. (2009) – *Partitioning geochemistry of arsenic and antimony, El Tatio Geyser Field, Chile*. Applied Geochemistry, 24, 664–676.

LEI G. (1996) – *Crystal structures and metal uptake capacity of 10Å-manganates: An overview*. Marine Geology, 133, 103- 112.

LIAKOPOULOS A., GLASBY G.P., PAPAVASSILIOU C.T. AND BOULEGUE J. (2001) – *Nature and origin of the Vani manganese deposit, Milos, Greece: an overview*. Ore Geology Reviews, 18, 181-209.

MANGAS J. AND ARRIBAS A. (1988) – *Hydrothermal fluid evolution of the Sn-W mineralization in the Parrilla ore deposit (Caceres, Spain)*. Journal of the Geological Society, 145, 147-155.

MARTINI I.P., OGGIANO G. AND MAZZI R. (1992) – *Siliciclastic-carbonate sequences of Miocene grabens of Northern Sardinia, Western Mediterranean Sea*. Sedimentary Geology, 76, 63-78.

MALINVERNO A. AND RYAN W.B.F. (1986) – *Extension in the Tyrrhenian Sea and shortening in the Apennines as results of arc migration driven by sinking of the lithosphere*. Tectonics, 5, 227-245.

MAYNARD J.B. (2003) – *Manganiferous Sediments, Rocks and Ore. In: Treatise on Geochemistry: meteorites, comets and planets*. Elsevier Lid., 1, 289-308.

MAYNARD J.B. (2010) – *The Chemistry of Manganese Ores through Time: A Signal of Increasing Diversity of Earth-Surface Environments*. Economic Geology, 105, 535-552.

MIURA H. (1986) – *The crystal structure of hollandite*. Mineralogical Journal, 13 (3), 119-129.

MOHAPATRA D., MISHRA D., CHAUDHURY G.R. AND DASB R.P. (2006) – *Effect of dissolved organic matter on the adsorption and stability of As(V) on manganese wad*. Separation and Purification Technology, 49, 223–229.

MORFORD J.L., MARTIN W.R. AND CARNEY C.M. (2009) – *Uranium diagenesis in sediments underlying bottom waters with high oxygen content*. Geochim. Cosmochim. Acta 73, 2920-2937.

MORRA V., SECCHI F. AND ASSORGIA A. (1994) – *Petrogenetic significance of peralkaline rocks from Cenozoic calc-alkaline volcanism from SW Sardinia, Italy*. Chemical Geology, 118, 109-142.

MURRAY J.W. (1975) – *The interaction of metal ions at the manganese dioxide-solution interface*. Geochim. Cosmochim. Acta, 39, 505-519.

NAHON D., BEAUVAIS A., BOEGLIN J.L., DUCLOUX J. AND NZIENGUI-MAPANGOU P. (1983) – *Manganese formation in the first stage of the lateritic manganese ores in Africa*. Chemical Geology, 40, 25-42.

NATH B.N., PLÜGER W.L. AND ROELANDTS I. (1997) – *Geochemical constraints on the hydrothermal origin of ferromanganese encrustations from the Rodriguez Triple Juntion, Indian Ocean*. In: Manganese Mineralization: Geochemistry and Mineralogy of Terrestrial and Marine Deposits, Nicholson K., Hein J.R., Bühn B. and Dasgupta S. Eds., Geological Society Special Publication, 119, 199-211

NICHOLSON K. (1992) – *Contrasting Mineralogical-Geochemical Signatures Of Manganese-Oxides: Guides To Metallogenesis*. Economic Geology, 87, 1253-1264.

NICHOLSON K. AND ELEY M. (1997) - *Geochemistry of manganese oxides: metal adsorption in freshwater and marine environments*. In: Nicholson K., Hein J., Bühn B., Dasgupta S. (Eds.), Geochemistry of manganese oxides: metal adsorption in freshwater and marine environments. Geological Society of London, Special Publications, 119, 309-326.

OGGIANO G., FUNEDDA A., CARMIGNANI L. AND PASCI S. (2009) – *The Sardinia-Corsica microplate and its role in the Northern Apennine Geodynamics: new insights from the Tertiary intraplate strike-slip tectonics of Sardinia*. Ital. Jour. Geosciences, 128, 527-539.

O'REILLY G.A. (1992) – *Petrographic and Geochemical Evidences for a Hypogene Origin of Granite-Hosted, Vein-Type Mn Mineralization at New Ross Mn Deposits, Lunenburg Country, Nova Scotia, Canada*. Economic Geology, 87, 1275-1300.

OUDET J., Münch Ph., Verati C., Ferrandini M., Melinte-Dobrinescu M., Gattacceca J., Cornée J.-J., Oggiano G., Quillévéré F., Borgomano J., Ferrandini J. (2010) – *Integrated chronostratigraphy of an intra-arc basin: 40Ar/39Ar datings, micropalaeontology and magnetostratigraphy of the early Miocene Castelsardo basin (northern Sardinia, Italy)*. Palaeogeography, Palaeoclimatology, Palaeoecology, 295, 293-306.

OUVRARD S., DE DONATO PH., SIMONNOT M.O., BEGIN S., GHANBAJA J., ALNOT M., DUVAL Y.B., LHOTE F., BARRES O. AND SARDIN M. (2005) – *Natural manganese oxide: combined analytical approach for solid characterization and arsenic retention*. Geochimica et Cosmochimica Acta, 69 (11), 2715-2724.

PLANK T. AND LANGMUIR C.H. (1998) – *The chemical composition of subducting sediment and its composition for the crust and mantle*. Chemical Geology, 145, 325-394.

POST J.E. (1999) - *Manganese oxide minerals: crystal structures and economic and environmental significance*. Proc. Natl. Acad. Sci. USA, 96, 3447-3454.

POST J.E., DREELE R.B. AND BUSECK P.R. (1982) – *Symmetry and cation displacements in hollandites: structure refinements of hollandite, cryptomelane and priderite*. Acta Crystallographica, B38, 1056-1065.

POST J.E. AND BURNHAM C.W. (1986) – *Modeling tunnel-cation displacements in hollandites using structure-energy calculations*. American Mineralogist, 71, 1178-1185.

RANDALL S.R., SHERMAN D.M. AND RAGNARSDOTTIR K.V. (1998) – *An extended X-ray absorption fine structure spectroscopy investigation of cadmium sorption on cryptomelane (KMn_8O_{16})*. Chemical Geology, 151, 95-106.

ROBB L. (2005) – *Introduction of ore-forming processes*. Blackwell Science Ltd, 377 pp..

ROY S. (1981) – *Manganese Deposits*. Academic Press, London. 458 pp.

ROY S. (1992) – *Environments and processes of manganese deposition*. Economic Geology, 87, 1218-1236.

ROY S. (1997) – *Genetic diversity of manganese deposition in the terrestrial geological record*. In: Nicholson K., Hein J., Bühn B., Dasgupta S. (Eds.), Manganese Mineralisation: Geochemistry and Mineralogy of Terrestrial and Marine Deposits. Geological Society of London, Special Publication, 119, 5-27.

ROY S. (2006) – *Sedimentary manganese metallogenesis in response to the evolution of the Earth system*. Earth Science Reviews, 77, 273-305.

SERRI G., INNOCENTI F. AND MANETTI P. (1993) – *Geochemical and petrological evidence of the subduction of delaminated adriatic continental lithosphere in the genesis of the neogene quaternary magmatism of central Italy*. Tectonophysics, 223 (1-2), 117-147.

SHAH M.T. AND MOON C.J. (2004) – *Mineralogy, geochemistry and genesis of the ferromanganese ores from Hazara area, NW Himalayas, northern Pakistan*. Jour. of Asian Earth Sciences, 23, 1-15.

SHAH M.T. AND MOON C.J. (2007) – *Manganese and ferromanganese ores from different tectonic settings in the NW Himalayas, Pakistan*. Jour. of Asian Earth Sciences, 29, 455-465.

SILLITOE R.H. (1997) – *Characteristics and controls of the largest porphyry copper–gold and epithermal gold deposits in the circum-Pacific region*. Australian Journal of Earth Sciences, 44, 373-388.

TAKENO N. (2005) – *Atlas of Eh-pH diagrams. Intercomparison of thermodynamic databases*. Geological Survey of Japan, 419, 285 pp.

TAYLOR S.R. AND MCLENNAN S.M. (1985) – *The Continental Crust: Its Composition and Evolution*. Blackwell, Oxford.

TEMPLE J.T. AND WALSH J.N. (1994) – *Use of element-mineral correlations to investigate fractionation of rare earth elements in fine-grained sediments*. Mineralogical Magazine, 58 (4), 533-541.

TOTH J.R. (1980) – *Deposition of submarine crusts rich in manganese and iron*. Geological Society of America Bullettin, 91 (1), 44-54.

VIGLIOTTI L. AND LANGENHEIM V.E. (1995) – *When did Sardinia stop rotating? New paleomagnetic results*. Terra Nova, 7, 424-435.

WEBB S.M., FULLER C.C., TEBO B.M. AND BARGAR J.R. (2006) – *Determination of uranyl incorporation into biogenic manganese oxides using x-ray absorption spectroscopy and scattering*. Environ. Sci. Technol., 40, 771-777.

ZHANG S., ZHAO P., XU Z., ZHENG M. (2001) – *Water/Rock Interactions and Changes in Chemical Composition during Zeolite Mineralization*. Chinese Journal of Geochemistry, 20, 226-232.

APPENDIX 1

CHEMICAL DATA

I.a **TABLE 1 – Chemical composition of Nurra Ironstones (HI and SI subsets)**

SAMPLE	HI	HI1	HI2	HI3	HI4	HI5	HI6	HI7	HI8	HI9	HI10	SI1	SI2	SI3	SI4	SI5	SI6	SI7	SI8	SI9	SI10	SI6N
wt. %																						
SiO_2	8,23	14,94	6,19	9,44	6,99	9,56	7,07	12,13	3,30	9,09	10,93	42,66	31,21	41,82	44,56	37,30	45,76	32,21	41,08	39,89	37,93	33,11
TiO_2	0,40	0,21	0,24	0,36	0,26	0,31	0,23	0,33	0,22	0,38	0,57	0,58	0,61	0,58	0,53	0,60	0,52	0,58	0,54	0,51	0,60	0,58
Al_2O_3	8,73	13,13	6,46	9,18	6,05	9,32	5,01	7,35	4,70	8,98	11,13	14,27	14,65	12,50	11,74	14,33	12,65	14,84	15,59	14,37	13,66	14,23
Fe_2O_3	57,23	26,97	71,04	52,59	68,80	52,41	61,33	46,50	69,11	58,77	56,45	30,56	38,65	32,44	31,37	35,94	29,40	38,15	30,04	33,64	34,95	36,89
MnO	0,29	0,08	0,16	0,33	0,10	0,42	0,18	0,39	0,16	0,17	0,29	0,08	0,06	0,05	0,05	0,06	0,06	0,06	0,07	0,06	0,06	0,07
MgO	2,59	1,98	1,65	2,17	1,35	2,31	1,72	2,14	1,66	1,88	2,81	2,81	2,34	1,89	1,62	2,40	2,09	2,45	2,97	2,79	2,18	2,12
CaO	2,52	2,65	5,06	4,34	4,51	4,08	4,22	5,94	4,39	3,90	3,01	0,35	1,41	0,81	1,49	0,34	0,55	0,93	1,06	0,58	1,00	1,10
Na_2O	0,52	0,83	1,06	1,00	1,06	0,99	1,03	0,99	1,05	0,30	0,31	0,31	0,35	0,34	0,28	0,31	0,93	0,98	0,93	0,93	0,31	1,02
K_2O	0,11	0,41	0,56	0,52	0,55	0,51	0,52	0,55	0,52	0,07	0,09	0,11	0,27	0,49	0,11	0,14	0,69	0,68	0,68	0,68	0,30	1,18
P_2O_5	1,00	0,65	1,86	1,57	1,87	1,34	1,56	2,68	1,70	1,71	1,24	0,29	0,95	0,69	1,32	0,22	0,23	0,55	0,48	0,20	0,68	0,41
LOI	18,39	38,14	5,72	18,49	8,44	18,74	17,12	17,92	13,19	14,74	13,17	7,96	9,50	8,39	6,93	8,35	7,12	8,57	6,55	6,35	8,33	9,28
Tot	100,01	99,99	100,00	99,99	99,98	99,99	99,99	96,91	100,0	99,99	100,00	99,98	100,00	100,00	100,00	99,99	100,00	100,00	99,99	100,00	100,00	99,99
ppm																						
Co	23	41	35	37	22	19	28	52	26	47	31	34	30	29	21	36	27	34	20	25	25	37
Cr	61	57	56	63	56	58	48	93	53	67	86	71	86	81	64	73	70	82	67	58	71	63
Cs							1,9				2,6										1,2	
Hf	2,4	1,7	1,2	2,8	1,5	3,4	1,1	1,6	1	2,2	3,9	3,3	4	3,8	3,2	3,6	3,1	3,4	4,4	3	3,9	4,5
Ni												310										
Rb							50												40	40		
Sc	17,5	25,4	22,4	27,1	21	22,3	16,8	28,6	18,8	22,8	24	13,1	22	21,7	18,2	13,2	13,7	19,1	14,4	11,3	18,5	20,7
U	2,4	2	2,9	3,5	3	2,7	2,3	5	3,8	2,3	2,1	1,1	2,5	2,1	2,4	1,8	1,8	2	1,5	1,9	2,5	2,5
Zn		170	80			90			60		60	110	120	80		130	80	180		90	140	120
V	297	226	284	333	347	331	359	311	334	276	329	111	247	266	231	122	102	221	120	110	189	228
Cu	57	26	84	61	93	73	65	75	70	70	67	37	39	47	60	42	31	29	47	25	45	55
Sr		99	79	81	63	64		61	11	24	15	181	174	133	159	32	34	90	122	20	233	58
Y	30	28	25	49	36	30	26	73	30	35	36	15	46	31	39	24	11	29	27	16	29	19
Zr	88	62	21	93	24	92	16	69	18	56	135	117	148	153	139	121	95	132	138	104	153	164

Nb	14	13	10	13	7	14	11	10	7	10	13	23	22	17	18	14	19	16	14	12	15	15
Pb	41	15	96	27	36	16	48	24	20	19	64	139	12	35	39	46	125	59	168	7	16	70
Th	18	9	24		22	10	6	13	3	15	20	16	15	23	12	19	13	18	14	15	15	19
V/Cr	4,87	3,97	5,07	5,29	6,20	5,70	7,47	3,34	6,30	4,12	3,83	1,56	2,87	3,28	3,61	1,67	1,45	2,70	1,79	1,89	2,66	3,62
La	27,4	33,5	18,8	34,4	21,6	18,7	23,2	24,4	14	25,7	41,6	39,7	42,6	41,9	41	41,4	45,7	40,1	49,7	41,8	42,8	35,4
Ce	58	70	47	77	54	43	51	62	38	60	84	67	81	76	80	69	77	74	91	62	78	70
Nd	39	28	24	28	22	21	23	39	15	24	41	44	56	54	45	41	34	44	51	37	51	44
Sm	6,2	7,2	6	8	6,3	6,1	5,9	9,5	4,9	7,6	8,4	6,5	8,1	7,3	8,3	5,4	6,5	7,1	9,6	5,1	7,3	6,6
Eu	1,5	2,1	2	2,1	1,9	1,5	1,7	2,7	1,5	1,8	2,1	2	2,1	1,8	2,2	1,3	2,2	2,1	3	1,5	1,5	1,5
Tb	1,2	< 0.5	0,9	1,5	1,4	1,3	1	0,9	1,2	1,7	1	0,9	< 0.5	1	1,7	< 0.5	0,7	1,2	1,4	0,8	< 0.5	< 0.5
Yb	5,4	4,3	5,9	6,9	6,7	5,8	5,7	10,6	5,7	5,7	5,5	2,4	5,5	4,5	4,8	3,3	2,3	4,1	4,1	2,4	3,7	4,1
Lu	0,85	0,67	0,89	1,06	0,99	0,91	0,86	1,62	0,92	0,9	0,87	0,41	0,86	0,68	0,72	0,58	0,42	0,66	0,67	0,41	0,62	0,64
ΣREE	139,55	145,77	105,49	158,96	114,89	98,31	112,36	150,72	81,22	127,40	184,47	162,91	196,16	187,18	183,72	161,98	168,82	173,26	210,47	151,01	184,92	162,24
Eu/Eu*	0,70		1,04	0,77	0,84	0,69	0,87	0,99	0,82	0,66	0,83	0,98		0,79	0,76		1,15	0,89	0,98	0,91		
Ce/Ce*	0,89	0,99	1,08	1,06	1,14	1,03	1,01	1,03	1,22	1,08	0,93	0,75	0,82	0,78	0,87	0,76	0,81	0,83	0,83	0,69	0,80	0,86
$(La/Yb)_{ch}$	3,43	5,26	2,15	3,37	2,18	2,18	2,75	1,56	1,66	3,05	5,11	11,18	5,23	6,29	5,77	8,48	13,43	6,61	8,19	11,77	7,82	5,83

$Ce/Ce^* = (3Ce/Ce_{ch})/(2La/La_{ch} + Nd/Nd_{ch})$; $Eu/Eu^* = Eu_{ch}/\sqrt{Sm_{ch} \cdot Gd_{ch}}$; $(La/Yb)_{ch} = (La/La_{ch})/(Yb/Yb_{ch})$. Chondrite values are from Taylor and McLennan (1985).

I.b TABLE 2 – Chemical composition of Tacchi Ironstones (MT and JP subsets)

SAMPLE	MT1	MT2	MT3	MT4	MT5	MT6	JP1	JP2	JP3	JP4	JP5	JP6	JP7	JP10	JP11	JP12
wt. %																
SiO_2	29,62	2,75	26,23	15,30	2,58	16,14	11,64	7,38	1,43	6,51	8,08	9,91	4,83	10,10	9,63	14,19
TiO_2	0,31	0,19	0,31	0,33	0,27	0,05	0,60	0,24	0,12	0,23	0,18	0,23	0,20	0,15	0,33	0,14
Al_2O_3	7,58	4,46	4,85	11,11	6,63	0,92	13,67	5,56	4,30	4,83	4,35	4,79	3,77	3,31	6,57	5,42
Fe_2O_3	50,02	77,95	55,31	55,67	74,30	69,42	56,83	72,26	78,76	74,58	71,15	72,74	78,19	73,04	67,50	66,78
MnO	0,16	0,22	0,14	0,18	0,10	0,17	0,16	0,24	0,30	0,12	0,24	0,06	0,08	0,08	0,07	0,10
MgO	0,64	0,64	0,48	0,71	0,61	0,44	0,63	0,46	0,50	0,45	0,50	0,48	0,47	0,44	0,72	0,48
CaO	0,43	0,42	1,26	2,57	1,75	1,86	1,72	1,13	1,36	0,78	2,88	0,67	0,31	1,04	2,85	1,24
Na_2O	0,33	0,33	0,30	0,36	0,37	0,28	0,74	0,39	0,38	0,38	0,35	0,31	0,26	0,27	0,32	0,28
K_2O	0,81	0,57	0,51	1,35	1,05	0,09	1,63	0,73	0,54	0,62	0,53	0,55	0,49	0,43	1,24	0,84
P_2O_5	1,22	1,42	1,65	2,64	1,74	1,33	1,64	1,39	1,57	1,40	2,06	0,77	0,85	1,58	2,11	1,51
LOI	8,88	11,05	8,96	9,79	10,60	9,30	10,73	10,21	10,74	10,10	9,68	9,48	10,55	9,56	8,65	9,02
Tot	100,00	100,00	100,00	100,01	100,00	100,00	99,99	99,99	100,00	100,00	100,00	99,99	100,00	100,00	99,99	100,00
ppm																
Ba			300	1800	400		300	1100	2900		900	100	200		300	200
Co	201	319	167	371	161	317	238	104	115	61	148	33	39	17	16	62
Cr	70	29	31	47	25	21	66	22	20	22	27	20	16	17	27	
Cs	4,1				3,3		5,5			3,1		2,5		3,2	4,7	2,3
Hf	2		1,3		1,4		2,3	1				1,5		1,3	2,5	1,9
Ni					400	420										
Rb	60				80		80		60				50		60	50
Sc	6,8	3,6	4,1	6,6	5,3	0,7	18,8	4,2	3,5	3,2	3,4	4,1	13,1	2	4,3	11,2
U	4,6	7,4	6,8	8,7	8,7	6,9	9,8	3,8	5,3	2,8	6,9	4,9	9,9	9,8	11	11,9
Zn	310	400	390	270	370	200	510	380	420	400	460	690	560	380	240	490
V	69	26	23	50	41	7	78	35	29	28	29	26	18	14	35	11
Cu	170	151	156	280	199	154	77	116	129	69	120	141	116	90	105	80
Sr	98		24	25	35		86	3	42							
Y	34	62	163	158	190	25	12	12	10	7	25	32	4	7	18	33

Zr	72		44	47			62					49	19	29	87	49
Nb	6	9	4	15	10	6	15	7	6	11	6	8	7	2	10	8
Pb	17	30	34	19	19	26	44	15	6	22	25	30	77	33	32	64
Th	7	2	10	9	21					2			3	6	5	11
V/Cr	0,98	0,89	0,75	1,06	1,63	0,33	1,19	1,58	1,45	1,27	1,09	1,32	1,14	0,80	1,29	
La	175	24,8	178	195	172	14,1	86,1	19,1	24,6	19,9	14,5	32,5	46,6	16,8	16,4	71,4
Ce	158	42	87	173	89	14	134	33	27	34	30	90	264	51	50	135
Nd	157	61	226	383	328	54	59	33	29	10	21	46	45	29	28	109
Sm	26,3	15,1	45	62,8	45,4	9,2	11,1	6,9	6,4	3,8	5,6	11,6	8,9	7,2	7,7	23,3
Eu	6,1	4,3	11,6	18,2	11,9	2,1	2,4	1,8	1,7	1	1,5	3,2	2	1,8	2	6
Tb	2,7	2,9	6,1	10	7	1,4	1,1	1,1	1,2	< 0.5	< 0.5	1,8	0,7	< 0.5	1,4	2,1
Yb	4,6	8,6	14,8	20,3	17,2	5,2	2,8	2,8	2,5	1,6	3,4	5,1	1,7	2	3,4	5,9
Lu	0,76	1,23	1,98	2,83	2,44	0,71	0,48	0,47	0,41	0,24	0,59	0,82	0,29	0,35	0,47	0,88
ΣREE	530,46	159,93	570,48	865,13	672,94	100,71	296,98	98,17	92,81	70,54	76,59	191,02	369,19	108,15	109,37	353,58
Eu/Eu*	0,80	0,83	0,83	0,89	0,81	0,71	0,75	0,80	0,78			0,85	0,81		0,77	0,91
Ce/Ce*	0,42	0,60	0,21	0,34	0,20	0,29	0,76	0,69	0,48	0,87	0,87	1,17	2,61	1,21	1,22	0,78
$(La/Yb)_{ch}$	25,71	1,95	8,13	6,49	6,76	1,83	20,78	4,61	6,65	8,40	2,88	4,31	18,52	5,68	3,26	8,18

$Ce/Ce^* = (3Ce/Ce_{ch})/(2La/La_{ch} + Nd/Nd_{ch})$; $Eu/Eu^* = Eu_{ch}/\sqrt{Sm_{ch} \cdot Gd_{ch}}$; $(La/Yb)_{ch} = (La/La_{ch})/(Yb/Yb_{ch})$. Chondrite values are from Taylor and McLennan (1985).

I.c TABLE 3 – Chemical composition of marine supergene Mn ores (*mar1*, *mar2* and *mar3* subgroup)

	mar1										*mar2*				*mar3*			
SAMPLE	**RS1**	**RS3**	**RS4**	**RS5**	**RS6**	**RS8**	**RS9**	**RS10**	**RS11**	**RS12**	**RS13**	**Mn1**	**Mn2**	**Mn3**	**Mn4**	**Mn5**	**RS20**	**RS21**
wt. %																		
SiO_2	2,71	4,34	16,59	32,22	17,33	32,39	15,43	3,94	4,60	2,87	16,19	4,17	4,04	10,13	25,87	19,33	10,73	8,58
Al_2O_3	0,81	1,59	5,72	12,87	5,59	13,07	4,26	1,99	2,13	1,10	4,99	1,37	1,31	3,13	8,03	5,62	3,08	2,32
Fe_2O_3	0,25	3,80	3,29	5,81	1,83	6,12	6,81	0,90	1,45	0,01	0,70	0,26	3,94	3,46	1,96	1,22	0,48	0,39
MnO	73,25	76,52	50,31	16,63	51,73	27,44	53,01	64,99	76,70	80,84	30,74	7,65	41,02	4,26	41,01	44,41	40,78	58,08
MgO	0,51	0,42	0,94	1,80	1,09	1,61	1,30	0,44	0,42	0,24	0,69	0,39	0,39	0,40	1,81	0,74	0,63	0,53
CaO	5,29	0,49	4,54	9,45	5,59	2,70	2,06	8,36	0,75	1,20	21,02	48,52	24,57	42,65	4,53	10,16	18,82	9,61
Na_2O	0,17	0,08	0,80	1,14	0,62	1,06	0,42	0,12	0,06	0,04	0,87	0,08	0,08	0,36	0,46	0,91	0,76	0,74
K_2O	0,16	0,37	3,99	3,11	1,28	2,02	1,05	0,66	0,37	0,16	2,27	0,21	0,14	0,92	2,53	1,88	0,80	0,51
TiO_2	0,02	0,06	0,36	0,52	0,22	0,52	0,23	0,07	0,07	0,01	0,10	0,02	0,02	0,08	0,21	0,13	0,07	0,06
P_2O_5	0,21	0,10	0,12	0,20	0,14	0,20	0,12	0,18	0,13	0,32	0,18	0,12	0,49	0,18	0,97	0,26	0,53	0,30
LOI	16,38	12,39	12,82	16,33	14,51	12,67	15,22	17,14	13,43	13,27	20,96	36,91	24,14	33,98	12,53	15,16	23,18	18,25
Tot	99,77	100,14	99,48	100,07	99,93	99,80	99,91	98,79	100,10	100,05	98,71	99,71	100,14	99,57	99,92	99,80	99,88	99,37
Mn/Fe	319,82	22,30	16,91	3,17	31,30	4,96	8,62	80,01	58,58	17897,50	48,62	32,34	11,52	1,36	23,16	40,42	93,54	163,73
SiO_2/Al_2O_3	3,34	2,73	2,90	2,50	3,10	2,48	3,63	1,98	2,16	2,61	3,25	3,04	3,08	3,24	3,22	3,44	3,49	3,71
ppm																		
As	706	1560	2350	777	653	643	786	1170	1880	226	304	21,3	178	99	125	82,2	46	82
Cr	23	27	32	43	32	35	42	35	33	36	31	4,5	7	12	12	4,5	59	40
Sb	63,3	276	91,4	19,4	168	25	43,3	918	1190	10,5	17,7	2,9	11,9	3,4	9,4	15,7	1,8	15,1
Sc	0,9	7,1	6,6	11,8	5,8	12,6	7,1	2,7	5,4	0,6	2,9	0,9	1,4	2,3	5	5,8	1,9	1,3
Be	1	4	2	2	3	2	2	21	10	2	3	0,5	3	2	3	4	0,5	3
Co	20	121	493	51	84	22	27	57	138	11	20	0,5	0,5	4	33	12	7	26
Ni	308	86	42	21	61	29	67	76	67	113	32	25	71	15	107	90	53	77
Zn	306	202	94	67	93	81	119	264	331	72	34	20	67	23	85	62	61	80
Cd	1,8	0,8	0,6	0,4	1,1	0,8	1,2	1,1	0,4	1,5	1,6	6	1,9	0,6	2,4	1,9	2,7	2,1
S	410	160	360	100	700	200	240	110	40	40	130	170	90	90	210	180	250	70

Cu	256	3190	2750	744	3790	127	104	293	70	27	111	32	71	23	42	57	24	23
Ag	18,5	21	13,2	2,2	12,6	5,6	14,2	18,3	19,7	14,3	7,2	1,8	9,5	0,3	14,4	15,1	9,2	15,5
Ga	89	115	90	59	81	68	86	96	118	121	76	10	40	4	29	32	90	97
Ge	13	14	16	9	10	5	8	12	22	6	2	0,5	3	0,5	2	3	4	3
Rb	5	8	49	46	24	32	51	6	7	6	52	10	8	31	81	52	26	15
Sr	800	443	2600	640	567	478	1803	1898	1011	136	776	241	147	121	1907	1021	334	815
Y	1,5	23	30	27	17	25	26	71	42	2	7	12	15	8	33	22	23	2
Zr	3,5	3,5	3,5	63	3,5	75	3,5	3,5	3,5	3,5	3,5	3,5	3,5	71	3,5	3,5	3,5	3,5
Nb	0,5	1	1	5	4	6	2	0,5	0,5	0,5	1	0,5	0,5	2	4	0,5	0,5	0,5
Mo	6	20	32	63	46	32	6	18	8	28	25	7	21	2	6	1,5	3	4
Sn	0,5	0,5	0,5	0,5	0,5	2	0,5	0,5	3	0,5	1	0,5	0,5	0,5	0,5	0,5	0,5	0,5
Cs	0,6	1,2	2,8	2,7	1,8	2,7	7,1	0,4	1,5	0,6	1,3	0,9	0,8	1	6,4	1,4	1,3	0,5
Ba	1162	2644	13630	4411	1658	837	520	16830	5020	8978	5045	3004	739	911	9700	4119	635	4257
Hf	0,1	0,5	1,3	3,8	1,7	3,8	1,2	0,4	0,4	0,1	1,3	0,6	0,4	1,7	2,3	1,1	1	0,8
Ta	0,05	0,05	0,05	0,4	0,2	0,5	0,05	0,05	0,05	0,05	0,05	0,05	0,05	0,1	0,4	0,05	0,05	0,05
W	2	13	0,5	3	110	10	7	47	54	1	45	4	14	12	31	5	10	25
Tl	49,6	20,8	868	538	68,9	64,4	8,4	7,1	2,2	0,9	16,3	1,9	0,8	0,8	48,4	2,8	0,4	1,6
Pb	39	55	35	15	36	24	38	38	46	35	20	7	24	10	32	32	25	44
Th	0,4	0,7	2,3	6,1	2,7	5,7	2,3	0,7	0,9	0,6	3,5	0,8	0,8	2,4	7,8	4,2	1,9	1,4
U	3,6	4,6	2,8	1	3,7	1,5	3,5	7,9	9,3	10,3	5	1,9	7,1	1	8	10,3	9,1	8,9
La	4,2	12,3	17	32,7	20,1	28,5	16,6	50,7	16	2,7	13,6	2,9	7,5	4,5	26,4	23,8	23,8	6,7
Ce	8,8	39,1	30	78,2	49,6	94,3	31,6	29,3	20,3	3,5	20,2	3,8	8,9	9,6	41,1	46	27,9	13,4
Pr	0,8	3,49	4,3	8,31	4,85	9,49	4,36	4,15	2,84	0,35	2,28	0,46	1,1	0,85	5,41	5,64	3,3	1,05
Nd	2,7	12,5	15,4	29	15,6	33,9	14,9	15,2	10,4	1,1	7	1,6	3,5	3,1	17,2	18	10,4	3,3
Sm	0,6	2,8	3,4	6,1	3,5	7	3,2	2,6	2,5	0,2	1,4	0,4	0,7	0,6	3,4	3,8	2,1	0,6
Eu	0,08	0,57	0,86	1,43	0,6	1,52	0,77	1,13	0,83	0,13	0,42	0,07	0,18	0,19	0,91	0,78	0,37	0,18
Gd	0,5	2,7	3,8	5,9	3	6,2	3,2	5,1	3,6	0,3	1,3	0,5	0,9	0,7	3,5	3,7	2,2	0,6
Tb	0,05	0,6	0,7	0,9	0,6	0,9	0,6	0,7	0,7	0,05	0,2	0,1	0,2	0,1	0,7	0,7	0,4	0,1
Dy	0,6	3,8	4,1	5,4	3,6	5,2	3,8	4,1	4,4	0,3	1,3	0,8	1,2	0,7	4,3	4,1	2,5	0,6
Ho	0,1	0,9	0,9	1,1	0,8	1,1	0,8	0,9	1	0,05	0,3	0,2	0,3	0,2	0,9	0,8	0,6	0,1

Er	0,4	3,2	3,3	3,5	2,4	3,1	3	2,8	3,4	0,4	1	0,7	1,1	0,5	3,1	2,6	1,9	0,5
Tm	0,07	0,55	0,54	0,53	0,39	0,48	0,49	0,34	0,48	0,08	0,16	0,13	0,19	0,08	0,5	0,41	0,31	0,08
Yb	0,4	3,9	3,5	3,5	2,6	3,2	3,3	1,8	2,9	0,6	1	0,9	1,3	0,6	3,3	2,7	1,9	0,5
Lu	0,06	0,63	0,56	0,53	0,39	0,47	0,51	0,24	0,47	0,1	0,15	0,16	0,22	0,09	0,53	0,42	0,28	0,07
ΣREE	19,36	87,04	88,36	177,10	108,03	195,36	87,13	119,06	69,82	9,86	50,31	12,72	27,29	21,81	111,25	113,45	77,96	27,78
Eu/Eu*	0,45	0,63	0,73	0,73	0,57	0,71	0,74	0,95	0,85	1,62	0,95	0,48	0,69	0,90	0,81	0,64	0,53	0,92
Ce/Ce*	1,06	1,39	0,81	1,09	1,15	1,34	0,86	0,36	0,66	0,74	0,79	0,71	0,65	1,09	0,77	0,91	0,66	1,08
$(La/Yb)_{ch}$	7,10	2,13	3,28	6,31	5,22	6,02	3,40	19,03	3,73	3,04	9,19	2,18	3,90	5,07	5,41	5,96	8,46	9,06

$Ce/Ce^* = (3Ce/Ce_{ch})/(2La/La_{ch} + Nd/Nd_{ch})$; $Eu/Eu^* = Eu_{ch}/\sqrt{Sm_{ch} \cdot Gd_{ch}}$; $(La/Yb)_{ch} = (La/La_{ch})/(Yb/Yb_{ch})$. Chondrite values are from Taylor and McLennan (1985).

I.d TABLE 4 – Chemical composition of continental hydrothermal Mn ores (*hyd1*, *hyd2* and *hyd3* subgroup)

	hyd1				*hyd2*							*hyd3*							
SAMPLE	**RS17**	**RS18**	**RS19**	**RS22**	**LP 1**	**LP 2**	**LP 3**	**LP 4**	**LP 5**	**LP mc**	**LP v**	**CF 1**	**CF 2**	**CF 3**	**CF 4**	**CF 5**	**CF 6**	**CF 7**	**CF 8**
wt. %																			
SiO_2	7,66	5,57	5,53	25,47	32,70	27,64	23,06	20,98	25,09	25,42	31,39	42,80	42,05	45,02	3,23	1,88	6,48	22,93	29,86
Al_2O_3	1,42	0,42	1,23	0,94	7,85	5,56	5,92	4,26	5,24	5,68	6,11	6,59	6,67	7,41	1,88	1,40	1,41	3,63	4,62
Fe_2O_3	0,19	0,005	0,38	0,16	2,37	1,55	1,74	1,34	3,07	1,77	1,68	1,83	1,71	2,03	0,09	0,01	0,21	1,60	2,58
MnO	78,14	81,67	79,30	62,33	40,76	48,13	53,19	58,40	52,23	49,96	45,62	31,31	35,41	31,16	75,95	79,95	72,91	56,78	49,11
MgO	0,14	0,08	0,16	0,15	0,37	0,52	0,36	0,15	0,24	0,60	0,26	0,15	0,08	0,15	0,25	0,13	0,62	0,12	0,06
CaO	0,39	0,34	0,50	0,37	0,84	0,73	0,75	0,21	0,44	0,97	0,72	0,17	0,15	0,10	0,18	0,13	0,41	0,14	0,17
Na_2O	0,15	0,03	0,15	0,05	2,47	0,97	1,63	1,15	0,40	1,12	1,72	1,78	2,58	2,50	0,52	0,42	0,01	1,16	1,90
K_2O	0,23	0,05	0,21	0,17	4,53	4,20	3,24	4,10	4,59	2,87	4,67	4,85	4,71	4,94	5,22	3,86	1,98	3,85	4,55
TiO_2	0,03	0,002	0,03	0,02	0,31	0,27	0,37	0,11	0,18	0,33	0,34	0,11	0,09	0,11	0,02	0,02	0,03	0,07	0,11
P_2O_5	0,21	0,17	0,10	0,15	0,52	0,17	0,21	0,28	0,29	0,17	0,38	0,01	0,03	0,05	0,02	0,02	0,02	0,01	0,02
LOI	11,13	11,86	12,39	9,81	7,18	10,09	9,61	9,11	8,00	10,85	6,95	10,31	6,22	6,27	11,74	11,71	15,95	9,10	6,75
Tot	99,69	100,18	99,99	99,61	99,91	99,82	100,09	100,09	99,78	99,74	99,83	99,91	99,70	99,74	99,10	99,51	100,02	99,38	99,74
Mn/Fe	466,70	18229,68	230,71	442,60	19,04	34,46	33,78	48,36	18,82	31,23	30,06	18,98	22,94	16,98	976,31	16989,56	385,00	39,23	21,10
SiO_2/Al_2O_3	5,39	13,36	4,49	27,22	4,17	4,98	3,89	4,93	4,79	4,47	5,14	6,50	6,31	6,08	1,71	1,34	4,60	6,31	6,46
ppm																			
As	74	79	70	114	193	172	159	165	159	116	213	93,1	101	87,5	207	399	756	297	294
Cr	96	91	77	4,5	11	4,5	4,5	4,5	4,5	4,5	4,5	4,5	4,5	4,5	8	7	12	4,5	4,5
Sb	31,4	31,9	54,2	87,9	6,2	3,9	5,4	4,5	4,5	8,2	3,5	4,1	3,6	8,3	19,7	50,2	61,3	13,6	4,5
Sc	5,3	4,9	3,6	3	6,2	3,5	2,6	4,6	5,9	3,2	6,2	1,6	1,7	1,5	1,5	1,2	0,9	0,9	1
Be	15	13	17	22	38	35	67	47	38	43	42	23	41	27	46	61	50	75	37
V	n.d.	n.d.	n.d.	n.d.	33	4,5	29	4,5	29	35	7	4,5	4,5	4,5	4,5	4,5	4,5	4,5	4,5
Co	12	21	16	17	23	37	125	26	26	69	32	10	28	4	19	21	13	88	31
Ni	37	53	37	32	36	45	58	55	49	41	35	40	54	36	77	69	62	49	46
Zn	125	121	93	45	256	419	343	490	438	231	187	1120	1540	1260	1180	869	597	1150	778
Cd	3,9	3,7	3,7	1,8	39,8	50,5	23,5	44,8	54,4	29,5	49,8	9,5	13	17,1	21,7	19,8	33,1	113	18,3

S	3	2	2	1	90	30	70	50	40	80	20	100	50	120	170	80	150	50	10
Cu	520	1330	258	956	3	5	31	4	4	6	5	13	7	28	31	11	21	21	3
Ag	20,2	20	21	15	9,6	12	13	14,3	13,3	11,1	8,9	6	8,4	6,6	20,7	19,1	19,7	14,5	12,7
Ga	107	129	130	103	16	13	16	18	16	16	15	25	24	28	24	17	13	25	18
Ge	11	9	13	6	3	2	4	6	4	2	10	5	5	7	11	12	8	20	9
Rb	9	2	7	3	89	107	79	94	97	69	115	170	178	187	64	45	22	109	134
Sr	377	401	529	462	1987	2174	1159	1741	2118	1780	1640	712	833	497	1790	1009	805	1568	978
Y	72	60	60	27	53	72	150	120	150	61	41	239	353	254	171	187	184	123	216
Zr	3,5	4	4	4	136	75	79	142	333	17	3,5	311	364	545	3,5	3,5	7	86	283
Nb	2	1	2	1	31	18	17	39	6	2	2	10	52	120	0,5	18	4	1	16
Mo	16	101	10	12	101	101	81	101	53	13	16	11	23	101	23	101	52	24	101
Sn	0,5	2	1	1	2	4	4	3	2	2	3	4	7	7	0,5	0,5	0,5	0,5	6
Cs	1,4	0	1	1	3,3	17,5	11,4	3,7	2,7	15,2	2,5	4	4,6	3,3	1,6	0,9	0,4	4,3	3,1
Ba	2209	1882	2828	4786	6824	6939	34370	10870	11160	18020	9871	2558	4223	2771	1224	1112	262	14030	7351
Hf	0,7	0,1	0,9	0,1	4,9	4,3	4,7	6,4	4,5	3,9	3,3	12,4	11,7	14,6	3,1	2,3	2,6	6,9	12,4
Ta	0,05	0,05	0,05	0,05	1,6	1,1	1,1	2,3	0,8	0,4	0,7	3,4	3,8	4,8	0,05	0,05	0,05	0,2	2,4
W	179	237	49	505	11	3	5	53	1	0,5	0,5	0,5	0,5	69	0,5	18	11	0,5	0,5
Tl	7,7	3,6	7,6	2,9	4,6	5	47,6	67	75,6	16	68,1	2,8	1	4,7	14,5	5,1	7,1	1001	263
Pb	48	48	49	35	76	88	325	52	48	321	48	38	79	99	180	69	46	170	45
Th	1,0	0,6	1,2	0,1	8	7,2	7,2	8,4	8,2	7	6,9	21,9	20,8	32	5	1,8	1,1	11,8	18,1
U	26,0	28,1	24,4	32,7	9,2	5,3	13,5	14,1	10,5	10,6	8,6	23,9	22,5	18,5	26,8	63,2	107	32	31,5
La	78,4	32,7	64,3	42,7	77,6	75,5	124	127	182	84,5	48,6	479	516	464	797	744	695	502	281
Ce	65,4	30,4	60,5	24,1	305	207	629	328	233	539	100	620	503	977	1420	563	634	1370	289
Pr	14,1	6,0	11,4	4,6	15,8	15,9	20,8	25	31,8	17,5	9,95	97,6	96,7	98	187	187	197	116	52
Nd	48,6	21,6	37,1	14,5	54,4	58,3	74	87,6	116	62,6	36,6	345	349	336	594	612	687	397	193
Sm	9,8	4,7	7,1	2,5	11,4	13,7	17,6	20,7	24,3	14,3	7,9	79,7	81,9	76,6	122	128	145	87,3	45,6
Eu	1,37	0,70	1,02	0,31	1,53	2,78	2,97	1	1,22	2,21	1,63	0,5	0,6	0,51	0,67	0,7	1,15	0,35	0,42
Gd	11,6	6,3	7,4	3,1	9,1	12,7	20,9	19,7	22,8	13,6	7	83,6	105	74,6	89,2	102	83,7	63,3	68,4
Tb	1,8	1,1	1,2	0,5	1,9	2,6	4,9	4,5	4,7	2,7	1,4	11,8	14,6	10,8	11	11,4	11,6	7,6	9,7
Dy	11,5	7,1	7,8	3,5	10,9	14,5	31,2	26,7	26,9	15,4	8,6	53,1	67,7	51	47,4	51,6	54,7	30,4	47

Ho	2,6	1,6	1,7	0,9	2,2	3	7,3	5,6	5,3	3,1	1,8	8,6	11,1	8,6	7,3	8	8,9	4,7	8,3
Er	7,9	5,5	5,7	3,2	6,4	8,4	22	15,9	14,7	8,7	5,3	20,2	25,8	20,8	17,7	19,4	21,5	11	19,2
Tm	1,12	0,82	0,84	0,55	1,04	1,1	3,29	2,22	2,07	1,26	0,74	2,7	3,25	2,8	2,39	2,57	2,71	1,4	2,46
Yb	6,70	4,90	5,10	3,90	6,3	6,5	20,3	13,4	12,5	8,2	4,7	14,1	15,7	14,6	12,1	12,9	13,9	7,2	12,1
Lu	0,99	0,76	0,76	0,65	0,9	1	3,32	2,09	1,89	1,28	0,72	1,77	1,95	1,85	1,39	1,52	1,74	0,9	1,58
ΣREE	261,88	124,17	211,92	105,02	504,47	422,98	981,58	679,41	679,18	774,35	234,94	1817,67	1792,30	2137,16	3309,15	2444,09	2557,90	2599,15	1029,76
Eu/Eu*	0,39	0,39	0,43	0,34	0,46	0,64	0,47	0,15	0,16	0,48	0,67	0,02	0,02	0,02	0,02	0,02	0,03	0,01	0,02
Ce/Ce*	0,43	0,48	0,49	0,34	1,95	1,34	2,68	1,30	0,67	3,15	1,02	0,64	0,50	1,03	0,84	0,35	0,40	1,29	0,53
$(La/Yb)_{ch}$	7,91	4,51	8,52	7,40	8,32	7,85	4,13	6,40	9,84	6,96	6,99	22,96	22,21	21,48	44,51	38,97	33,79	47,11	15,69

$Ce/Ce^* = (3Ce/Ce_{ch})/(2La/La_{ch} + Nd/Nd_{ch})$; $Eu/Eu^* = Eu_{ch}/\sqrt{Sm_{ch} \cdot Gd_{ch}}$; $(La/Yb)_{ch} = (La/La_{ch})/(Yb/Yb_{ch})$. Chondrite values are from Taylor and McLennan (1985).

APPENDIX 2

BASIC PRINCIPLES OF ANALYTICAL METHODS

II.a X-ray Diffraction Analysis

X-ray diffraction (XRD) is an important tool in mineralogy for identifying, quantifying and characterizing minerals in complex mineral assemblages. The interaction of waves with periodic structures produces diffraction effects if the wavelength and the periodicity of the crystals, are of similar magnitude. Considering that atoms have diameters of the order of Angströms (1 Å = 10^{-10} m), unit cells have dimensions of several Å. This implies that crystals with sizes of microns or larger consist of billions of unit cells, which repeat periodically in all three dimensions. Electromagnetic waves with wavelengths of the order of 10^{-10} m are called X-rays. The electric field of such waves interacts with the charges of all electrons of an atom, which then emit an almost spherical wave with the same wavelength as the incident radiation. The amplitude of this outgoing wave is proportional to the number of electrons in the atom, and, hence, to the atomic number. Light elements with few electrons, such as carbon or oxygen, are therefore "poor" scatterers for X-rays, whereas heavy elements, such as lead, are "good" scatterers (Stanjek and Häusler 2004).

Detection limits are severely influenced by this effect. The amplitude of the scattered wave is described by the atom form factor (*f*). Due to interference within individual atoms, especially larger ones, the amplitude of the outgoing wave and hence the atom form factor varies also with the scattering angle 2θ.

Without any diffraction effects, the incidence of a primary X-rays beam onto a sample volume would produce scattering in all directions. Diffraction redistributes intensity from the whole scattering sphere into distinct directions. Therefore, intensity peaks arise in certain directions, whereas in directions between peaks the intensity decreases drastically. The intensity integrated over the sphere, however, remains constant due to energy conservation. In what directions do we observe such peaks, also called reflections? One way of describing these directions is the notion of scattering lattice planes and interference between the wavelets scattered by neighbouring lattice planes. Constructive interference and hence a so called Bragg reflection is obtained when the path of the wavelet scattered of the lower of the two planes is longer by an integer number of wavelengths λ than that of the wavelet scattered off the upper plane.

A reflection will thus occur when $n\lambda = 2d \cdot \sin\theta$. This is the so-called Bragg's equation, where λ is the wavelength of the radiation, n is an integer number, θ is

the angle between the lattice planes and the incident beam and d is the distance of the lattice planes for which the peak occurs.

X-ray powder diffraction is widely used for analyzing the phase composition of a sample and its crystal-chemical features. The method allows fine-grained and poorly crystalline samples to be studied. A resultant powder diffraction pattern (a set of peaks related to interatomic distances or d-spacings and peak intensities) is compared with reference data for minerals. The most complete source of diffraction data is Powder Diffraction File (PDF) database. This includes experimentally obtained patterns and patterns calculated on the basis of a known crystal structure.

Phase identification involves comparison of a set of experimental d-spacings and intensities values with those in a database. Quantitative phase analysis is based on the correlation between the intensity of diffraction peaks for a phase and the abundance of the phase in a sample. Investigations are carried out by a variety of procedures including the internal standard method, the adsorption-diffraction method, the standard addition method and the Rietveld method (Snyder and Bish 1989).

II.b X-ray Fluorescence Analysis

X-ray fluorescence spectrometry (XRF) is currently the most widely used analytical technique in the determination of the major and trace elements chemistry of rock samples. It is versatile and can analyze up to 80 elements over a range of sensitivities, detecting contents from 100% down to a few ppm. The XRF is a rapid method and large numbers of precise analyses can be made in a relatively short time. The limitation of this method is that elements lighter than Na (atomic number=11) cannot be analyzed. X-ray fluorescence spectrometry is based upon the excitation of a powdered rock sample by X-ray. A primary X-rays beam excites secondary X-rays (X-ray fluorescence) which have wavelengths characteristic of the elements present in the sample. The intensity of the secondary X-rays is used to determine the element contents by reference to calibration standards, with appropriate corrections being made for instrumental errors and the effects the composition of the sample has no its X-ray emission intensities. Alternatively, the X-rays may be detected without being separated into different frequencies, using a detector which measures energy as well as intensity of the X-rays.

This method, known as energy-dispersive X-ray fluorescence, is currently under investigation for routine trace elements analysis (Rollinson 1993 and reference therein).

II.c Instrumental Neutron Activation Analysis

Neutron activation analysis is a useful method for the simultaneous determination of a large number (about 25-40) of major, minor and trace elements in small geological sample, without necessarily destroying the sample.

The method allows the highly selective determination of elements (especially rare earth elements, Sc, Cr, Co, Rb, Hf, Ta, W, Th, U and other elements of the platinum group) in the ppm and ppb concentration range with or without chemical treatment. There are, indeed, two approaches for this method: instrumental neutron activation analysis (INAA) employs a powdered rock or mineral sample without chemical treatment; radiochemical neutron activation analysis (RNAA) involves the chemical separation of selected elements (Rollinson 1993). Among these, INAA is used here for the chemical analysis of ironstones and Mn ores.

INAA is based on the "activation", for up to 30 hours, of a rock sampleby neutrons flux within a neutron reactor. During the irradiation, the naturally occurring stable isotopes of all elements that constitute the rock and mineral samples are transformed into higher-mass radioactive (unstable) isotopes by neutron capture reactions (e.g. $^{23}Na+n \longrightarrow {}^{24}Na+\gamma_{prompt}$). The activated nucleus then decays with a characteristic half-live $t_{1/2}$ and with γ-ray emission at one or more characteristic energies (e.g. $^{24}Na \longrightarrow {}^{24}Mg+\beta^{-}+\gamma$). Generally, the intensities of these radiations are proportional to the amount of the isotopes present and thus the amount of the radioactive nuclide is determined by measuring the intensity of the characteristic gamma-ray lines in the gamma spectrum.

Because irradiated mineral samples contain radionuclides of different half-lives, the resulting activity and gamma spectra of a sample change with time and it is therefore necessary to count at various time intervals (several hours, days and weeks) after the end of irradiation. After taking different half-life corrections, decay time, counting time and other correction factor into account, the results are quantified by comparison with standards which have been irradiated and counted together with the samples (Koeberl 1995).

For these measurements, a specialized instrumentation is necessary and it consist of a gamma-ray detector, the electronic signal processing and the amplification part, a multichannel analyzer for storage of all measured signals and a computer system for data evaluation.

II.d Inductively Coupled Plasma-Mass Spectrometry

Inductively Coupled Plasma-Mass Spectrometry (or ICP-MS) is an analytical technique used for elemental determinations and was commercially introduced in 1983. ICP-MS has many advantages over other elemental analysis techniques such as atomic absorption and optical emission spectrometry and they are linked to a superior detection capability, particularly for the rare-earth elements (REEs), Ta, Nb, Hf, Th and U (typically less than 0,05 ng/ml), and ability to obtain isotopic information (Jarvis 1990; Hall et al. 1990).

An ICP-MS combines a high-temperature ICP (Inductively Coupled Plasma) source with a mass spectrometer. The ICP source converts the atoms of the elements in the sample to ions. These ions are then separated and detected by the mass spectrometer. The sample is typically introduced into the ICP plasma as an aerosol, either by aspirating a liquid or dissolved solid sample into a nebulizer or using a laser to directly convert solid samples into an aerosol. Once the sample aerosol is introduced into the ICP torch, it is completely desolvated and the elements in the aerosol are converted first into gaseous atoms and then ionized towards the end of the plasma. Once the elements in the sample are converted into ions, they are then brought into the mass spectrometer via the interface cones.

The ions coming from the system are positively charged, so the electrostatic lens, which also has a positive charge, serves to collimate the ion beam and focus it into the entrance aperture or slit of the mass spectrometer. Different types of ICP-MS systems have different types of lens systems. The simplest employs a single lens, while more complex systems may contain as many as 12 ion lenses. Once the ions enter the mass spectrometer, they are separated by their mass-to-charge ratio. The most commonly used type of mass spectrometer is the quadrupole mass filter which act as sequential filter and separate up to 2400 amu (atomic mass units) per second. This speed is the reason for that the quadrupole ICP-MS is often considered to have simultaneous multi-elemental analysis properties. The ability to filter ions on their mass-to-

charge ratio allows ICP-MS to supply isotopic information, since different isotopes of the same element have different masses.

The instrument may be operated in a number of ways. Spectra can be collected over the complete mass range, allowing a qualitative investigation of a sample to be made. This feature is particularly useful to establish simply which elements are present in a sample. Alternatively, semiquantitative measurements can be made using a single standard solution containing about six elements across the mass range. A response curve for these elements is established and unknown samples measured against this curve. Finally, fully quantitative data may be obtained using either external calibration procedures or isotope dilution (Jarvis 1995).

II.e Scanning Electron Microscopy and EDS Analysis

The scanning electron microscope (SEM) consists of an electron gun and a number of electromagnetic lenses, all within an evacuated column where a electrons beam is accelerated by a high voltage and then focused by two condenser lenses onto the thin specimen. Finally, the objective focused the beam onto the sample surface and the beam is moved or scanned across an area. At any instant, signals being generated by the beam can be collected by appropriate detectors and one of them used to control the intensity on a cathode ray tube. Latter is scanned synchronously with the incident beam so that an image of the area as it is scanned is build up on the cathode ray tube. Thus, the scanning electron microscope permits the observation and characterization of heterogeneous organic and inorganic materials on a nanometer (nm) to micrometer (μm) scale and it provides information about the surface structure of the specimen. The popularity of the SEM, in fact, stems from its capability of obtaining three-dimensional-like images of the surfaces of a very wide range of materials (Goldstein et al. 2003).

In the SEM, the examined sample is irradiated with a primary (incident) electrons beam, which interact with the sample in a volume named "interaction volume". The depth of penetration of the electrons below the sample surface is maximum when the beam is normal to the sample surface and increases as the average atomic number and density of the sample decrease and as the beam energy increase.

The electrons interact with the sample by both elastic (i.e. without loss of energy) and inelastic scattering. A fraction of the incident electrons are adsorbed while the others are scattered out of the specimen. Among these, the electrons which are produce by elastic interaction are named backscattered electrons. Their intensity increase with increasing atomic number of observed material and has a cosine angular distribution about the incident beam direction for normal incidence. Tilting the sample increases the intensity of the beck scattered electrons and caused the angular distribution to become asymmetrically peaked away from the beam; the contrast from differences in the average atomic number is reduced at grazing incidence and high contrast topographic images are obtained.

The electrons, which lose energy by inelastic scattering processes, produce secondary electrons, continuum X-rays, characteristic X-rays and infrared, visible and ultraviolet radiations. Among these, secondary electrons are of particular interest for mineralogical and textural observations. The number of emitted secondary electrons increases approximately with the secant angle of the surface tilt of the sample causing topographic contrast in images. Secondary electrons are sensitive to surface fields caused by voltage or magnetic differences. The spatial resolution for secondary electron images is of the order of the beam diameter.

The secondary electron emission, confined to a very small volume near the beam impact area for certain choice of the beam energy, permits images to be obtained at a resolution approximating the size of the focused electron beam. The three-dimensional appearance of the images is due to the large depth of field of the scanning electron microscope as well as to the shadow relief effect of the secondary and backscattered electron contrast.

In the SEM, characteristic X–rays are also emitted as a result of electron bombardment. The analysis of characteristic X-radiation emitted from the samples can yield both qualitative identification and quantitative elemental information from regions of a specimen nominally 1 μm in diameter and 1μm in depth under normal operating conditions.

The radiations are collected by two types of electron detector. The solid state detector is a semiconductor device which generates a current when struck by an electron, the current being proportional to the energy of the electron. This detector has a good response to high energy backscattered electrons but is relatively insensitive to the low energy secondary electrons. The scintillator-

photomultiplier type of detector is commonly used to collect backscattered and secondary electrons and convert them into light photons.

Specimen preparation is generally minimal with SEM. Sample are fixed to the specimen stage in an orientation which will optimize the generation and collection of the signal of interest. The samples need to be conducting to avoid charge build-up and possible thermal damage. Gold is often used as a coating when topographic information are required, as it gives a good secondary electron signal. Carbon, indeed, is used when information about the composition is required, as with backscattered electrons or X-ray signals, as the gold layer adsorb and obscures the signals from the sample (Pennock 1995).

REFERENCES

GOLDSTEIN J., NEWBURY D.E., JOY D.C., ECHLIN P., LYMAN C.E., LIFSHIN E. (2003) - *Scanning electron microscopy and X-ray microanalysis*. Springer Ed., vol. 1, 689 pp.

JARVIS K.E. (1990) – *A critical evaluation of two sample preparation techniques for low level determination of some geologically incompatible elements by inductively coupled plasma mass spectrometry*. Chemical Geology, 83, 89-103.

JARVIS K.E. (1995) – INDUCTIVELY COUPLED PLASMA MASS SPECTROMETRY. In: Advanced Mineralogy. Methods and Instrumentation: Results and Recent developments. A.S. Marfunin Ed., Springer-Verlag, vol. 2, 337-340.

KOEBERL C. (1995) – *Neutron Activation Analysis*. In: Advanced Mineralogy. Methods and Instrumentation: Results and Recent developments. A.S. Marfunin Ed., Springer-Verlag, vol. 2, 322-329.

HALL G.E.M., PELCHAT J.C. AND LOOP J. (1990) – *Determination of zirconium, niobium, hafnium and tantalum at low levels in geological materials by inductively coupled plasma mass spectrometry*. J. Anal. at Spectrom, 5, 339-349.

PENNOCK G.M. (1995) – *Scanning Electron Microscopy and Image Formation*. In: Advanced Mineralogy. Methods and Instrumentation: Results and Recent developments. A.S. Marfunin Ed., Springer-Verlag, vol. 2, 273-279.

ROLLINSON H. (1993) – *Using geochemical data: evaluation, presentation interpretation*. Longman Ed., 352 pp.

SNYDER R.L. AND BISH D.L. (1989) – *Quantitative analysis. In: Modern powder diffraction. Reviews in mineralogy*. Bish D.L. and Post J.E. (Eds), vol. 20, Mineralogical Society of America, 101-144.

STANJEK H. AND HÄUSLER W. (2004) – *Basics of X-ray Diffraction*. Hyperfine Interactions, 154, 107-119.